LUND UNIVERSITY

Finite Element Analysis of Structure-Acoustic Systems; Formulations and Solution Strategies

Carlsson, Håkan

1992

[Link to publication](#)

Total number of authors:
1

FINITE ELEMENT ANALYSIS
OF STRUCTURE-ACOUSTIC SYSTEMS;
FORMULATIONS AND SOLUTION STRATEGIES

Håkan Carlsson

FINITE ELEMENT ANALYSIS
OF STRUCTURE-ACOUSTIC SYSTEMS;
FORMULATIONS AND SOLUTION STRATEGIES

Håkan Carlsson

To My Family

ACKNOWLEDGEMENTS

Lund in April 1992

Håkan Carlsson

ABSTRACT

This thesis is concerned with the finite element analysis of the small—amplitude coupled vibration problem of an acoustic fluid enclosed in a flexible and/or rigid container structure. The governing equations for linear elastic solids and inviscid acoustic fluids are derived by a continuum mechanics approach. Modified equations for an acoustic fluid interpenetrating a rigid incompressible porous material are given.

The coupled structure—acoustic vibration problem is discretized by a finite element technique resulting in eleven formally equivalent symmetric and unsymmetric systems of equations. The advantages and restrictions connected to the use of various formulations are discussed with respect to the undamped problem. Suitable formulation found for the coupled analysis is then generalized to also incorporate various damping effects.

Non—modal reduction techniques that use a set of orthogonolized load—dependent Krylov vectors are described and are successfully applied to proportionally or non—proportionally damped structure—acoustic problems. The basic idea is that, in the case of spatially invariant loading situations, the information of the loading distribution is used in a procedure where the original system of equations is transformed into a much smaller system without solving the corresponding eigenvalue problem.

Matrix—vector iteration schemes based on the Lanczos algorithm are used for the reduction of the symmetric systems of equations, whereas for the unsymmetric systems an iteration scheme based on the Arnoldi algorithm is developed. The applications of the Lanczos process and the Arnoldi process respectively to harmonic and transient analysis of structure—acoustic systems are new and are illustrated in numerical examples for both structural and fluid loading.

Key words: Finite element method, coupled problem, fluid—structure interaction, structure—acoustic interaction, acoustics, non—proportional damping, reduction methods, reduced basis, Lanczos method, Arnoldi method.

CONTENTS   Page

1 INTRODUCTION

1.1 Background

The present thesis has been carried out at the Division of Structural Mechanics at Lund University and is a result of the ongoing research activities within the field of fluid—structure interaction. These activities started in 1983 and has evolved to play a significant role in the research within the division. The first thesis on this subject was presented by Sandberg in 1986 [66] and has been followed by a licentiate thesis by Carlsson in 1990 [9—11].

In the thesis by Sandberg, finite element formulations of the coupled fluid—structure interaction problem were derived. Basic equations were assumed for an inviscid fluid, and the choice of primary variables for the mathematical description of the fluid domain discussed. Symmetric and unsymmetric systems of equations were given for the undamped problem and numerical examples showed the characteristics of the solution to fluid—structure interaction problems.

In [9], the governing equations for acoustic fluids were closely studied and compared to the governing equations for linear—elastic solids. Further, alternative finite element formulations for the coupled structure—acoustic problem were added to those found in [66]. Finite element results were compared favourably to analytical solutions to one— and three—dimensional model problems. A large—scale structure—acoustic problem found in automobile design was studied in [10] and revealed both the potential and the limitations of using finite element analysis in this type of problems. As a result of that study, a non—modal solution strategy for the coupled problem was proposed in [11], using a load—dependent reduction technique in order to minimize the computational effort.

The dynamic response of structures like marine platforms, ships and dams may be significantly affected by the presence of the surrounding fluid. The primary interest in the design process of these types of structures is their structural strength and stability, and no particular interest is directed towards the fluid domain other than the fluid causing a loading effect on the structure. Further, the geometry of the boundaries of the fluid is such that pressure waves are radiated away to infinity and are not reflected back on the surface of the structure to produce added fluid loading. A general background to research in this area is given below.

The increased use of light—weight materials in automobiles and aircraft has created an interest in not only studying the structural motion but also in predicting fluid pressure levels and displacement fields in these vehicles to ensure passenger comfort. These systems differ significantly from the unbounded systems, in that the structure is in contact with a fluid contained within a finite volume, and by physical boundaries that wholly or partly comprise the surface of the structure. The introduction of acoustic modes in the fluid volume may require the two physically separated domains to be analyzed in a coupled analysis by necessity, especially when considering small fluid volumes, measured in acoustic wavelength. Coupling is important when a structural mode frequency is close to an acoustic mode frequency and also if structural modes have frequencies below the lowest acoustic mode. In this case, the cavity acts as an added stiffness. A review of current solution methods for the structure—acoustic problem in general can be found in [26] and for the structure—acoustic analysis of automobile compartments in particular in [10]. In principle, one can classify these methods into analytical techniques (like Green's Function Analysis, Modal—Interaction Models and Statistical Energy Analysis) and numerical techniques (like Finite Element Methods and Boundary Element Methods).

One advantage of the analytical techniques is that they lend themselves to asymptotic approximations, so that physical interpretation of the solutions may readily be achieved. However, very often it is not possible to obtain analytical solutions to the problems in question because of the material and/or kinematic complexity of the system modelled. Visualizing structure—acoustic systems, the vibrational behaviour may generally be expressed in terms of series—solutions to the governing equations, but it is generally not possible to derive analytical expressions for the terms in the series, unless the systems and their boundaries are particularly simple.

Numerical techniques are not restricted to particular models and can be performed to any degree of precision desired, subject to the limitations of the computer precision, speed and storage. The finite element method (FEM) is a highly systematized tool for discretization of complex—shaped static and dynamic systems where the continuum problem is transformed into a solvable matrix problem [79]. The method has been under continuous development during the last 30 years and a brief review of its historical background and different fields of application is given in reference [48].

The first paper on the application of finite element methods for the solution of problems in acoustics was published in 1966 [33]. In this paper both fluid pressure and fluid displacement formulations for calculating the modes of three—dimensional cavities with hard and flexible walls were presented. This paper laid the foundation for more than twenty years of research in FE—analysis of acoustic problems. A brief survey of this research is presented in [62]. Finite element techniques have been developed for, in principle, three types of acoustic problems. These are:

- the prediction of the acoustic pressure in a cavity which is enclosed by rigid/flexible walls (the interior problem)

- the prediction of the acoustic pressure radiated from a vibrating structure which is immersed in an infinite acoustic medium (the exterior problem)

- the propagation of acoustic waves in ducts with and without mean flow.

The majority of papers on acoustic finite element analysis use a pressure formulation for describing the fluid vibration, see [62]. This choice of primary variable in the fluid domain gives unsymmetric systems of equations when coupled to a displacement—based structural model. Unsymmetric systems of this form arise if two coupled, conservative mechanical systems interact through conjugate variables like forces and displacements [30]. The interaction effect between the fluid and structure domain may be studied in a decoupled manner by transferring field variables from one field to another at each time step in a so—called staggered solution. An overview of these techniques is given in [70] and is applied to interior structure—acoustic systems in [71]. Equivalent symmetric formulations of the coupled problem exist, and these forms are of great interest because computer—based eigenvalue methods that take advantage of sparsity, are more highly developed and require less computer storage than the unsymmetric counterpart [34]. The eigenvalues and their corresponding eigenvector play an important role in analyzing mechanical systems. The eigenvalues may be used as an error estimate for the discretization procedure, whereas the eigenvectors may reveal physical insight into the mechanical behaviour of the studied system, or may be used in a reduction procedure in order to decrease the number of unknowns in the system of equations to be solved.

Actually, a number of alternative formulations which produce symmetric systems of equations have been suggested, based upon displacement, a velocity—potential or simultaneous pressure and displacement—potential representation of the acoustic medium. Some of these formulations have been incorporated in the major commercial general purpose FE—codes. A velocity potential is used in ADINA [59], introducing a third system "damping" matrix. ASKA utilizes a mixed two—field formulation with both a pressure and displacement—potential variable in the fluid domain [35]. All these implementations facilitate symmetric eigenvalue calculations, although the first two lead to a non—standard quadratic eigenvalue problem. The implementation in ASKA is, to the author's knowledge, the only implementation in the major FE—codes leading to an eigenvalue of generalized form. This implementation was suggested in the thesis by Sandberg [66].

Unsymmetric formulations using fluid pressure in the fluid region are implemented in ABAQUS [1], ANSYS [2] and MSC/NASTRAN [42] and in the special purpose code SYSNOISE [75]. In a previous study [10], ABAQUS was used to solve simultaneously the acoustic pressure and structural displacement field due to harmonic structural force excitation of an idealized automobile compartment. Although the finite element mesh was rather coarse from an engineering point of view, the model comprised approximately 20,000 degrees—of—freedom. Typically, to compute the response function for a given loading configuration required 4.5 CPU minutes per frequency on a large—scale computer. An unsymmetric eigenvalue solver is not available in ABAQUS and hence no modal reduction could be performed. The analysis was performed without damping, thus allowing all calculations to be made in real arithmetic. In the case of damping the computational effort would have increased considerably. It was concluded in [10] that an efficient solution strategy, including the choice of primary variables in the fluid domain and a suitable reduction technique, is of extreme importance to make the problem of interacting structure—acoustic systems practically solvable by the finite element method.

A discretization procedure such as the finite element method results in the equations of motion generally expressed as

$$\mathbf{M}\,\ddot{\mathbf{u}} + \mathbf{C}\,\dot{\mathbf{u}} + \mathbf{K}\,\mathbf{u} = \mathbf{f}(t) \tag{1.1}$$

in which $\mathbf{M}$, $\mathbf{C}$ and $\mathbf{K}$ are the $n \times n$ mass, damping and stiffness matrices respectively. $\mathbf{f}(t)$ is the $n \times 1$ time—dependent external load and $\mathbf{u}$ is the $n \times 1$ solution vector describing the response of the system.

The Rayleigh–Ritz approximation method [17] is widely used in large–scale finite element analysis to reduce the number of equations into a smaller number before the dynamic response is calculated. The method is a general formalism where the essential idea is to express an approximate solution u_m by a set of linearly independent vectors $Y_m = [y_1, y_2, \dots y_m]$ as in

$$u(t) \simeq u_m(t) = Y_m x(t) \tag{1.2}$$

in which the amplitude of these vectors stored in $x(t)$, are the generalized coordinates. The m's are here less than n, the number of degrees–of–freedom in the unreduced system, and the quality of the approximation depends entirely on the chosen set of vectors, Y_m.

Because of their orthogonality properties the eigenvectors have been frequently used in the matrix Y_m. In particular, in the low frequency domain this choice of vectors is advantageous since the dynamic response is dominated by the lowest modes of the system. However, it has been shown that the use of load–dependent Ritz vectors [78], [6] or Lanczos vectors [50] can yield even more accurate results, with fewer vectors, than if the exact (load–independent) eigenvectors are used. The improvement in accuracy is gained due to the fact that in the standard mode superposition procedure, eigenvectors which are orthogonal to the loading are not excited even if their frequency is contained in the loading. In situations with spatially invariant load distributions, the knowledge of this distribution can therefore be used to incorporate in Y_m, only those vectors that are non–orthogonal to the loading, thus improving the quality of Y_m and hence u_m in Eq. (1.2).

Regarding finite element analysis of structure–acoustic systems, two observations can be made. Firstly, the number of equations increases rapidly with the frequency of interest and especially in 3–D applications. An accurate and computationally efficient reduction method is therefore necessary for analysis of full–scale models. Secondly, typical tasks in the transient case may be to study the wave propagation caused by a local structural impact load or by a sudden discharge of mass in a fluid point. In the harmonic case the response function may be calculated for a load function with a given spatial distribution and ultimately within a specific frequency range.

In most structural and acoustic models presently employed, proportional damping of Rayleigh type of modal damping is assumed for convenience and for lack of a more realistic representation. The eigenvectors of the damped system are assumed to be the same as those of the undamped system. These assumptions are invalid for structures and fluids with non–proportional damping. For example, applying discrete viscous dampers to the structure

or the frictional retardation to flow through a porous medium can hardly be described as being proportional to the system mass and stiffness matrices.

Guided by these observations of the system at hand and the improved reduction methods referenced above, the present thesis is concerned with formulations and solution techniques for proportionally or non—proportionally damped coupled structure—acoustic problems. Presently available finite element programs for structure—acoustic analysis are primarily intended for harmonic analysis. Therefore, in this work we will give more general expressions suitable also for transient analysis.

1.2   Aim and scope of the present work

This thesis is concerned with the finite element modelling of small—amplitude vibrations in structure—acoustic systems, see Fig. 1.1. We assume the structure to be linear—elastic and totally or partly filled with an inviscid or slightly viscous compressible fluid. Non—proportional damping is introduced through discrete mechanical devices, locally reacting surfaces and/or by considering viscous flow in porous materials. Alternatively, proportional damping may be considered. Various loading situations will be taken into account, such as harmonic and transient structural and fluid loadings.
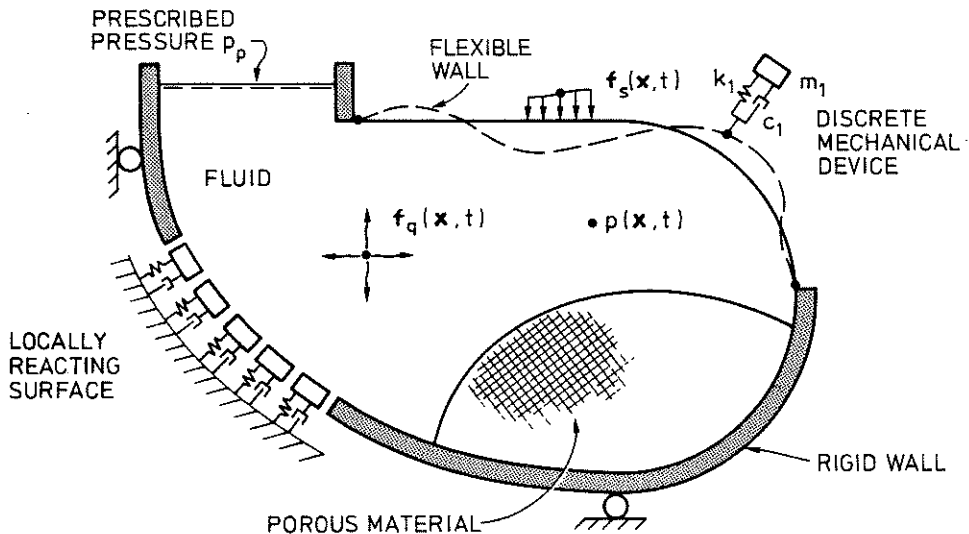
Fig. 1.1   Linear—elastic structure filled with a compressible fluid.

Fig. 1.1 also illustrates the scope of the present work with respect to application. We are only concerned with the interior problem, i.e. an acoustic fluid enclosed in a flexible and/or

rigid container structure. The possible effect of a surrounding fluid is not considered unless it may be modelled by a locally reacting surface.

The aim of the present study is to find a framework for an efficient numerical technique applicable to interacting structure—acoustic systems. This framework includes a complete understanding of the mathematical description of both linear—elastic solids and acoustic fluids and the approximations introduced. Considering the coupled system, different finite element formulations leading to symmetric and unsymmetric systems of equations will be investigated. Finally, efficient reduction techniques will be proposed for the dynamic analysis of damped and undamped structure—acoustic systems.

Examples of applications are found in the analysis of

- fluid—carrying spacecraft
- aircraft fuselages
- launch vehicles
- rocket engines
- fluid—carrying ground vehicles
- automobile cavities
- box—welded beams
- inflated tires
- mufflers
- liquid—filled tanks or containers
- nuclear power safety relief systems
- cavity—connected piping systems
- sound transmission between enclosures
- light weight floors and wall constructions
- small glass—fronted rooms
- sound insulation of windows
- sound insulation between small rooms
- loudspeaker design
- ear acoustics
- ducts
- environmental effects of machinery
- submerged structures
- transducers

1.3   Summary of contents

The contents of the present work may be summarized as:

- to derive structural and fluid governing equations suitable for small—amplitude coupled vibration problems (Chapter 2)

- to study various symmetric and unsymmetric finite element formulations, and their connections, for damped and undamped interacting structure—acoustic systems (Chapter 3)

- to study different reduction techniques based on load—dependent vector algorithms suitable for structure—acoustic analysis (Chapter 4)

- to perform numerical studies on model problems (Chapter 5)

and finally

- to make concluding remarks on this work together with some suggestions for future research and development (Chapter 6).

1.4 Notations

Notations are explained in the text where they first occur. Most of the notations are also listed in APPENDIX A. Some general remarks can be made however. Unless otherwise stated, scalar functions are written in lowercase Greek ρ, ψ or italic p, q letters, whereas vector—valued functions are written in lowercase italic letters with subscript, like u_i, or in boldface, like $\mathbf{u}$. Further, vectors are written in boldface with lowercase sans serif roman $\mathbf{u}$ and matrices in boldface with uppercase sans serif roman $\mathbf{K}$.

Comparing computational effort in different algorithms we will use the notion of flop, i.e. a single floating point operation. A dot product or saxpy operation of length n involves $2n$ flop because there are n multiplications and n adds in either of these vector operations, see [34] for further details.

For brevity, we will use the notation *matrix pencil* ($\mathbf{K}$, $\mathbf{M}$), referring to "a given pair of matrices $\mathbf{K}$ and $\mathbf{M}$" [60].

2 GOVERNING EQUATIONS FOR SOLIDS AND FLUIDS

2.1 Introduction

A mathematical description and derivation of fluid equations for fluid—structure interaction problems was given in [66]. The main effort was to describe the mathematics of the fluid and the fluid—structure interaction, and only passing attention was given to the physics of the structural and fluid parts, respectively. In this chapter we will enrich the mathematical modelling of the structural and fluid components in structure—acoustic systems. We will relate the approximations introduced in the theoretical fluid model to the approximations introduced in the theoretical structure model. Further, we will exemplify the approximations and limitations in the theory, in terms of physical data. The presentation in this chapter follows mainly the one given in [9]; however, it is extended to include the description of acoustic wave propagation in a porous medium.

The governing equations for solids and fluids will be derived, starting with particle kinematics and deformation measures. Two laws of physics, the conservation of mass and the conservation of linear momentum, are used to derive the continuity equation and the equations of motion. These laws must always be fulfilled and are not restricted to any particular material. By appropriate deformation measures and introduced constitutive equations, the equations of motion for linear elastic solids and acoustic fluids can be stated. In the case of small—amplitude vibrations, a spatial description is shown to be applicable for both solids and fluids. The approximations introduced in the fluid and solid domains are both based on a small displacement gradient assumption implying small density variations, and on an assumption of small displacement velocities.

The discretized differential equations in Chapter 3 are due to the linear form of the governing equations. Further, the reduced base techniques studied in Chapter 4 are based on superposition principles. Therefore, it is of interest to recognize the limit for linear behaviour in structure—acoustic systems. Many of the relations shown below can be found in books on continuum mechanics; here reference [72] is used in general. The resulting governing equations for an undamped acoustic fluid derived below are identical to the equations given in [66]. However, in this study we also derive the governing equations for an acoustic fluid penetrating a porous medium.

2.2   Basic equations for a continuum
2.2.1   Particle kinematics and deformation measures

We introduce a fixed rectangular Cartesian coordinate system with base vectors e_i. All subsequent vector and tensor components refer to these base vectors.

The displacement vector u of a studied particle from its position X in the reference configuration at time $t=0$ to its current position x at time t may be expressed in <u>material description</u> as

$$u\,(X,t) = x(X,t) - X \tag{2.1}$$

or in <u>spatial description</u> as

$$u\,(x,t) = x - X(x,t) \tag{2.2}$$

Thus, the velocity vector v in material description is

$$v\,(X,t) = \frac{\partial u(X,t)}{\partial t} = \frac{\partial x(X,t)}{\partial t} \tag{2.3}$$

and the acceleration vector a is

$$a\,(X,t) = \frac{\partial^2 x(X,t)}{\partial t^2} \tag{2.4}$$

In spatial description the velocity of a particle which occupies the point x at time t is

$$v\,(X(x,t),t) = v(x,t) \tag{2.5}$$

whereas the acceleration in the same point x at time t is expressed as

$$a = \frac{\mathrm{d}v}{\mathrm{d}t} = \frac{\partial v}{\partial t} + (v \cdot \nabla)v \tag{2.6}$$

where $\nabla = [\frac{\partial \cdot}{x_1}, \frac{\partial \cdot}{x_2}, \frac{\partial \cdot}{x_3}]$, is the del operator and the operator $\frac{\mathrm{d} \cdot}{\mathrm{d}t} = [\frac{\partial \cdot}{\partial t} + (v \cdot \nabla) \cdot]$ the material time derivative.

Studying motions of deformable bodies, we will make use of the deformation gradient tensor F defined by

$$F_{iR} = \frac{\partial x_i}{\partial X_R} = \delta_{iR} + \frac{\partial u_i}{\partial X_R} \qquad (i, R = 1, 2, 3) \qquad (2.7)$$

where δ_{ij} is the Kronecker delta. Capital letter indices are used for components of vectors and tensors related to the reference configuration. Various exact measures of deformation exist in both material and spatial description. In material description the Lagrangian strain tensor is defined by

$$G = \tfrac{1}{2}(F^T F - I) \qquad (2.8)$$

where I is the unit tensor.

In component form Eq. (2.8) is given by

$$G_{RS} = \frac{1}{2}\left[\frac{\partial u_R}{\partial X} + \frac{\partial u_S}{\partial X} + \frac{\partial u_i}{\partial X_R}\frac{\partial u_i}{\partial X_S} \right] \qquad (2.9)$$

For the problem studied in this work it is reasonable to adopt the small displacement gradient approximation where we assume

$$\left| \frac{\partial u_i}{\partial X_R} \right| << 1 \qquad (i, R = 1, 2, 3) \qquad (2.10)$$

which enables us to simplify Eq. (2.9) to the infinitesimal strain tensor defined by

$$E_{RS} = \frac{1}{2}\left[\frac{\partial u_R}{\partial X_S} + \frac{\partial u_S}{\partial X_R} \right] \qquad (2.11)$$

We observe that the components E_{RS} are linear in the displacement components u_R. Eq. (2.10) also carries the implication of small rotations. It can also be shown that Eq. (2.10) implies that at the same order of approximation we get

$$\frac{\partial u_R}{\partial X_S} \approx \frac{\partial u_i}{\partial x_j} \qquad (2.12)$$

and thus Eq. (2.11) may be rewritten as

$$E_{ij} = \frac{1}{2}\left[\frac{\partial u_i}{\partial x_j} + \frac{\partial u_j}{\partial x_i} \right] \qquad (2.13)$$

Discussing the validity of neglecting viscous effects in the fluid region we will make use of the rate–of–deformation tensor defined by

$$D_{ij} = \frac{1}{2} \left[\frac{\partial v_i}{\partial x_j} + \frac{\partial v_j}{\partial x_i} \right] \qquad (2.14)$$

where v_i is the velocity component in a fluid point. Thus, D_{ij} is linear in the velocity components and is measured in the current configuration. D_{ij} is an exact measure of deformation rate whereas E_{ij} is an approximate measure of deformation.

2.2.2   Continuity equations

For later use we will formulate the continuity equation in both spatial and material form. We start with the general case including a source function $q = q(\mathbf{x},t)$.

In spatial form we express the mass conservation in terms of the velocity components. Consider an arbitrary region V fixed in space at time t and with surface S. The mass conservation can be stated as

$$\int_V \frac{\partial \rho}{\partial t} \, dV = - \int_S \rho v \cdot \mathbf{n} \, dS + \int_V q \, dV \qquad (2.15)$$

where $\rho = \rho(\mathbf{x},t)$ is the current density, $v(\mathbf{x},t)$ the velocity field, $\mathbf{n}(\mathbf{x},t)$ the outward normal to S and $q = q(\mathbf{x},t)$ the added fluid mass per unit volume and time in V. Because of the source function q the Eq. (2.15) may actually be referenced as a mass balance equation rather than a mass conservation equation.

By applying the divergence theorem to the surface integral we obtain

$$\int_V \left\{ \frac{\partial \rho}{\partial t} + \nabla \cdot (\rho v) - q \right\} \, dV = 0 \qquad (2.16)$$

and because V is arbitrary we get

$$\frac{\partial \rho}{\partial t} + \nabla \cdot (\rho v) = q \qquad (2.17)$$

which is seen to be the usual expression for conservation of mass in spatial form if the source function vanishes ($q{=}0$).

For convenience we may rewrite Eq. (2.17) using the identity

$$\nabla(\rho v) = \rho(\nabla \cdot v) + (v \cdot \nabla)\rho \tag{2.18}$$

and get

$$\frac{d\rho}{dt} + \rho(\nabla \cdot v) = q \tag{2.19}$$

where $\frac{d\rho}{dt}$ is the material time derivative of the density ρ.

In absence of a source function q, the continuity equation in material form simply states that the mass of the material in a (material) volume element remains constant during deformation. It can be shown that the volume dV of an element with volume dV_o in the reference configuration can be expressed as

$$dV = \det F \, dV_o \tag{2.20}$$

where F is the deformation gradient tensor defined by Eq. (2.7). Conservation of mass then implies

$$\rho_0 = \det F \, \rho \tag{2.21}$$

where ρ_0 is the density of the referential volume element and ρ the current density of the deformed volume element. From Eq. (2.7) follows that

$$\det F = \det \left[\delta_{iR} + \frac{\partial u_i}{\partial X_R} \right] = 1 + \frac{\partial u_i}{\partial X_R} + a \left[\frac{\partial u_i}{\partial X_R} \right]^2 \tag{2.22}$$

Making use of the small displacement gradient approximation (2.10) and Eq. (2.12) we get

$$\det F \approx 1 + \frac{\partial u_i}{\partial x_i} = 1 + E_{ii} = 1 + \nabla \cdot u \approx (1 - \nabla \cdot u)^{-1} \tag{2.23}$$

where $E_{ii} = \nabla \cdot u$ is the dilatation or change of volume per unit initial volume of the element. Hence, by Eq. (2.21) and (2.23) the continuity equation in material form approximately can be written

$$\rho = \rho_0(1 - \nabla \cdot u) \tag{2.24}$$

The material form Eq. (2.24) is derived in absence of a source function, and hence less general than the spatial form Eq. (2.17). It is noted that Eq. (2.24) is applicable to both solids and fluids when no source function has to be considered. In most cases this form is impractical for fluids because it relates the current density to a reference state. However, for fluid vibrations around a fixed point in such a reference state, Eq. (2.24) is suitable whenever $q = 0$.

2.2.3   Equations of motion

We consider a fixed region V at time t containing a certain amount of particles and bounded by a surface S. The conservation law of linear momentum states that the time rate of change of linear momentum of the particles in V is equal to the vector sum of all surface tractions or S and body forces in V. Thus, we instantaneously have

$$\frac{d}{dt} \int_V \rho\, v\, dV = \int_S t^{(n)}\, dS + \int_V \rho\, b\, dV \qquad (2.25)$$

where $v = v\,(x,t)$ is the velocity field, $t^{(n)} = t^{(n)}(x,t)$ is the traction force acting on S and $b = b(x,t)$ is the body forces acting on the particles in V.

In a given fixed rectangular Cartesian coordinate system with base vectors e_i, there is a traction vector $t^{(i)}$ associated with each one of the base vectors e_i, and these traction vectors can be written in component form

$$t^{(i)} = \sigma_{ij}\, e_j \qquad (i,j = 1,\ 2,\ 3) \qquad (2.26)$$

where the quantities σ_{ij} are the stress components. It can be shown that σ_{ij} are components of a second—order tensor, the Cauchy stress tensor, that completely describes the state of stress of the body and that the traction on any surface with normal n in the current configuration can be expressed in direct notation as

$$t^{(n)} = n \cdot \sigma, \qquad \sigma = \sigma^T \qquad (2.27)$$

where the second—order tensor σ is the Cauchy stress tensor, and where the second equality can be proved by applying the conservation law of angular momentum to the body identified by the region V considered above. Applying the divergence theorem to the surface integral in Eq. (2.25) then yields

$$\frac{d}{dt} \int_V \rho\, v\, dV = \int_V \nabla\cdot\sigma\, dV + \int_V \rho\, b\, dV \tag{2.28}$$

Using Reynold's transport theorem the left—hand—side of Eq. (2.28) takes the form

$$\frac{d}{dt} \int_V \rho\, v\, dV = \int_V \frac{\partial(\rho v)}{\partial t}\, dV - \int_S \rho\, v\,(n\cdot v)\, dS \tag{2.29}$$

Then using the divergence theorem to the surface integral and rearranging terms Eq. (2.28) can be written as

$$\frac{d}{dt} \int_V \rho\, v\, dV = \int_V \left\{ \frac{\partial(\rho v)}{\partial t} + \nabla\cdot(\rho v \otimes v) \right\} dV \tag{2.30}$$

where the tensor $v \otimes v$ is the dyadic product of the two vectors. Noting that the integrand of the right hand side can be written as

$$v \left[\frac{\partial\rho}{\partial t} + \nabla\cdot(\rho\, v) \right] + \rho \left[\frac{\partial v}{\partial t} + (v\cdot\nabla)\, v \right] \tag{2.31}$$

and using Eqs. (2.6) and (2.17), Eq. (2.28) becomes

$$\int_V \left\{ v\, q + \rho\frac{dv}{dt} \right\} dV = \int_V \nabla\cdot\sigma\, dV + \int_V \rho b\, dV \tag{2.32}$$

Because the region V is arbitrary we find the equation of motion to be

$$\nabla\cdot\sigma + \rho b = \rho\frac{dv}{dt} + qv \tag{2.33}$$

expressed in spatial description. This equation is different from the corresponding equation obtained in [66] with respect to the added fluid mass term qv. In [66] the added mass was considered as being a mass *inflow* with the velocity v_q, and the contribution to Eq.(2.33) became $q(v-v_q)$ instead of qv. In the present study, however, we will think of the source term as being just the increase of mass in fluid points.

2.3 Constitutive equations

2.3.1 Constitutive equations for a linear elastic solid

For an isotropic linear elastic solid under isothermal conditions, the constitutive equations may be expressed as

$$\sigma_{ij} = \lambda \; E_{kk} \; \delta_{ij} + 2 \; \mu \; E_{ij} \qquad (2.34)$$

where λ and μ are constants which satisfy

$$\lambda = \frac{\nu E}{(1+\nu)(1-2\nu)} \; , \qquad \mu = G = \frac{E}{2(1+\nu)} \qquad (2.35)$$

where E is Young's modulus, ν is Poisson's ratios and G is the shear modulus. Typically for steel, λ and μ are of order 10^{11} Pa so that strain of order 10^{-3} are associated with stresses of order 10^8 Pa. In other words, steel (and some other materials) support large loads without significant deformation and hence without significant density variations.

Eq. (2.34) may serve as an approximation for a variety of solid materials in motions with small displacement gradients according to Eq. (2.10).

2.3.2 Constitutive equations for a linear viscous fluid

In contrast to solids fluids cannot support shear stresses when in equilibrium. The constitutive equation for a fluid relates stress to the rate—of—deformation tensor D_{ij} defined by Eq. (2.14). In a linear isotropic viscous fluid the shear stress on the shear planes is assumed to be proportional to the shear rate, and may be written in the form

$$\sigma_{ij} = \left\{- \; p(\rho, \; \theta) + \lambda(\rho, \; \theta) \; D_{kk}\right\} \delta_{ij} + 2\mu(\rho, \; \theta) \; D_{ij} \qquad (2.36)$$

where $p(\rho, \; \theta)$ is the current fluid pressure, θ the fluid temperature and where λ and μ are material constants (to be determined by experiments). The pressure p is positive reflecting that fluids in rest are unable to sustain hydrostatic tension. The dependence of the pressure p on the density ρ and temperature θ is discussed in Section 2.3.3.

It is noted that Eq. (2.36) represents an exact expression for a linear viscous fluid, since no approximation of the rate—of—deformation measure is involved. (In contrast to Eq. (2.34) for a linear elastic solid).

Eq. (2.36) can be rewritten as

$$\sigma_{ij} = \left\{ -p(\rho, \ \theta) + (\lambda + \tfrac{2}{3} \ \mu) \ D_{kk} \right\} \delta_{ij} + 2\mu(D_{ij} - \tfrac{1}{3}D_{kk} \ \delta_{ij}) \qquad (2.37)$$

where $(\lambda + \tfrac{2}{3}\mu)$ can be identified as the coefficient of volume (or bulk) viscosity and μ the coefficient of shear viscosity. Commonly, Stokes' relation

$$3\lambda + 2\mu = 0 \qquad (2.38)$$

is assumed, leading to

$$\sigma_{ij} = -p(\rho, \ \theta) \ \delta_{ij} + 2\mu(\rho, \ \theta) \ (D_{ij} - \tfrac{1}{3}D_{kk} \ \delta_{ij}) \qquad (2.39)$$

which is an adequate model for many liquids and gases and in particular for water and air. The viscosity is sensitive to temperature but the dependence on density is usually negligible. Some values of μ are listed in Table 2.1.

Table 2.1   (Dynamic) viscosity μ (Ns/m^2) for air, water and glycerin [38].

Air	at	0^{0}C	17.1 $\cdot$	10^{-6}
"	at	20^{0}C	18.2 $\cdot$	10^{-6}
"	at	60^{0}C	20.7 $\cdot$	10^{-6}
Water	at	0^{0}C	1.8 $\cdot$	10^{-3}
"	at	20^{0}C	1.0 $\cdot$	10^{-3}
"	at	60^{0}C	0.5 $\cdot$	10^{-3}
Glycerin	at	0^{0}C	12.1	

2.3.3 Constitutive equations for a linear inviscid fluid

Under some flow conditions the shear stresses occurring in liquid and gases are small compared with the normal stresses. In such circumstances we can neglect the shear viscosity in Eq. (2.39), $\lambda = \mu = 0$, and the constitutive fluid equation becomes simply

$$\sigma_{ij} = - p(\rho, \theta) \, \delta_{ij} \tag{2.40}$$

The function $p(\rho, \theta)$ for gases and liquids will be studied next. For *gases* (over wide ranges of temperature and density, we have

$$p = R \, \rho \, \theta / m \tag{2.41}$$

where R is the universal gas constant, m the mean molecular weight of the gas and θ the absolute temperature.

A barotropic model for both gases and liquids where the fluid is only dependent on the density is preferable in our applications, i.e. $p=p(\rho)$. Eq. (2.41) for gases under adiabatic conditions, i.e. conditions when no heat transfer occurs in the fluid, may be written as

$$p = p_0 \left(\frac{\rho}{\rho_0}\right)^\gamma \tag{2.42}$$

where γ is the ratio of specific heat at constant pressure to the specific heat at constant volume, while p_0 and ρ_0 are the reference pressure and density, respectively.

The barotropic and adiabatic model above is found by experiments to be more accurate than an alternative isothermal model when studying sound propagation in gases. Local fluctuations in temperature do occur during the propagation of the wave, but so rapidly that heat liberated locally by gas compression is reabsorbed by the gas during the expansion phase without any heat transfer into neighbouring regions.

Linearization of Eq. (2.42) using the first two terms of a Taylor expansion yields

$$p = p_0 + (\rho - \rho_0)\left[\frac{dp}{d\rho}\right]_{\rho=\rho_0} = p_0 + (\rho - \rho_0)c^2 \tag{2.43}$$

where according to (2.42) and (2.41)

$$c^2 = \left[\frac{dp}{d\rho}\right]_{\rho=\rho_0} = \gamma \cdot \frac{R\theta_0}{m} \qquad (2.44)$$

where θ_0 is the absolute temperature in the reference state. The constant c is subsequently identified as the speed of sound, and for air ($\gamma = 1.40$, $m = 28.96 \cdot 10^{-3}$ kg, $R = 8.314$ (J/Mole°K)) we get

$$c = 20.047 \, \theta_0^{\frac{1}{2}} \qquad (m/s) \qquad (2.45)$$

Typically, for air at temperature 20°C ($\theta_0 = 293$ °K) we get $c = 343.1$ m/s. For comparison, the "isothermal" speed of sound is easily found from (2.43) and (2.41) to be $c = (R\theta_0/m)^{\frac{1}{2}}$ and thus a factor of $\gamma^{\frac{1}{2}}$ less than the "adiabatic" speed. For air at temperature 20 °C the isothermal speed of sound will be $c = 343.1/\sqrt{1.40} = 290.0$ m/s.

For *liquids*, p is well approximated by

$$p = p_0 + K_1(\theta)[\rho - \rho_0)]/\rho_0(\theta) \qquad (2.46)$$

where $K_1(\theta)$ is the isothermal bulk modulus and $\rho_0(\theta)$ is the density in the reference state with pressure p_0 and temperature θ_0. Typically K_1 is of order 10^9 N/m² and this expression for p is valid for values of $(\rho - \rho_0)$ up to about 0.05 [38].

A barotropic model is easily achieved from Eq. (2.46) because K_1 and ρ_0 are relatively insensitive to θ_0. In fact they are nearly identical and thus, the constitutive expression for the pressure of liquids may be approximated by

$$p = p_0 + \frac{K}{\rho_0}(\rho - \rho_0) \qquad (2.47)$$

where now the bulk modulus K is temperature independent and p_0 and ρ_0 as before are the reference values of pressure and density respectively.

The speed of sound in liquids can thus be approximated by the relation

$$c^2 = \left[\frac{dp}{d\rho}\right]_{\rho=\rho_0} = \frac{K}{\rho_0} \qquad (2.48)$$

For water, typical values are $K = 2.25 \cdot 10^3$ MPa and $c = 1500$ m/s.

In summary, for a linear inviscid compressible fluid we use the constitutive equation

$$\sigma_{ij} = - \, p(\rho) \; \delta_{ij} \tag{2.49}$$

where $p(\rho)$ is expressed by a linear equation of state

$$p(\rho) = p_0 + c^2(\rho - \rho_0) \tag{2.50}$$

and where in this last expression the speed of sound c is estimated for gases by Eq. (2.44) and for liquids by Eq. (2.48). It should be noted that the linear model of (2.50) is valid only for small departures of ρ from ρ_0, say within a 2 % variation of ρ around ρ_0.

2.4 Governing equations
2.4.1 Navier's equation of motion for solids

The equations used in classical elastodynamics are based on the equation of motion of a continuum according to Eq. (2.33) (with no source function), the infinitesimal strain tensor Eq. (2.13) and the constitutive equation (2.34). Thus, we have in tensor component notation

$$\frac{\partial \sigma_{ij}}{\partial x_j} + \rho \; b_i = \rho \frac{d v_i}{d t} \; , \; \sigma_{ij} = \sigma_{ji} \tag{2.51}$$

$$E_{ij} = \frac{1}{2} \left[\frac{\partial u_i}{\partial x_j} + \frac{\partial u_j}{\partial x_i} \right] \tag{2.52}$$

$$\sigma_{ij} = \lambda \; E_{kk} \; \delta_{ij} + 2 \, \mu \; E_{ij} \tag{2.53}$$

All quantities in Eqs. (2.51–53) are expressed as functions of spatial coordinates, which is consistent with the small displacement gradient assumption used to derive the infinitesimal strain tensor in Eq. (2.52).

The system of equations (2.51–53) provides 15 equations and 16 unknowns (σ_{ij}, E_{ij}, u_i, ρ). However, we may replace the current density ρ with the density in the reference configuration which is consistent with the small displacement gradient assumption according to Eq. (2.10), and hence by Eq. (2.24)

$$\rho = \rho_0(1 - \nabla \cdot \pmb{u}) \approx \rho_0 \tag{2.54}$$

The equation of motion in vector notation reads

$$\nabla \cdot \sigma + \rho_0 \, b = \rho_0 \left[\frac{\partial v}{\partial t} + (v \cdot \nabla) \, v \right] \tag{2.55}$$

where we have used Eq. (2.6) to rewrite the material time derivative on the right hand side of Eq. (2.51). This equation is nonlinear in v due to the presence of the convection term $(v \cdot \nabla)v$. However, if small displacement velocities are assumed this term can be neglected. Thus we have

$$\nabla \cdot \sigma + \rho_0 \, b = \rho_0 \, \frac{\partial^2 u}{\partial t^2} \tag{2.56}$$

where $u = u\,(x,t)$ is the displacement vector field defined by Eq. (2.2).

In combination with Eqs. (2.52–53) we get Navier's equation of motion for an isotropic linear elastic solid,

$$(\lambda + \mu) \, \nabla(\nabla \cdot u) + \mu \nabla^2 u + \rho_0 b = \rho_0 \, \frac{\partial^2 u}{\partial t^2} \tag{2.57}$$

where $\nabla^2 \equiv \nabla \cdot \nabla$ is the Laplace operator.

The derivation above of Navier's equation for solids was made in order to identify the approximations involved, i.e. the small displacement gradient assumption and the assumption of small displacement velocities, and for later comparison with the fluid equations in subsequent sections.

In practice the structures to be considered in fluid–structure interaction problems generally have one small dimension like shells and plates or two small dimensions like beams. These structures will thus be vibrating mainly in the transverse direction. The differential equations for these types of structures can be found by imposing suitable boundary conditions on Eq. (2.57) or by direct derivation from equilibrium equations, and they will not be stated here.

2.4.2   Navier—Stokes' equation

Most current work in fluid mechanics is directed towards finding solutions to the so—called Navier—Stokes' equation. These equations are readily found from the equation of motion for a continuum according to Eq. (2.33), the rate of deformation tensor Eq. (2.14) and the constitutive equations for a linear viscous fluid Eq. (2.39). Thus, we will combine the following equations

$$\frac{\partial \sigma_{ij}}{\partial x_j} + \rho \ b_i = \rho\frac{dv_i}{dt} + q \ v_i \tag{2.58}$$

$$D_{ij} = \frac{1}{2} \left[\frac{\partial v_i}{\partial x_j} + \frac{\partial v_j}{\partial x_i} \right] \tag{2.59}$$

$$\sigma_{ij} = -p \ (\rho, \ \theta) \ \delta_{ij} + 2 \ \mu(D_{ij} - \frac{1}{3}D_{kk} \ \delta_{ij}) \tag{2.60}$$

Assuming μ constant, independent of temperature, and a barotropic pressure i.e. $p = p(\rho)$, the Navier—Stokes' equation (here with source term) will be

$$-\nabla p + \frac{1}{3}\mu \ \nabla(\nabla \cdot v) + \mu \ \nabla^2 v + \rho b = \rho\frac{dv}{dt} + qv \tag{2.61}$$

and provides, together with the continuity equation in spatial form according to Eq. (2.17), four scalar equations and four unknowns (v and ρ).

Comparing the equation of motion for fluids (2.61) with the corresponding equation for solids (2.57), we note that they are identical in structure. Under certain circumstances (see Section 2.4.3) approximations similar to those found in Eq. (2.57) may be employed in Eq. (2.61), i.e. the convective term on the right—hand side can be neglected and the current density ρ be replaced by the reference value ρ_0. These approximations are employed, in the following for shorter expressions, when discussing dissipation of energy during wave propagation through slightly viscous fluids like air and water. For simplicity we will study one—dimensional wave propagation in which Eq. (2.61) (in absence of body forces and source function) becomes

$$-\frac{\partial p}{\partial x_1} + \frac{4}{3} \ \mu \ \frac{\partial^2 v_1}{\partial x_1^2} = \rho_0 \ \frac{dv_1}{dt} \tag{2.62}$$

By the continuity equation, Eq. (2.17), and the linear equation of state, Eq. (2.50), one gets

$$\frac{1}{c^2} \frac{\partial p}{\partial t} = - \rho_0 \frac{\partial v_1}{\partial x_1} \tag{2.63}$$

Differentiating Eq. (2.62) with respect to x_1 and by use of Eq. (2.63) we achieve the dissipative wave equation expressed in the fluid pressure p

$$\frac{\partial^2 p}{\partial x_1^2} + \frac{4}{3} \mu \frac{1}{\rho_0 c^2} \frac{\partial^3 p}{\partial x_1^2 \partial t} = \frac{1}{c^2} \frac{\partial^2 p}{\partial t^2} \tag{2.64}$$

A solution of Eq. (2.64) can be written in the form [22]

$$p(x_1,t) = \hat{p} \cos \left(\omega t - \frac{\omega}{c} x_1 \right) e^{-\eta x_1} = \mathrm{Re} \left[\hat{p} \; e^{i \omega t - \left(i \frac{\omega}{c} + \eta \right) x_1} \right]$$

where η is the attenuation coefficient, $\hat{p}$ the pressure amplitude and ω the angular frequency. Substituting in Eq. (2.64) and assuming $\eta^2 << \left(\frac{\omega}{c} \right)^2$ we may solve for η and get

$$\eta = \frac{2}{3} \frac{\mu}{\rho_0 c^3} \omega^2 \approx 26.3 \; \frac{\mu f^2}{\rho_0 c^3}$$

The pressure drop $e^{-\eta x_1}$ thus increases with frequency and dynamic viscosity μ. Introducing in this expression the values of μ, ρ_0 and c we can estimate how small the viscous damping is for different fluids at different frequencies, see Table 2.2.

Table 2.2   Pressure drop factor $e^{-\eta x_1}$ (–), for a distance of 100 meters (x_1=100 m) and at different frequencies, due to viscous damping.

f (Hz)	100	10000	20000
Air (20^{0}C)	1.0	0.9	0.67
Water (20^{0}C)	1.0	1.0	0.99
Glycerin (0^{0}C)[1]	0.99	0.48	0.05

[1] For wave speed c = 1500 m/s

It is clear from Table 2.2 that the influence of fluid viscosity can be neglected studying free spaces with air or water in the low frequency range. Wave propagation through a porous material is discussed in Section 2.6.

2.4.3 Governing equations for an acoustic fluid

In this section we study the compressible flow of inviscid fluids. The approximations introduced lead to a model for an acoustic fluid which is found to be reasonably valid for small amplitude wave propagation in liquids and gases.

The governing equations for a compressible inviscid fluid are the equations of motion for a continuum, Eq. (2.33), the continuity equation, Eq. (2.19), and the constitutive equation for a linear inviscid compressible fluid, Eqs. (2.49–50). In summary,

$$\rho \frac{\mathrm{d} v}{\mathrm{d} t} + \nabla p = \rho b - q v \tag{2.65}$$

$$\frac{\mathrm{d}\rho}{\mathrm{d} t} + \rho(\nabla \cdot v) = q \tag{2.66}$$

$$p = p_0 + c^2(\rho - \rho_0) \tag{2.67}$$

The first two equations can be simplified on the assumption of small particle velocities compared to the wave propagation velocity, i.e. $|v| \ll c$. We begin with the equations of motion (2.65) and note that

$$\frac{\mathrm{d} v}{\mathrm{d} t} = \frac{\partial v}{\partial t} + (v \cdot \nabla) v \tag{2.68}$$

$$\frac{\mathrm{d}\rho}{\mathrm{d} t} = \frac{\partial \rho}{\partial t} + (v \cdot \nabla)\rho \tag{2.69}$$

Substituting these expressions in Eqs. (2.65) and (2.66) respectively yields

$$\rho \left(\frac{\partial v}{\partial t} + (v \cdot \nabla) v \right) + \nabla p = \rho b - q v \tag{2.70}$$

$$\frac{\partial \rho}{\partial t} + (v \cdot \nabla)\rho + \rho(\nabla \cdot v) = q \tag{2.71}$$

Because $\nabla p = c^2 \nabla \rho$ we rewrite Eq. (2.70)

$$\rho \frac{\partial v}{\partial t} + \rho(v \cdot \nabla)v + c^2 \nabla \rho = \rho b - qv \qquad (2.72)$$

We multiply Eq. (2.71) by c^2 and Eq. (2.72) by v and get

$$c^2 \frac{\partial \rho}{\partial t} + c^2(v \cdot \nabla)\rho + c^2 \rho(\nabla \cdot v) = c^2 q \qquad (2.73)$$

$$v\rho \frac{\partial v}{\partial t} + v\rho(v \cdot \nabla)v + v \cdot c^2 \nabla \rho = v \cdot \rho b - v \cdot qv \qquad (2.74)$$

Substituting Eq. (2.74) into Eq. (2.73)

$$c^2 \frac{\partial \rho}{\partial t} + v\rho b - vqv - v\rho \frac{\partial v}{\partial t} - v\rho(v \cdot \nabla)v + c^2 \rho \nabla \cdot v = c^2 q \qquad (2.75)$$

and rearranging

$$c^2 \frac{\partial \rho}{\partial t} + \rho(c^2 \nabla \cdot v - v \cdot (v \cdot \nabla) - v\rho \frac{\partial v}{\partial t} = -v\rho b + (c^2 + v \cdot v)q \qquad (2.76)$$

For low particle velocities compared to the wave propagation velocity, i.e. $|v| \ll c$ the following terms can be neglected in Eq. (2.76); $v \cdot (v \cdot \nabla)v$ in comparison with $c^2 \nabla \cdot v$, and $(v \cdot v)$ in comparison with c^2, see also [66].

Thus, Eq. (2.76) can be written as

$$c^2 \left[\frac{\partial \rho}{\partial t} + \rho \nabla \cdot v - q \right] = v \left(\rho \frac{\partial v}{\partial t} - \rho b \right) \qquad (2.77)$$

which by use of Eq. (2.71) on the left hand side and because v is arbitrary can be rewritten as

$$c^2(-\nabla \rho) = \rho \frac{\partial v}{\partial t} - \rho b \qquad (2.78)$$

or equivalently

$$\rho \frac{\partial v}{\partial t} + \nabla p = \rho b \qquad (2.79)$$

Comparing Eq. (2.79) with the original equation of motion (2.65) we have thus neglected the convective term $(v \cdot \nabla)v$ and the influence of the added fluid mass q on the assumption of $|v| \ll c$.

The continuity equation, Eq. (2.71), can be simplified in the same manner. We multiply Eq. (2.71) by v and add the approximative equations of motion, Eq. (2.79), to get

$$v \frac{\partial \rho}{\partial t} + v (v \cdot \nabla) + v\rho(\nabla \cdot v) + \rho \frac{\partial v}{\partial t} + c^2 \nabla \rho = vq + \rho b \tag{2.80}$$

and rearrange to

$$v \frac{\partial \rho}{\partial t} + v\rho(\nabla \cdot v) - vq + (v (v \cdot \nabla)\rho + c^2 \nabla \rho) = - \rho \frac{\partial v}{\partial t} + \rho b \tag{2.81}$$

Again, for low particle velocities $|v| \ll c$, we can neglect $v (v \cdot \nabla)\rho$, in comparison with $c^2 \nabla \rho$.

Thus, Eq. (2.81) can be written as

$$v \left[\frac{\partial \rho}{\partial t} + \rho(\nabla \cdot v) - q \right] = - \rho \frac{\partial v}{\partial t} - c^2 \nabla \rho + \rho b \tag{2.82}$$

where the right hand side is zero according to Eq. (2.78). Again, v is arbitrary and thus

$$\frac{\partial \rho}{\partial t} + \rho(\nabla \cdot v) = q \tag{2.83}$$

Comparing Eq. (2.83) with the original continuity equation (2.66) we have neglected the convective term $(v \cdot \nabla)\rho$ due to the assumption that $|v| \ll c$.

Further, we define functions p_d and ρ_d by the relations

$$p(\mathbf{x}, t) = p_o(\mathbf{X}) + p_d(\mathbf{x}, t) \tag{2.84}$$

$$\rho(\mathbf{x}, t) = \rho_o(\mathbf{X}) + \rho_d(\mathbf{x}, t) \tag{2.85}$$

where $p_o(\mathbf{X})$ and $\rho_o(\mathbf{X})$ are referred to the initial (referential state) and $p_d(\mathbf{x}, t)$ and $\rho_d(\mathbf{x}, t)$ are referred to a disturbed state satisfying the condition

$$p_d(\mathbf{x}, t)\big|_{t=0} = \rho_d(\mathbf{x}, t)\big|_{t=0} = 0 \tag{2.86}$$

Frequently we will use the word "dynamic" in this study when referring to the disturbed state.

We assume that the initial state is homogeneous, i.e.

$$p_o(\mathbf{X}) = p_o \quad , \quad \rho_o(\mathbf{X}) = \rho_o \tag{2.87}$$

where p_o and ρ_o are constants.

Substituting these definitions in Eq. (2.79), (2.83) and (2.67) we get

$$(\rho_o + \rho_d)\frac{\partial v}{\partial t} + \nabla p_d = (\rho_o + \rho_d)b \tag{2.88}$$

$$\frac{\partial \rho_d}{\partial t} + (\rho_o + \rho_d)(\nabla \cdot v) = q \tag{2.89}$$

$$p_d = c^2 \rho_d \tag{2.90}$$

By means of Eqs. (2.88) and (2.89) we have four equations for the four unknowns (v, ρ_d). We may note that both equations are nonlinear with respect to the terms $\rho_d\, \partial v / \partial t$ and $\rho_d(\nabla \cdot v)$ respectively. However, to an approximation consistent with the linear equation of state Eq. (2.50) these terms may be neglected as stated below.

For small departures of ρ from ρ_o, i.e. if the dynamic density is far less than the reference value, we may write

$$\rho = \rho_o + \rho_d = \rho_o(1 + \frac{\rho_d}{\rho_o}) \approx \rho_o \tag{2.91}$$

Substituting this result into the equations above we achieve the governing equations for an acoustic fluid, see also [66]

$$\rho_o\, \frac{\partial v}{\partial t} + \nabla p_d = \rho_o b \tag{2.92}$$

$$\frac{\partial \rho_d}{\partial t} + \rho_o\, \nabla \cdot v = q \tag{2.93}$$

$$p_d = c^2 \rho_d \tag{2.94}$$

The linearization of the fluid equations and the assumption of an inviscid fluid model made above will be discussed next. The equation of motion and the continuity equation are simplified due to the assumption of small particle velocity compared to the wave propagation velocity. This assumption may be justified by studying the particle velocity v in a plane wave where $v_1 = p_d/\rho_0 c$. For air $\rho_0 c \approx 414$ kg/m^{2}s, and for water $\rho_0 c \approx 1.5 \cdot 10^6$ kg/m^{2}s. According to Subsection 2.3.3, linear relations between pressure and density are assumed for density variations of up to a few percent. For liquids like water, a two percent variation in density corresponds to a pressure variation of about 20 MPa (by Eq. (2.47)) and this is an enormous pressure encountered in almost all practical situations. However, despite this high pressure the maximal particle velocity would be only 13 m/s, which is far less than c=1500 m/s.

For gases the case is somewhat different because a gas may behave in a highly compressible fashion. A two percent density variation corresponds to a pressure variation of approximately 3 kPa by use of Eq. (2.43) for γ=1.4. The maximum particle velocity in a plane wave will then be 7 m/s, and thus about 20 percent of the wave propagation speed (343 m/s). A dynamic pressure of 3 kPa is about 161 dB expressed in sound pressure level and is beyond the threshold of pain, but less than, for example, the maximum pressure in the vicinity of exhausts of jet engines.

From this discussion we conclude that, for liquids, the density variation defines the limit of the acoustic approximation, whereas for gases the convective term sets the limit. Further, we may observe the meaning of the approximation in Eq. (2.91) when comparing it with Eq. (2.24). The amount of the variation in density around the reference state can be expressed by Eq. (2.24) as

$$\left| \frac{\rho_d}{\rho_0} \right| = \left| \frac{\rho - \rho_0}{\rho_0} \right| = \left| \nabla \cdot u \right| << 1 \qquad (2.95)$$

where the last comparison follows from Eq. (2.10). The assumption made in Eq. (2.91) is thus consistent with the small displacement gradient assumption.

2.5   Undamped fluid equations for structure–acoustic analysis

2.5.1   Nonhomogeneous wave equation in terms of dynamic pressure

In this section we will derive the undamped equations used for structure–acoustic problems.

Differentiating the mass balance equation, Eq. (2.93), with respect to time and making use of Eq. (2.94) result in

$$\frac{1}{c^2}\frac{\partial^2 p_{\mathrm d}}{\partial t^2} + \nabla\cdot(\rho_{\mathrm o}\frac{\partial v}{\partial t}) = \frac{\partial q}{\partial t} \qquad (2.96)$$

Substituting Eq. (2.92) into this expression yields

$$\frac{1}{c^2}\frac{\partial^2 p_{\mathrm d}}{\partial t^2} + \nabla\cdot(\rho_{\mathrm o}b - \nabla p_{\mathrm d}) = \frac{\partial q}{\partial t} \qquad (2.97)$$

which rewritten is the nonhomogeneous wave–equation expressed in the dynamic pressure $p_{\mathrm d}$

$$\frac{\partial^2 p_{\mathrm d}}{\partial t^2} - c^2\,\nabla^2 p_{\mathrm d} = c^2\,\frac{\partial q}{\partial t} - c^2\,\rho_{\mathrm o}\,\nabla\cdot b \qquad (2.98)$$

where c is identified as the speed of the propagating wave.

2.5.2   Mixed formulations in terms of fluid displacement–potential and fluid pressure

Taking the curl of both sides of the equation of motions, Eq. (2.92), yields

$$\tilde{\nabla}\,(\rho_{\mathrm o}\,\frac{\partial v}{\partial t} + \nabla p_{\mathrm d}) = \tilde{\nabla}(\rho_{\mathrm o}\,b) \qquad (2.99)$$

where $\tilde{\nabla}$ is the curl operator.

The curl of a gradient is zero and hence $\tilde{\nabla}(\nabla p_{\mathrm d}) = 0$. Further, if we assume the body force to be derivable from a potential function $\beta(\mathbf{x},t)$, that is

$$b = \nabla\beta \qquad (2.100)$$

then $\tilde{\nabla} b = 0$ and Eq. (2.99) results in

$$\tilde{\nabla}\left(\frac{\partial v}{\partial t}\right) = 0 \tag{2.101}$$

We note that every velocity field which can be decomposed into one irrotational and one equivolumal part such as

$$v(\mathbf{x},t) = \nabla\,\varphi(\mathbf{x},t) + \tilde{\nabla}\,h(\mathbf{x}) \tag{2.102}$$

is a solution of Eq. (2.101) since

$$\tilde{\nabla}\left(\frac{\partial v(\mathbf{x},t)}{\partial t}\right) = \tilde{\nabla}\left(\nabla\,\frac{\partial\varphi(\mathbf{x},t)}{\partial t}\right) = 0 \tag{2.103}$$

If $v(\mathbf{x},t)$ is irrotational at some time $\tilde{\nabla}\,h(\mathbf{x})$ must vanish identically and the velocity field $v(\mathbf{x},t)$ remains irrotational. Since we have assumed that $v(\mathbf{x},t) = \frac{\partial u_f(\mathbf{x},t)}{\partial t}$ it follows from a similar argument that the displacement field once irrotational also remains irrotational.

An irrotational fluid displacement field is automatically enforced by introducing a displacement–potential ψ such that

$$u_f = \nabla\psi \tag{2.104}$$

where u_f is the fluid displacement. In the finite element formulation, use of this representation of the displacement field, will make sure that spurious modes associated with unrestrained fluid rotations will be avoided.

Integrating the mass balance equation (2.93) with respect to time and assuming the initial system to be undeformed and at rest, i.e. $\left.\frac{\partial u_f(\mathbf{x},t)}{\partial t}\right|_{t=0} = u_f(\mathbf{x},t)\big|_{t=0} = 0$, we get

$$\rho_d + \rho_0\nabla\cdot u_f = Q \quad,\quad Q = \int_0^t q\,d\tau \tag{2.105}$$

where we also have used Eq. (2.86), and where we note that Q is the total added fluid mass per volume during time t. Eq. (2.105) is equivalent to the continuity equation in material form according to Eq. (2.24) if we omit the source term Q. Finally by substituting Eq. (2.104) into

Eq. (2.92) and further Eqs. (2.94) and (2.104) into Eq. (2.105), we obtain the following governing equations for an inviscid acoustic fluid

$$\rho_0 \nabla \frac{\partial^2 \psi}{\partial t^2} + \nabla p_{\mathrm{d}} = \rho_0 \nabla \beta \tag{2.106}$$

$$\frac{1}{\rho_0 c^2} p_{\mathrm{d}} + \nabla^2 \psi = \frac{1}{\rho_0} Q \tag{2.107}$$

These linear equations are the basis for the symmetric fluid–structure interaction models used in this study. They have the advantage of giving a symmetric system of equations in fluid analysis (with rigid walls) and in a coupled analysis where the fluid is interacting with a flexible structure. Further, by integration of the continuity equation, Eq.(2.93), we avoid working with velocity terms in the final equations and the associated eigenvalue problem will be of a so–called generalized form.

2.5.3   Nonhomogeneous wave equation in terms of displacement–potential

Eqs. (2.106) and (2.107) represent two useful relations between fluid pressure and fluid displacement–potential. Firstly, Eq. (2.107) implies that

$$p_{\mathrm{d}} = -\rho_0 c^2 \nabla^2 \psi + c^2 \, Q \tag{2.108}$$

where $\rho_0 c^2$ is identified as the bulk modulus described in Section 2.3.3. Secondly, Eq. (2.106) may be written

$$\nabla(\rho_0 \frac{\partial^2 \psi}{\partial t^2} + p_{\mathrm{d}} - \rho_0 \beta) = 0 \tag{2.109}$$

or by use of Eq. (2.108)

$$\nabla(\rho_0 \frac{\partial^2 \psi}{\partial t^2} - \rho_0 c^2 \nabla^2 \psi + c^2 Q - \rho_0 \beta) = 0 \tag{2.110}$$

where the function inside the brackets is independent of position and depends on time only. Therefore, we can add an extra function of time to ψ without changing the fluid displacement field [66], and hence with no loss of generality rewrite Eq. (2.110) as

$$\rho_0 \frac{\partial^2 \psi}{\partial t^2} - \rho_0 c^2 \nabla^2 \psi = -c^2 Q + \rho_0 \beta \tag{2.111}$$

which is the nonhomogeneous wave–equation for the fluid expressed in the fluid–displacement potential. In the absence of source term and body forces we get by means of Eq. (2.108)

$$p_{\mathrm{d}} = -\rho_0 \, \frac{\partial^2 \psi}{\partial t^2} \qquad\qquad\qquad (2.112)$$

which is the spatially integrated form of the equation of motion, Eq. (2.106).

Other expressions for the wave equation using either the fluid density, the fluid velocity field, or the fluid displacement field as the primary variable may be found in reference [66].

2.6   Damped fluid equations for structure–acoustic analysis
2.6.1   Introduction

In Section 2.4.2 it was shown that the fluid viscosity can be neglected when studying wave propagation in slightly viscous fluids like air and water in the low frequency range. The undamped fluid equations based on this assumption were derived in Section 2.5. However, in the analysis of wave propagation through a porous material, the frictional retardation of the fluid flow is to be considered also for slightly viscous fluids. Fluid equations for an acoustic fluid interpenetrating a porous medium are given in [47]. A discretized form of this fluid model was used in an uncoupled (rigid wall) frequency analysis of mufflers in [16], and simulated results were reported to agree perfectly well with experiments. Absorption elements for rigid porous materials have also been developed in [19–21].

In this work we will adopt the theory presented in [16,47] and modify the linearized fluid equations derived in Section 2.5 to include the effect of introducing a porous material in the fluid domain. In the referred work the main interest was models for frequency analysis. In addition, we will also consider the corresponding equations for transient analysis.

2.6.2   Fluid equations for a porous medium

The governing equations, Eqs. (2.92–94) for an acoustic fluid occupying a fluid domain were derived in the previous section within a theory for continuous media. In this section we will assume that the fluid is interpenetrating a perfectly rigid and incompressible porous solid. The pores are randomly interconnected but in such a way that the medium can be looked upon as isotropic. The irregularities of the size and orientation of the pores will average out if the volume under consideration is large enough. Local variation in the fluid velocity as it

passes through the pores will occur. The fluid velocity in this model will therefore be assumed to represent the mean volume velocity, i.e. the mean volume of fluid passing across a unit area normal to the flow, per second. In this way the velocity field will be continuous in the normal direction at the intersurface between the porous medium and the free fluid.

The governing equations for an acoustic fluid were derived in Section 2.4.3 on the assumption that $|v| \ll c$, where v is the particle velocity and c is the speed of sound. If this restriction on the particle velocity is applied also to the mean volume velocity in a porous medium, we may neglect the convective terms also in the porous model. Further, the space occupied by the fluid is given by actual volume multiplied with a volume porosity factor, defined as

$$\Omega_v = [(\text{volume}) - (\text{volume of solid})]/\text{volume}. \tag{2.113}$$

In the present notation, Eqs. (2.92–2.94) for the free medium will be modified with respect to porosity and read

$$\rho_0 \, \nabla \, \frac{\partial^2 \psi}{\partial t^2} + \nabla p_d = \rho_0 \, b \tag{2.114}$$

$$\Omega_v \, \frac{\partial \rho_d}{\partial t} + \rho_0 \, \nabla^2 \, \frac{\partial \psi}{\partial t} = q \tag{2.115}$$

$$p_d = c^2 \rho_d \tag{2.116}$$

where we have introduced the volume porosity Ω_v in the continuity equation Eq.(2.115), [16,47]. For gases at low frequencies it is likely that the heat liberated locally by gas compression will be absorbed by the fibre material and thus the isothermal speed of sound c for the fluid in the pores (rather than the adiabatic speed) should be used in Eq. (2.116), see Section 2.3.3.

In order to consider the frictional retardation of the fluid flow in the pores we will introduce a velocity dependent body force as shown below. In this manner we are able to model a viscous flow through the pores although the fluid is considered inviscid when the porous material is removed. Hence, the constitutive equation for a linear inviscid compressible fluid Eq. (2.49) is still used, and the derivations made in Section 2.4.3 will hold.

We define a specific disturbance force $b_d(x,t)$ referred to the disturbed state by the relation

$$b(\mathbf{x},t) = b_o(\mathbf{X}) + b_d(\mathbf{x},t) \tag{2.117}$$

where $b_o(\mathbf{X})$ is the specific body force at time $t=0$ and

$$b_d(\mathbf{x},t)\big|_{t=0} = 0 \tag{2.118}$$

We assume the initial state homogeneous and hence $b_o(\mathbf{X}) = 0$.

The specific disturbance force $b_d(\mathbf{x},t)$ is assumed to result from the interaction between the fluid and the solid material in the porous medium. This contribution is expressed by the relation

$$b_d = -\, r\, \frac{1}{\rho_o}\, \nabla \varphi \tag{2.119}$$

where r is a viscous flow resistance or "drag coefficient" and $\varphi(\mathbf{x},t)$ is the fluid velocity potential, the fluid flow being assumed irrotational.

The flow resistance r for air penetrating a fibre material like mineral wool is found to be frequency dependent and may be calculated from the following expression given in [16]

$$r = r_s \, \max \, \{0.6 + 0.55 \, \sqrt{\omega/r_s}, \, 1\} \tag{2.120}$$

where ω is the angular frequency, r_s the static flow resistance, defined as the pressure drop required to force a unit volume flow through the material [47]. For frequencies less than 1 kHz, $r \approx r_s$, see also [7].

If Eq. (2.119) is used in Eq. (2.114) we get

$$\rho_o \nabla \frac{\partial^2 \psi}{\partial t^2} + \, r \nabla \frac{\partial \psi}{\partial t} + \nabla p_d = 0 \tag{2.121}$$

The inertia term $\rho_o \nabla \frac{\partial^2 \psi}{\partial t^2}$ in Eq. (2.121) will be modified to include the change of inertia of the fluid as it moves through the pores. In the low–frequency range the velocity profile will not be uniform within the pores. For a circular section in straight pores the profile will be parabolic at low frequencies, and the fluid density ρ_o should be increased to an effective density $\rho_e = 4/3 \, \rho_o$ [21].

At high frequencies the velocity profile is nearly uniform and $\rho_e = \rho_0$. The effective density in the direction of the pores may be defined by

$$\rho_e = (\min \{1 + 0.46 \sqrt{r_s/\omega}, \, 4/3\}) \cdot \rho_0 \qquad (2.122)$$

where again r_s is the static flow resistance and ω is the angular frequency. For uniformly distributed pores the ratio ρ_e/ρ_0 is multiplied by a factor of 3 [80]. The effective density ρ_e is frequency dependent. For a material with $r_s = 8000$ Ns/m⁴, the ratio ρ_e/ρ_0 is equal to $4/3$ for $f \leq 2.3$ kHz and thus $\rho_e = 4\rho_0$ is to be used in the calculations.

The governing differential equations were derived on the basis that the fibres do not move, i.e. they were assumed perfectly rigid. In practice, there may be some movement in the fibres and this motivates a modification of Eq. (2.121). If both elastic effects and intertia effects in the porous material are considered the model will be very complex due to the propagating waves in the fibres. However, if only inertia effects are considered, these extra inertia forces may be introduced in the fluid equations by additionally increasing the fluid density to what was motivated by the nonhomogeneous velocity profile according to Eq. (2.122). The effective density may in this case be calculated by means of a structure factor k_s [80] according to

$$\rho_e = k_s \, \rho_0 \qquad (2.123)$$

and this factor may take values between 1.5 and 5 [47].

The effective density ρ_e is introduced in Eq. (2.121) and by means of Eq. (2.116) we may write

$$\rho_e \nabla \frac{\partial^2 \psi}{\partial t^2} + r \, \nabla \frac{\partial \psi}{\partial t} + \nabla p_d = 0 \qquad (2.124)$$

$$\Omega_v \frac{1}{\rho_0 c^2} \, p_d + \nabla^2 \psi = \frac{1}{\rho_0} \, Q \qquad (2.125)$$

where Eq. (2.115) has been integrated once with respect to time assuming the system to be initially at rest.

These equations are the basis in this study for the coupled structure–acoustic analysis including fluid domains with porous materials.

2.6.3 Damped nonhomogeneous wave equations

We take the gradient of Eq. (2.124) and yield

$$\rho_e \nabla^2 \frac{\partial^2 \psi}{\partial t^2} + r \nabla^2 \frac{\partial \varphi}{\partial t} + \nabla^2 p_d = 0 \tag{2.126}$$

Differentiating Eq. (2.125) with respect to time and substituting in Eq. (2.126) gives

$$\rho_e \left[\Omega_v \frac{1}{\rho_o} \frac{\partial q}{\partial t} - \Omega_v \frac{1}{\rho_o c^2} \frac{\partial^2 p_d}{\partial t^2} \right] + r \left[\Omega_v \frac{1}{\rho_o} q - \Omega_v \frac{1}{\rho_o c^2} \frac{\partial p_d}{\partial t} \right] + \nabla^2 p_d = 0$$

$$\tag{2.127}$$

and after rearrangement

$$\frac{\partial^2 p_d}{\partial t^2} + \frac{r}{\rho_e} \frac{\partial p_d}{\partial t} - \frac{1}{\Omega_v} \frac{\rho_o}{\rho_e} c^2 \nabla^2 p_d = \frac{r}{\rho_e} c^2 q + c^2 \frac{\partial q}{\partial t} \tag{2.128}$$

where the undamped speed of sound in the porous medium c_p is identified as

$$c_p^2 = \frac{1}{\Omega_v} \frac{\rho_o}{\rho_e} c^2 \tag{2.129}$$

For gases, c is likely to be the isothermal speed of sound in free air. This speed is thus reduced by increased porosity Ω_v and by an increased structure factor.

Alternatively we may derive the damped nonhomogeneous wave equation expressed in terms of the fluid displacement—potential. Eq. (2.125) is equal to

$$p_d = -\frac{1}{\Omega_v} \rho_o c^2 \nabla^2 \psi + \frac{1}{\Omega_v} c^2 Q \tag{2.130}$$

and substitution in Eq. (2.124) results in

$$\nabla \left(\rho_e \frac{\partial^2 \psi}{\partial t^2} + r \frac{\partial \psi}{\partial t} - \frac{1}{\Omega_v} \rho_o c^2 \nabla^2 \psi + \frac{1}{\Omega_v} c^2 Q \right) = 0 \tag{2.131}$$

With no loss of generality we can rewrite this equation to

$$\frac{\partial^2 \psi}{\partial t^2} + \frac{r}{\rho_e} \frac{\partial \psi}{\partial t} - \frac{1}{\Omega_v} \frac{\rho_o}{\rho_e} c^2 \nabla^2 \psi = -\frac{1}{\Omega_v} \frac{c^2}{\rho_e} Q \tag{2.132}$$

where we observe the similarity to Eq. (2.128). However, the loading term is somewhat simpler in this case.

2.7 Boundary conditions
2.7.1 Essential and natural boundary conditions

In the *structural* domain, prescribed displacements are essential boundary conditions whereas quantities proportional to spatial derivatives of the displacements are natural boundary conditions.

In the *fluid* domain a prescribed pressure is an essential boundary condition whereas prescribed fluid displacements are natural boundary conditions.

At the *rigid* wall the fluid displacement (and its time derivatives) is zero in the normal direction to the surface. Hence, the natural boundary condition is

$$u_f \cdot n = \nabla \psi \cdot n = 0 \tag{2.133}$$

where u_f is the fluid displacement field and n the outward normal to the fluid domain, see Fig. 2.1.

From Eqs. (2.106) and (2.133) we obtain, in the absence of body forces,

$$\nabla p_d \cdot n = 0 \tag{2.134}$$

which expresses the natural boundary condition for the fluid in the pressure p_d. The pressure and displacement—potential themselves are free at the rigid wall and hence no essential boundary conditions should be specified at the rigid wall.

2.7.2 Fluid–structure interface, S_{fs}

At the *flexible* wall the following kinematic boundary condition should be satisfied

$$\boldsymbol{u}_f \cdot \mathbf{n} = \nabla \psi \cdot \mathbf{n} = \boldsymbol{u}_s \cdot \mathbf{n} \qquad \text{on } S_{fs} \tag{2.135}$$

where $\boldsymbol{u}_s$ is the structural displacement field and $\mathbf{n}$ the outward unit normal vector to the fluid domain, see Fig. 2.1.

That is, the normal motion of the fluid and the normal motion of the structure will coincide.
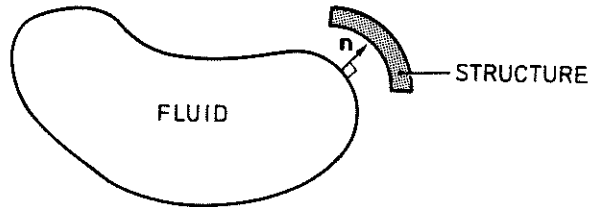
Fig. 2.1   The outward unit normal vector $\mathbf{n}$ to the fluid domain.

2.7.3 Surface with prescribed pressure, S_P

On a *fixed* surface the displacements perpendicular to the surface are assumed to be zero (rigid wall case) and we prescribe the dynamic fluid pressure on the surface by

$$p_d = p_P \qquad \text{on } S_P \tag{2.136}$$

or alternatively, if the fluid is modelled by a fluid displacement–potential, by

$$\frac{\partial^2 \psi}{\partial t^2} = -\frac{p_d}{\rho_0} \qquad \text{on } S_P \tag{2.137}$$

according to Eq. (2.112). On a *free* surface, gravitational waves may be modelled by [66, 79]

$$p_d = \rho_0 g (\boldsymbol{u}_f \cdot \mathbf{n}) + p_P \qquad \text{on } S_P \tag{2.138}$$

where g is the gravity acceleration and $(\boldsymbol{u}_f \cdot \mathbf{n})$ is the elevation of the current surface relative to the mean surface. In this way we are able to model both gravitational waves and a superposed external pressure, see [66] for details.

3   FINITE ELEMENT FORMULATIONS OF THE COUPLED VIBRATION PROBLEM

3.1   Introduction

In this chapter we derive the finite element equations through weak formulations of the governing equations followed by the Galerkin choice of weighting functions, see [37].

The structural part is discretized by a conventional displacement—based finite element method. For the discretization of the fluid, one is faced with various choices of primary variable. The primary fluid variable may be a vector field of fluid—particle displacements or velocities, or a scalar field such as the pressure, density, velocity—potential or displacement—potential. Using, for example, a pressure formulation, the coupled equations for structure—acoustic interaction analysis have unsymmetric matrices caused by the appearance of a coupling term between fluid pressure and structural displacement [66].

A number of formulations of the coupled system which produce symmetric coefficient matrices have been suggested. These formulations are based upon a displacement, velocity-potential or simultaneous pressure and displacement—potential representation of the acoustic medium. The use of a fluid displacement field leads directly to a symmetric vibration problem of the conventional mass—stiffness form, see for example [66], and no coupling term needs to be evaluated between the fluid and structural domain. However, the fluid degrees—of—freedom is substantially increased compared to the scalar field formulations (3 freedoms/node instead of 1 freedom/node) and a large number of spurious modes are introduced corresponding to rotational fluid motions at zero frequency. In order to prevent a rotational fluid displacement field, a rotational stiffness term may be included in the expression for the fluid stiffness matrix [66]. Another approach to avoid spurious displacement modes is to use a reduced integration technique, see [15].

The use of scalar fields such as pressure, displacement—potential or velocity—potential automatically enforces irrotationality of fluid motions, hence eliminating the spurious modes and minimizing the number of degrees—of—freedom to one per acoustic node. The pressure formulation has unsymmetric coefficient matrices due to the coupling as mentioned above, and so has the displacement—potential formulation [66].

A fluid velocity—potential proposed in [25, 59] transfers the unsymmetric coupling terms in the systems mass and stiffness matrices to a system "damping" matrix. All three system matrices are symmetric.

A mixed formulation of the fluid domain with the simultaneous use of two scalar fields – pressure and displacement—potential – was introduced for free vibration analysis in [46] and for transient analysis in [66]. The resulting three—field formulation has a state vector consisting of three subvectors: u_s—structural displacement, Ψ—fluid displacement—potential and p—fluid pressure. This system leads to symmetric eigenvalue problems of generalized form. An alternative three—field form with the same subvectors, u_s, Ψ and p, but with superior properties from a computational point of view was also given in [66].

Symmetrization of established unsymmetric systems of equations by a matrix—scaling technique has been studied in [29] and by eigenvector augmentation in [30].

Lately, the alternative three—field form derived in [66] by a weak formulation was established in [31] by a variational formulation, and used as a base for deriving ten formally equivalent formulations of the coupled problem. This technique is also used in this chapter in order to compare different formulations. The expressions given here have been modified to include a fluid source term. Further, the symmetric formulation based on the fluid velocity—potential derived in [25, 59] is also easily found in the present notation. Thus eleven formulations are given for the coupled structure acoustic system.

A comparison of different coupled systems of equations is made with respect to computational efficiency and stability. The main interest is the interaction between the structure and fluid domain, respectively. Hence, this comparison is made for the undamped structure—acoustic system.

Finally, suitable symmetric forms found in this comparison will then be generalized to include non—proportional damping effects recognized for example when introducing a porous medium in the fluid domain.

3.2   Semidiscrete structural equations of motion

In order to formulate a general structure–acoustic interaction capability in our model we will consider two types of structural "members". According to Fig. 1.1 the interaction between the fluid domain and the structure domain is considered for a flexible wall and for a locally reacting surface, respectively. The principal difference between these two structural members is also illustrated in Fig. 3.1. Contrary to the continuous structure no wave propagation will occur in the transverse direction to the motion of the locally reacting surface. These special, locally reacting surface elements may be used to model vibrating panels, small in size compared to the acoustic wave length, or acoustic absorbers, described by their specific acoustic properties [42].

$\cdot \; p_d(\mathbf{x}, t)$

a)

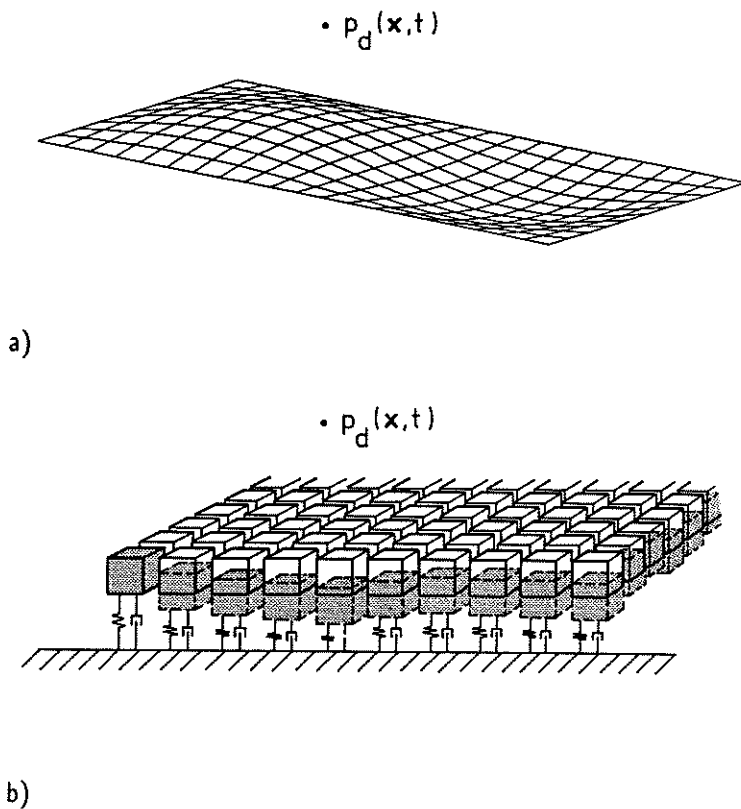$\cdot \; p_d(\mathbf{x}, t)$

b)

Fig. 3.1   Structural members subjected to a dynamic fluid pressure field $p_d(x, t)$.
a) Continuous structure illustrated by a vibrating plate.
b) Locally reacting surface modelled as a set of individual single degree-of-freedom systems.

3.2.1 Continuous structure

The motion of the continuous structure is governed by

$$L(u_s) = f_s(x,t) + f_f(x,t) \tag{3.1}$$

where L is a partial differential operator with respect to time and space, u_s is the structural displacement field, which depends on the coordinate x and time t, and f_s is an external time-dependent structural load. At the fluid–structure interface S_{fs}, the fluid loading f_f acting on the structure is defined by

$$f_f(x,t) = p_d(x,t) \; n \tag{3.2}$$

where p_d is the ambient dynamic fluid pressure and n is the outward unit normal vector to the fluid domain, see Fig. 2.1.

The discretized formulation of the structure is based on the expansion of the structural displacement as

$$u_s = \sum_j N_s^j(x) \; u_s^j(t) \tag{3.3}$$

where $N_s^j(x)$ is the displacement shape function of the structure and $u_s^j(t)$ is the discrete value of the structural displacement at a nodal point j.

The resulting semidiscrete equations of motion take the form

$$M_s \ddot{u}_s + C_s \dot{u}_s + K_s u_s = f_s^e + f_f \tag{3.4}$$

where M_s, C_s and K_s are the symmetric mass, damping and stiffness matrices at the reference state. The (tangent) stiffness matrix K_s may include structural prestresses through the geometric stiffness. f_s^e is the structure load vector due to externally applied forces on the structure and f_f is the structure load vector due to the coupling effects according to Eq. (3.2). Using the shape function set $\{N_s\}$ in the structural domain gives

$$(f_f)_i = \int_{S_{fs}} N_s^i \cdot n \; p_d \; dS \tag{3.5}$$

where S_{fs} is the wet surface of the structure and p_d is the dynamic fluid pressure.

3.5

3.2.2 Locally reacting surface

The equation of motion in an arbitrary point x can be expressed as

$$\bar{m}(\mathbf{x})\ddot{u}_{rs}(\mathbf{x},t) + \bar{c}(\mathbf{x})\dot{u}_{rs}(\mathbf{x},t) + \bar{k}(\mathbf{x})u_{rs}(\mathbf{x},t) = p_d(\mathbf{x},t)\mathbf{n} \qquad (3.6)$$

where $\bar{m}(\mathbf{x})$, $\bar{c}(\mathbf{x})$ and $\bar{k}(\mathbf{x})$ are the mass damping and stiffness distributions, respectively. $p_d(\mathbf{x},t)$ is the ambient dynamic fluid pressure and $\mathbf{n}$ is the outward normal vector to the fluid domain.

By definition, the displacement field u_{rs} in Eq. (3.6) along the locally reacting surface need not be continuous. However, we will assume that the discontinuous displacement of the surface can be described by

$$u_{rs}(\mathbf{x},t) = \sum_j N_{rs}^j \ u_{rs}^j(t) \qquad (3.7)$$

where $N_{rs}^j(\mathbf{x})$ is the displacement shape function of the surface and $u_{rs}^j(t)$ is the discrete value of the displacement at a nodal point j, see Fig. 3.2.
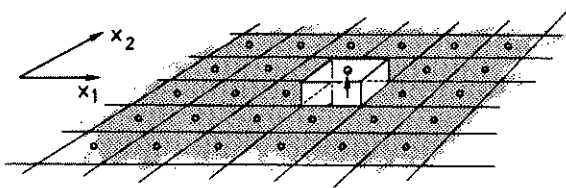
Fig. 3.2   Displacement shape function $N_{rs}^j(\mathbf{x})$ for a locally reacting surface

The corresponding weak form of Eq. (3.6) will be

$$\int_{S_{rs}} w\ \bar{m}(\mathbf{x})\ \ddot{u}_{rs}\ dS + \int_{S_{rs}} w\ \bar{c}(\mathbf{x})\dot{u}_{rs}\ dS + \int_{S_{rs}} w\ \bar{k}(\mathbf{x})\ u_{rs}\ dS = \int_{S_{rs}} w\ p_d\ \mathbf{n}\ dS \qquad (3.8)$$

Following a Galerkin procedure and using $w(\mathbf{x}) = N_{rs}(\mathbf{x})$ we get the matrix equations for a locally reacting surface

$$\mathbf{M}_{rs}\, \ddot{\mathbf{u}}_{rs} + \mathbf{C}_{rs}\, \dot{\mathbf{u}}_{rs} + \mathbf{K}_{rs}\, \mathbf{u}_{rs} = \mathbf{f}_f \qquad (3.9)$$

where

$$(\mathbf{M}_{rs})_{ij} = \int\limits_{S_{rs}} N_{rs}^{i}\, \bar{m}(\mathbf{x})\, N_{rs}^{j}\, dS \qquad (3.10)$$

$$(\mathbf{C}_{rs})_{ij} = \int\limits_{S_{rs}} N_{rs}^{i}\, \bar{c}(\mathbf{x})\, N_{rs}^{j}\, dS \qquad (3.11)$$

$$(\mathbf{K}_{rs})_{ij} = \int\limits_{S_{rs}} N_{rs}^{i}\, \bar{k}(\mathbf{x})\, N_{rs}^{j}\, dS \qquad (3.12)$$

$$(\mathbf{f}_f)_i = \int\limits_{S_{rs}} N_{rs}^{i}\, \mathbf{n} \cdot p_d\, dS \qquad (3.13)$$

For the type of shape functions shown in Fig. 3.2., Eq. (3.9) will be of diagonal form. For a complete description of the locally reacting surface we need an infinite number of nodal points.

3.3 Transient equations for undamped coupled systems

3.3.1 Introduction

In this section we will derive the transient equations for the coupled structure—acoustic system. The main interest here is the coupling between the structure domain and the fluid domain, respectively. No damping effects will therefore be considered at this point.

For convenience we will make no notational distinction between the flexible wall and the locally reacting surface with respect to the structure—acoustic coupling. The notation u_s for the structural displacement vector may thus also represent the displacement of the locally reacting surface u_{rs} in the equations below. Likewise, the notation $N_s(\mathbf{x})$ for the structural displacement shape function may also represent $N_{rs}(\mathbf{x})$, i.e. the displacement shape function for the locally reacting surface. Since no direct coupling between the flexible wall and the locally reacting surface takes place, the structural matrices and structural displacement vectors below may always be partitioned into uncoupled structural submatrices and subvectors if required.

3.3.2 Symmetric three—field forms

The linear undamped fluid equations (2.106–107) derived in Chapter 2 are discretized below. The equations are based on the dynamic pressure p_d and the fluid displacement—potential ψ. For brevity we will use $^{\cdot}$ for time derivatives $\partial/\partial t$. Thus the governing differential equations are

$$\rho_0 \, \nabla\ddot{\psi} + \nabla p_d = \rho_0 b \tag{3.14}$$

$$\frac{1}{\rho_0 c^2} \, p_d + \nabla^2\psi = \frac{1}{\rho_0} \, Q \tag{3.15}$$

where b is assumed to be derivable from a potential function $b = \nabla\beta$, according to Eq. (2.100).

The corresponding weak forms of these equations above are established by using $\nabla w(\mathbf{x})$ as a weighting function for Eq. (3.14) and $w(\mathbf{x})$ as a weighting function for Eq. (3.15), resulting in the following integral equations

$$\rho_0 \int_V \nabla w \cdot \nabla\ddot{\psi} \; dV + \int_V \nabla w \cdot \nabla p_d \; dV = \rho_0 \int_V \nabla w \cdot b \; dV \tag{3.16}$$

and

$$\frac{1}{\rho_0 c^2} \int_V w p_d \ dV - \int_V \nabla w \cdot \nabla \psi \ dV + \int_S w \nabla \psi \cdot \mathbf{n} \ dS = \frac{1}{\rho_0} \int_V w Q \ dV \qquad (3.17)$$

where Gauss's theorem has been used on the left—hand side of (3.17) and S is the boundary of the fluid domain.

Expanding p_d and ψ in different shape function sets $\{N_P\}$ and $\{N_\psi\}$ such that

$$p_d(\mathbf{x}, t) = \sum_j N_p^j(\mathbf{x}) \ p_j(t) \qquad (3.18)$$

and

$$\psi(\mathbf{x}, t) = \sum_j N_\psi^j(\mathbf{x}) \ \Psi_j(t) \qquad (3.19)$$

and running w over $\{N_\psi\}$ in Eq. (3.16) and over $\{N_P\}$ in Eq. (3.17) results in

$$\rho_0 \mathbf{K_f} \ \ddot{\Psi} + \mathbf{B} \mathbf{p} = \mathbf{f_b} \qquad (3.20)$$

$$\frac{1}{\rho_0 c^2} \mathbf{M_f} \ \mathbf{p} - \mathbf{B}^T \Psi + \mathbf{M_c^T} \ \mathbf{u_s} = \mathbf{f_q} \qquad (3.21)$$

where

$$(M_f)_{ij} = \int_V N_p^i \ N_p^j \ dV \qquad (3.22)$$

$$(K_f)_{ij} = \int_V \nabla N_\psi^i \cdot \nabla N_\psi^j \ dV \qquad (3.23)$$

$$(M_c)_{ij} = \int_{S_{fs}} N_s^i \cdot \mathbf{n} \ N_p^j \ dS \qquad (3.24)$$

$$(B)_{ij} = \int_V \nabla N_\psi^i \cdot \nabla N_p^j \ dV \qquad (3.25)$$

$$(f_q)_i = \frac{1}{\rho_0} \int_V N_p^i \ Q \ dV \qquad (3.26)$$

$$(f_b)_i = \rho_0 \int_V \nabla N_\psi^i \cdot \mathbf{b} \ dV \qquad (3.27)$$

($i =$ row index, $j =$ column index).

The coupling between structure and fluid is taken into account in the fluid equations by the boundary integral in Eq. (3.17), viz.

$$\int\limits_{S_{fs}} w \nabla \psi \cdot \mathbf{n} \, dS = \int\limits_{S_{fs}} N_P \nabla \psi \cdot \mathbf{n} \, dS = \int\limits_{S_{fs}} N_P \, u_s \cdot \mathbf{n} \, dS = \int\limits_{S_{fs}} N_P \, N_s \cdot \mathbf{n} \, dS \, \mathbf{u_s} \quad (3.28)$$

where we use the continuity condition Eq. (2.135) to replace $\nabla \psi \cdot \mathbf{n}$ by $u_s \cdot \mathbf{n}$, resulting in the coupling matrix $\mathbf{M_c}$, see Eq. (3.24). This matrix is thus evaluated along the wet surface S_{fs} and is simply a cross—integration of structural and fluid shape functions. $\mathbf{M_c}$ is thus a very sparse pressure—to—displacement transformation matrix. The non—zero entries of $\mathbf{M_c}$ depend on the geometry of the fluid—structure interface and on the primary—variable shape functions there.

Finally, using Eq. (3.24) in Eq. (3.5), resulting in $\mathbf{f_f} = \mathbf{M_c p}$, and moving this term from the right to the left hand side in the structural equations we achieve

$$\mathbf{M_s \ddot{u}_s} + \mathbf{K_s u_s} - \mathbf{M_c p} = \mathbf{f_s^e} \qquad (3.29)$$

Assembling the three matrix equations (3.29), (3.20) and (3.21) we get the coupled and symmetric system of equations as

$$\begin{bmatrix} \mathbf{M_s} & 0 & 0 \\ 0 & \rho_0 \mathbf{K_f} & 0 \\ 0 & 0 & 0 \end{bmatrix} \begin{bmatrix} \ddot{\mathbf{u}}_s \\ \ddot{\boldsymbol{\Psi}} \\ \ddot{\mathbf{p}} \end{bmatrix} + \begin{bmatrix} \mathbf{K_s} & 0 & -\mathbf{M_c} \\ 0 & 0 & \mathbf{B} \\ -\mathbf{M_c^T} & \mathbf{B^T} & -\dfrac{1}{\rho_0 c^2}\mathbf{M_f} \end{bmatrix} \begin{bmatrix} \mathbf{u}_s \\ \boldsymbol{\Psi} \\ \mathbf{p} \end{bmatrix} = \begin{bmatrix} \mathbf{f_s^e} \\ \mathbf{f_b} \\ -\mathbf{f_q} \end{bmatrix}$$

$$\begin{array}{r} (3.30a) \\ (3.30b) \\ (3.30c) \end{array}$$

This system of equations was derived for the free vibration problem in [29] and for the transient problem (as above) in [66].

Considering the fluid equations in this system, they are formulated by a so—called mixed method. Since there exists a linear dependence between $\boldsymbol{\Psi}$ and $\mathbf{p}$, either one of these variables can be eliminated as will be shown later in Section 3.3.2.

It is practical from a programming point of view (but not necessary) to use the same shape functions for p_d and ψ, i.e.

$$N_\psi \equiv N_P \qquad (3.31)$$

and thus both vectors $\boldsymbol{\Psi}$ and $\mathbf{p}$ are of equal dimension and evaluated at the same nodes. Then $\mathbf{K_f} = \mathbf{B}$ and the system of equations simplifies to

$$
\begin{bmatrix} M_s & 0 & 0 \\ 0 & \rho_0 B & 0 \\ 0 & 0 & 0 \end{bmatrix} \begin{bmatrix} \ddot{u}_s \\ \ddot{\Psi} \\ \ddot{p} \end{bmatrix} + \begin{bmatrix} K_s & 0 & -M_c \\ 0 & 0 & B \\ -M_c^T & B^T & -\dfrac{1}{\rho_0 c^2} M_f \end{bmatrix} \begin{bmatrix} u_s \\ \Psi \\ p \end{bmatrix} = \begin{bmatrix} f_s^e \\ f_b \\ -f_q \end{bmatrix}
$$

(3.32a)
(3.32b)
(3.32c)

This form (and its condensed version shown in Section 3.3.2) is used in the numerical examples in Chapter 5. This system of equations (3.32) may also be used as a base for deriving other symmetric three–field forms as reported in reference [31], although no fluid loadings were taken into account in that study. The fluid source load f_q included here in Eq. (3.21c) will therefore be retained in the derivations below, resulting in more general formulations compared to those found in [12].

Eq. (3.32b) is the discretized equation of motion for the fluid domain, cf. Eq. (3.14). We rewrite Eq. (3.32b) and in the absence of body forces, $f_b = 0$, we obtain

$$
B(\rho_0 \ddot{\Psi} + p) = 0
$$

(3.33)

Two conditions may be considered regarding the solution to the eigenvalue problem in Eq. (3.33). Firstly, by Eq. (3.25) we note that the matrix B is generally singular and hence B^{-1} does not exist. However, as will be discussed later in Section 3.4.1 a solution to Eq. (3.33) exists and is a vector αe where e is a vector of all ones. The coefficient α can take on any value expressing the indeterminacy of this zero–mode. In particular for $\alpha = 0$ we get

$$
p = -\rho_0 \ddot{\Psi}
$$

(3.34)

Secondly, if the fluid pressure is prescribed in any point in the fluid domain the singularity of B in Eq. (3.33) is removed. In this case B^{-1} exists and Eq. (3.34) follows directly. Eq. (3.34) is the discrete analog to the continuous relation Eq. (2.112) for the dynamic pressure.

In order to achieve an alternative form of Eq. (3.32), we differentiate Eq. (3.32c) twice in time and multiply by $-\rho_0$, use Eq. (3.34) in (3.32) and premultiply Eq. (3.34) by $\dfrac{1}{\rho_0 c^2} M_f$ to obtain

$$
\begin{bmatrix} M_s & \rho_0 M_c & 0 \\ \rho_0 M_c^T & -\rho_0 B^T & \dfrac{1}{c^2} M_f \\ 0 & \dfrac{1}{c^2} M_f & 0 \end{bmatrix} \begin{bmatrix} \ddot{u}_s \\ \ddot{\Psi} \\ \ddot{p} \end{bmatrix} + \begin{bmatrix} K_s & 0 & 0 \\ 0 & 0 & 0 \\ 0 & 0 & \dfrac{1}{\rho_0 c^2} M_f \end{bmatrix} \begin{bmatrix} u_s \\ \Psi \\ p \end{bmatrix} = \begin{bmatrix} f_s^e \\ \rho_0 f_q \\ 0 \end{bmatrix}
$$

(3.35a)
(3.35b)
(3.35c)

This form was derived from a variational principal in [46] and by a weak formulation of the governing equations in [66]. The latter derivation was the most general, whereas the final expression included both fluid source loads f_q and fluid body forces f_b.

Two more symmetric forms can be derived. A third symmetric system is obtained by integrating Eq.(3.32a) twice in time, assuming the initial system to be at rest, multiplying Eq. (3.32c) by ρ_0 and eliminating the pressure by using Eq. (3.34) and then adding the trivial equation $K_s u_s - K_s u_s = 0$ as a third matrix equation

$$
\begin{bmatrix} 0 & 0 & 0 \\ 0 & \frac{\rho_0}{c^2} M_f & 0 \\ 0 & 0 & K_s \end{bmatrix}
\begin{bmatrix} \ddot{u}_s \\ \ddot{\Psi} \\ u_s \end{bmatrix}
+
\begin{bmatrix} -M_s & -\rho_0 M_c & -K_s \\ -\rho_0 M_c^T & \rho_0 B^T & 0 \\ -K_s & 0 & 0 \end{bmatrix}
\begin{bmatrix} u_s \\ \Psi \\ \overset{**}{u}_s \end{bmatrix}
=
\begin{bmatrix} -\overset{**}{f^e_s} \\ -\rho_0 f_q \\ 0 \end{bmatrix}
\qquad
\begin{matrix} (3.36a) \\ (3.36b) \\ (3.36c) \end{matrix}
$$

where superposed stars denote integration with respect to time.

Finally, a fourth symmetric three—field form is obtained by multiplying Eq. (3.32c) by ρ_0 and eliminating the pressure from this equation and from Eq. (3.32a) by use of Eq. (3.34), and then adding the trivial equation $M_s u_s - M_s u_s = 0$ as a third matrix equation, thus

$$
\begin{bmatrix} 0 & 0 & -M_s \\ 0 & \frac{\rho_0}{c^2} M_f & -\rho_0 M_c^T \\ -M_s & -\rho_0 M_c & -K_s \end{bmatrix}
\begin{bmatrix} \ddot{u}_s \\ \ddot{\Psi} \\ u_s \end{bmatrix}
+
\begin{bmatrix} M_s & 0 & 0 \\ 0 & \rho_0 B^T & 0 \\ 0 & 0 & 0 \end{bmatrix}
\begin{bmatrix} u_s \\ \Psi \\ \overset{**}{u}_s \end{bmatrix}
=
\begin{bmatrix} 0 \\ -\rho_0 f_q \\ -f^e_s \end{bmatrix}
\qquad
\begin{matrix} (3.37a) \\ (3.37b) \\ (3.37c) \end{matrix}
$$

In summary, including Eq. (3.19) that enables use of different shape functions for pressure and fluid displacement—potential, five symmetric three—field forms have been derived. The last four systems obtained above, Eqs. (3.32), (3.35), (3.36) and (3.37), are found to be formally equivalent for the choice of identical fluid shape functions $N_\psi = N_p$.

3.3.2   Symmetric two—field forms

Studying the symmetric three—field forms above, we observe that all of them have a zero row matrix in the system mass matrix or system stiffness matrix, and thus one field variable may be eliminated in each one of these system of equations.

Assuming that all matrix inverses below exist, such a condensation process yields the following symmetric two—field forms, formally equivalent to (3.32), (3.35), (3.36) and (3.37) above.

The pressure degrees—of—freedom can be eliminated from Eq. (3.32) by solving for p in Eq. (3.32c), i.e.

$$\mathbf{p} = -\rho_o c^2 \ \mathbf{M}_f^{-1} [\mathbf{M_c}^T \mathbf{u}_s - \mathbf{B}^T \ \mathbf{\Psi} - \mathbf{f}_q]$$

(3.38)

Substituting the last equation in Eq. (3.32) results in

$$\begin{bmatrix} \mathbf{M}_s & 0 \\ 0 & \rho_o \mathbf{B} \end{bmatrix} \begin{bmatrix} \ddot{\mathbf{u}}_s \\ \ddot{\mathbf{\Psi}} \end{bmatrix} + \begin{bmatrix} \mathbf{K}_s + \rho_o c^2 \mathbf{M_c} \mathbf{M}_f^{-1} \mathbf{M}_c^T & -\rho_o c^2 \mathbf{M_c} \mathbf{M}_f^{-1} \mathbf{B}^T \\ -\rho_o c^2 \mathbf{B} \ \mathbf{M}_f^{-1} \ \mathbf{M}_c^T & \rho_o c^2 \mathbf{B} \ \mathbf{M}_f^{-1} \mathbf{B}^T \end{bmatrix} \begin{bmatrix} \mathbf{u}_s \\ \mathbf{\Psi} \end{bmatrix} =$$

$$= \begin{bmatrix} \mathbf{f}_s^e + \rho_o c^2 \mathbf{M_c} \mathbf{M}_f^{-1} \mathbf{f}_q \\ \mathbf{f}_b - \rho_o c^2 \mathbf{B} \ \mathbf{M}_f^{-1} \mathbf{f}_q \end{bmatrix}$$

(3.39)

We solve for $\ddot{\mathbf{\Psi}}$ in Eq. (3.35) and obtain

$$\ddot{\mathbf{\Psi}} = \frac{1}{\rho_o} \ \mathbf{B}^{-T} \ [\rho_o \ \mathbf{M}_c^T \ \ddot{\mathbf{u}}_s + \frac{1}{c^2} \ \mathbf{M}_f \ \ddot{\mathbf{p}} - \rho_o \ \ddot{\mathbf{f}}_q]$$

(3.40)

Eliminating $\mathbf{\Psi}$ from Eq. (3.35) gives

$$\begin{bmatrix} \mathbf{M}_s + \rho_o \mathbf{M_c} \mathbf{B}^{-1} \mathbf{M}_c^T & \frac{1}{c^2} \mathbf{M_c} \mathbf{B}^{-1} \mathbf{M}_f \\ \frac{1}{c^2} \mathbf{M}_f \mathbf{B}^{-1} \mathbf{M}_c^T & \frac{1}{\rho_o c^4} \mathbf{M}_f \mathbf{B}^{-1} \mathbf{M}_f \end{bmatrix} \begin{bmatrix} \ddot{\mathbf{u}}_s \\ \ddot{\mathbf{p}} \end{bmatrix} + \begin{bmatrix} \mathbf{K}_s & 0 \\ 0 & \frac{1}{\rho_o c^2} \mathbf{M}_f \end{bmatrix} \begin{bmatrix} \mathbf{u}_s \\ \mathbf{p} \end{bmatrix} =$$

$$= \begin{bmatrix} \mathbf{f}_s^e + \rho_o \mathbf{M_c} \mathbf{B}^{-T} \ddot{\mathbf{f}}_q \\ \frac{1}{c^2} \mathbf{M}_f \mathbf{B}^{-T} \ddot{\mathbf{f}}_q \end{bmatrix}$$

(3.41)

To eliminate the first row in Eq. (3.36) we solve for $\mathbf{u}_s$ in Eq. (3.36a), i.e.

$$\mathbf{u}_s = \mathbf{M}_s^{-1} \ [-\rho_o \ \mathbf{M}_c \ \mathbf{\Psi} - \mathbf{K}_s \ \overset{**}{\mathbf{u}}_s + \overset{**}{\mathbf{f}_s^e}]$$

(3.42)

resulting in

$$\begin{bmatrix} \frac{\rho_0}{c^2}\mathbf{M}_f & 0 \\ 0 & \mathbf{K}_s \end{bmatrix} \begin{bmatrix} \ddot{\Psi} \\ \mathbf{u}_s \end{bmatrix} + \begin{bmatrix} \rho_0\mathbf{B}^T + \rho_0^2\mathbf{M}_c^T\mathbf{M}_s^{-1}\mathbf{M}_c & \rho_0\mathbf{M}_c^T\mathbf{M}_s^{-1}\mathbf{K}_s \\ \rho_0\mathbf{K}_s\mathbf{M}_s^{-1}\mathbf{M}_c & \mathbf{K}_s\mathbf{M}_s^{-1}\mathbf{K}_s \end{bmatrix} \begin{bmatrix} \Psi \\ \overset{**}{\mathbf{u}}_s \end{bmatrix} =$$

$$= \begin{bmatrix} -\rho_0\mathbf{f}_q - \rho_0\mathbf{M}_c^T\mathbf{M}_s^{-1}\overset{**}{\mathbf{f}}{}_s^e \\ -\mathbf{K}_s\mathbf{M}_s^{-1}\overset{**}{\mathbf{f}}{}_s^e \end{bmatrix} \qquad (3.43)$$

Finally, solving for $\mathbf{u}_s$ in Eq. (3.37c) yields

$$\mathbf{u}_s = \mathbf{K}_s^{-1}\left[-\mathbf{M}_s\ddot{\mathbf{u}}_s - \rho_0\mathbf{M}_c\ddot{\Psi} + \mathbf{f}_s^e\right] \qquad (3.44)$$

and eliminating the third row in Eq. (3.37) results in

$$\begin{bmatrix} \mathbf{M}_s\mathbf{K}_s^{-1}\mathbf{M}_s & \rho_0\mathbf{M}_s\mathbf{K}_s^{-1}\mathbf{M}_c \\ \rho_0\mathbf{M}_c^T\mathbf{K}_s^{-1}\mathbf{M}_s & \frac{\rho_0}{c^2}\mathbf{M}_f + \rho_0^2\mathbf{M}_c^T\mathbf{K}_s^{-1}\mathbf{M}_c \end{bmatrix} \begin{bmatrix} \ddot{\mathbf{u}}_s \\ \ddot{\Psi} \end{bmatrix} + \begin{bmatrix} \mathbf{M}_s & 0 \\ 0 & \rho_0\mathbf{B} \end{bmatrix} \begin{bmatrix} \mathbf{u}_s \\ \Psi \end{bmatrix} =$$

$$= \begin{bmatrix} \mathbf{M}_s\mathbf{K}_s^{-1}\mathbf{f}_s^e \\ -\rho_0\mathbf{f}_q + \rho_0\mathbf{M}_c^T\mathbf{K}_s^{-1}\mathbf{f}_s^e \end{bmatrix} \qquad (3.45)$$

3.3.3 Unsymmetric two—field forms

It was stated in Sections 2.5.1 and 2.5.3 that the governing equations for an acoustic fluid, i.e. the equations of motion and the continuity equation, could be combined into the (nonhomogeneous) wave equation expressed in the pressure field p Eq. (2.98) or the displacement potential field ψ Eq. (2.111). A weak formulation of the fluid domain described in any of these scalar variables generates unsymmetric systems of equations when coupled to a displacement-based weak formulation of the structure domain [66]. These unsymmetric two—field forms can be found in the present notation without starting over with a weak formulation of the single—field fluid equations.

In order to achieve fluid equations expressed in the fluid pressure we eliminate the fluid displacement—potential from Eq. (3.32). We differentiate Eq. (3.32c) twice in time and premultiply the resulting equation with $(-\rho_0)$. Finally, we use Eq. (3.34) and get

$$
\begin{bmatrix} \mathbf{M}_s & 0 \\ \rho_0 \mathbf{M}_c^T & \frac{1}{c^2}\mathbf{M}_f \end{bmatrix} \begin{bmatrix} \ddot{\mathbf{u}}_s \\ \ddot{\mathbf{p}} \end{bmatrix} + \begin{bmatrix} \mathbf{K}_s & -\mathbf{M}_c \\ 0 & \mathbf{K}_f \end{bmatrix} \begin{bmatrix} \mathbf{u}_s \\ \mathbf{p} \end{bmatrix} = \begin{bmatrix} \mathbf{f}_e \\ \rho_0 \ddot{\mathbf{f}}_q \end{bmatrix} \tag{3.46}
$$

In the same manner the fluid pressure may be eliminated from Eq. (3.32) by a direct substitution of Eq. (3.34) in Eq. (3.32). The resulting system of equations expressed in structure displacements and fluid displacement—potential thus reads

$$
\begin{bmatrix} \mathbf{M}_s & \rho_0 \mathbf{M}_c \\ 0 & \frac{1}{c^2}\mathbf{M}_f \end{bmatrix} \begin{bmatrix} \ddot{\mathbf{u}}_s \\ \ddot{\mathbf{\Psi}} \end{bmatrix} + \begin{bmatrix} \mathbf{K}_s & 0 \\ -\mathbf{M}_c^T & \mathbf{K}_f \end{bmatrix} \begin{bmatrix} \mathbf{u}_s \\ \mathbf{\Psi} \end{bmatrix} = \begin{bmatrix} \mathbf{f}_s^e \\ -\mathbf{f}_q \end{bmatrix} \tag{3.47}
$$

Further, if the structure is considered non—flexible the last matrix equations in (3.46) is simply

$$
\frac{1}{c^2}\mathbf{M}_f\ddot{\mathbf{p}} + \mathbf{K}_f\mathbf{p} = \rho_0\ddot{\mathbf{f}}_q - \rho_0\mathbf{M}_c^T\ddot{\tilde{\mathbf{u}}}_s \tag{3.48}
$$

where $\ddot{\tilde{\mathbf{u}}}_s$ is the prescribed structural acceleration vector.

Likewise, the last matrix equation of Eq. (3.47) is

$$
\frac{1}{c^2}\mathbf{M}_f\ddot{\mathbf{\Psi}} + \mathbf{K}_f\mathbf{\Psi} = -\mathbf{f}_q + \mathbf{M}_c^T\tilde{\mathbf{u}}_s \tag{3.49}
$$

where $\tilde{\mathbf{u}}_s$ is the prescribed structural displacement vector.

The fluid response to a moving boundary can thus be determined by either Eq. (3.48) or Eq. (3.49). For zero structural motion, i.e. the fluid is surrounded by rigid walls, the last term vanishes in these equations and the discretized versions of the undamped nonhomogeneous wave equation, expressed in the dynamic fluid pressure p_d and the fluid displacement—potential ψ respectively, are obtained.

3.3.4 Symmetric two—field form of quadratic type

A fluid velocity—potential has been proposed for the coupled structure—acoustic problem in [25, 59]. The resulting coupled system of equation in this case may also be derived from Eq. (3.47) by introducing a fluid velocity—potential vector Φ defined as

$$\Phi = \dot{\Psi} \tag{3.50}$$

corresponding to the time derivative of the fluid displacement—potential field given by Eq. (2.104). We differentiate the second matrix equation in Eq. (3.47) with respect to time, multiply by $(-\rho_0)$ and substitute Eq. (3.50) into the resulting systems of equations to get

$$\begin{bmatrix} M_s & 0 \\ 0 & -\frac{\rho_0}{c^2}M_f \end{bmatrix} \begin{bmatrix} \ddot{u}_s \\ \ddot{\Phi} \end{bmatrix} + \begin{bmatrix} 0 & \rho_0 M_c \\ \rho_0 M_c^T & 0 \end{bmatrix} \begin{bmatrix} \dot{u}_s \\ \dot{\Phi} \end{bmatrix} + \begin{bmatrix} K_s & 0 \\ 0 & -\rho_0 K_f \end{bmatrix} \begin{bmatrix} u_s \\ \Phi \end{bmatrix}$$

$$= \begin{bmatrix} f_s^e \\ \rho_0 \tilde{f}_q \end{bmatrix} \tag{3.51}$$

Actually, this expression is more general than the expressions given in [25, 59] since no fluid loading was considered in their work.

3.4 Computational considerations for undamped systems

It has been shown in the previous sections that the eleven fluid—structure interaction formulations are formally equivalent. However, the various forms have different behaviour in terms of numerical stability and computational efficiency. In this section we focus on some circumstances that may affect the choice of form.

First, some general comments on the appearance of the coefficient matrix in dynamic analysis. This matrix is formed as a combination of the system mass, damping and stiffness matrices. In a transient analysis, an implicit time integrator can be used, such as the Newmark method. The system of equations to be solved in each time step is, in this case, of the principal form

$$[M + \gamma \Delta t C + \beta(\Delta t)^2 K] \ddot{x}_{n+1} = f_{n+1} - C \tilde{\dot{x}}_{n+1} - K \tilde{x}_{n+1} \tag{3.52}$$

where γ and β are the integrator parameters that determine the stability and accuracy characteristics of the algorithm and Δt is the time step. $\tilde{\dot{x}}_{n+1}$ and $\tilde{x}_{n+1}$ are predictor values of $\dot{x}_{n+1}$ and x_{n+1} respectively; see ref. [37] for more details. An explicit scheme is achieved for $\beta = 0$ and M and C diagonal.

Turning to the coupled eigenvalue problems associated to the transient equations given above, those are of so—called generalized form, i.e.

$$\lambda_i \ M \ z_i = K \ z_i \tag{3.53}$$

where λ_i is the m:th eigenvalue and z_i the corresponding eigenvector. Premultiplying Eq. (3.53) by z_i^T we may form the Rayleigh quotient

$$\lambda_i = \frac{z_i^T K z_i}{z_i^T M z_i} \tag{3.54}$$

where the nominator and denominator are the generalized stiffness and generalized mass respectively. The eigenvalue problem may be spectrally transformed [17], where the system stiffness matrix K is replaced by

$$K_\sigma = [K - \sigma M] \tag{3.55}$$

where σ is the frequency shift. By introducing a positive shift σ the eigenvalues are decreased by σ. Most common eigenvalue solvers for sparse matrices, e.g. the Subspace Iteration Method or the Lanczos Method, see ref. [37] for details, require a nonsingular stiffness matrix K and so do the reduced base techniques proposed in Chapter 4 in this study. Depending on the structure of M, this condition may thus be satisfied by a shift.

3.4.1   Rigid—body structural modes and constant potential mode (CPM)

If the structure is not fully supported, K_s is singular and

$$K_s \ u_r = 0 \tag{3.56}$$

where u_r is a structural displacement vector corresponding to a rigid—body motion. It is clear from the Rayleigh quotient that the eigenvalue becomes zero but finite for this rigid—body structural mode. When K_s is singular, form (3.45) does not exist.

From Eq. (3.23) and (3.25) we note that the matrices K_f and B are singular and

$$K_f \, e = B \, e = 0 \qquad\qquad (3.57)$$

where e denotes a vector of all ones eventually multiplied with a scalar α. This condition expresses that a constant potential generates no pressure or displacements, i.e. under the constant potential mode the potential is nonzero but all fluid displacements and dynamic pressure vanish. This is in contrast with the rigid—body structural mode where the displacements are nonzero but the strains vanish. Thus, compared to the rigid—body mode, the CPM has no physical significance and is spurious.

Considering the three—field forms (3.32) and (3.35), those are both affected by the CPM mode, i.e. the singularity of the B matrix. In these systems of equations the B matrix appears in the system mass matrix and may cause a Rayleigh quotient of the form 0/0. This is easily found by using the eigenvector $z^T = [0 \; e^T \; 0]$ in the expression for the Rayleigh quotient (3.54) and with system mass and stiffness matrices according to Eq. (3.32) and Eq. (3.35). In both cases one obtains

$$\lambda = \frac{0}{\rho_0 e^T B e} = \frac{0}{0} \qquad\qquad (3.58)$$

which represents a so—called defective eigenproblem where every λ is an eigenvalue. If one attempts to solve such a problem numerically, nonsensical results can be expected [31].

For the case of a totally enclosed fluid, with no free surface, the remedy is easy using system (3.32), while the CPM mode complicates the use of (3.35). In Eq. (3.32) we may avoid the 0/0—mode by simply setting $\Psi = 0$ at one arbitrary node in the fluid domain, leaving the pressure free. Eqs. (3.32b) and (3.32c) are the discretized weak formulations of the governing fluid equations (3.14) and (3.15), containing only spatial derivatives of the displacement—potential; therefore suppressing one degree—of—freedom in the potential in (3.32b) does not change the eigenvalues of the system of equations. On the other hand, using Eq. (3.35) and suppressing one degree—of—freedom in the displacement—potential automatically enforces an invalid prescribed fluid pressure through Eq. (3.35c), i.e. through Eq. (3.34). This superior property of Eq. (3.32) as compared to Eq. (3.35) when analyzing a totally enclosed fluid is overlooked in ref. [31] where Eq. (3.35) is proposed for the free

vibration problem. However, the use of Eq. (3.35) in this case requires the introduction of a Lagrange multiplier to avoid the 0/0—mode as shown in ref. [32].

When the fluid pressure *can* be prescribed in a fluid point, the singularity of **B** is automatically removed in Eq. (3.35). Because of Eq. (3.34) a prescribed pressure corresponds to a prescribed displacement—potential and the CPM mode is removed by reducing the numbers of equations in Eq. (3.35b) according to the vector of prescribed pressures. Using Eq. (3.32) one degree—of—freedom is prescribed in the displacement—potential and the prescribed pressures are conveniently introduced in Eq. (3.32c).

Considering the two—field form (3.39), the indeterminacy of the fluid displacement—potential is easily removed by suppressing the potential in one arbitrary fluid node. If no essential boundary condition is applied to the fluid, e.g. when the fluid has no free surface, the inverse to **B** does not exist on account of Eq. (3.57) and consequently the two—field forms (3.40) emanating from Eq. (3.35) do not exist.

As mentioned above, the three—field forms are very sparse. Furthermore, the coefficients in the system stiffness matrix in some of these forms show a substantial variation in magnitude. For example, the system stiffness matrix in Eq. (3.32) includes both the structural stiffness matrix K_s and the fluid mass terms according to $1/\rho_s c^2$ M_f. Typically, K_s is proportional to Young's modulus and of order 10^{11}, whereas the fluid terms are in the range between 10^{-6} (air) and 10^{-9} (water). The system stiffness matrix will thus have a very high condition number, approximately 10^{20}, and be ill—conditioned. However, in comparison, the condensed two—field forms Eq. (3.39) are well—conditioned and they are therefore advantageous within this respect.

The unsymmetric two—field systems (3.46) and (3.47) have two eigenvectors (left and right) for each eigenvalue λ. It is shown in [31] that these systems possess zero roots but are not defective. These systems have the advantage of utilizing only one variable in the fluid domain and being sparse.

Finally, it should be observed that all eleven symmetric and unsymmetric algebraic eigenproblems given above possess real eigenvalues, since a linear combination of the system stiffness and mass matrices, that is positive—definite, can be found for all forms. A positive—definite linear combination of **K** and **M** is a sufficient but not a necessary condition for real eigenvalues [37]. Thus, despite the unsymmetric matrices in forms (3.46) and (3.47) these systems also possess real eigenvalues [81]. Complex eigenvalues are normally encountered for in physically non—conservative systems and they are not considered in this comparison.

3.4.2   Computational efficiency and stability

The symmetry in the three—field systems of equations above is achieved at the cost of two scalar unknowns instead of one at each node in the fluid domain and also a very sparse structure of the coefficient matrices. The smaller size of the system of equations, in the two—field forms as compared to the three—field forms, is achieved at the cost of either a full system stiffness matrix, see Eqs. (3.39) and (3.41), or a full system mass matrix, see Eqs. (3.43) and (3.45).

Comparing the two condensed systems of equations (3.39) and (3.41), the former (3.39) has a full system stiffness matrix, whereas the latter (3.41) has a banded stiffness matrix. Therefore, Eq. (3.41) may be the most efficient of the two whenever this form exists, i.e. when the fluid has a free surface. If a free surface does not exist, i.e. when the fluid is totally enclosed by the structure, Eq. (3.39) has to be used instead. The tedious work of forming the system stiffness matrix in this case may be limited by using a diagonal (lumped) fluid mass matrix when suitable.

The structural and fluid mass matrices, M_s and M_f respectively, can often be made diagonal by an appropriate lumping technique. A diagonal form of these matrices facilitates the use of Eqs (3.39) and (3.43), since these systems require the inverse of M_s and M_f. Using an explicit time integrator, the unsymmetric two—field forms (3.46) and (3.47) are especially advantageous when M_s and M_f are diagonal. Substituting these equations in Eq. (3.52) results in a coefficient matrix that is upper or lower triangular (for $\beta = 0$), and the equations can be solved directly in each step by a forward or backward reduction without prior factorization.

Further, in the transient case, the two—field forms Eq. (3.43) and Eq. (3.29) both require additional matrix—vector operations on the applied structural forces. Additional matrix—vector operations are also needed using form Eq. (3.39) and Eq. (3.41) if fluid loading is incorporated. Furthermore, this fluid load needs to be two—times differentiable with respect to time when used in Eq. (3.41). The pressure is not used explicitly in Eq. (3.39) and the pressure needs to be resolved by Eq. (3.38), when requested.

Considering the two unsymmetric forms, we also make the following observation. The shifted system coefficient matrix assembled as $[K - \sigma M]$, according to Eq. (3.55), can be made symmetric by multiplying the last matrix row in Eq. (3.46) or the first matrix row in Eq. (3.47) by $(-1/\rho_0)$. Thus, in a harmonic analysis we are able to form a symmetric system of equations with respect to the coupling terms if the density is considered to be equal in all fluid regions.

3.4.3 Limit conditions

From the two—field formulations above we may identify four interesting limit conditions leading to four one—variable systems of equations. These forms, if applicable, are useful for perturbation analysis, see also [3]. Starting with Eq. (3.39), we note that for a *hypercompressible* fluid with a small bulk modulus ($K = \rho_0 c^2 \rightarrow 0$), this equation tends towards

$$\mathbf{M}_s \ddot{\mathbf{u}}_s + \mathbf{K}_s \ddot{\mathbf{u}}_s = \mathbf{f}_s^e \tag{3.59}$$

which is simply the in—vacuo structural problem. By Eq. (3.41) we can derive the limit condition for an *incompressible* fluid ($c \rightarrow \infty$) i.e.

$$(\mathbf{M}_s + \rho_0 \mathbf{M}_c \mathbf{B}^{-1} \mathbf{M}_c^T) \ddot{\mathbf{u}}_s + \mathbf{K}_s \mathbf{u}_s = \mathbf{f}_s^e + \rho_0 \mathbf{M}_c \mathbf{B}^T \ddot{\mathbf{f}}_q \tag{3.60}$$

where we observe the presence of an "added mass" matrix. For the incompressible case the fluid is thus acting like an extra mass attached to the structure. The contribution from this extra mass increases when the fluid density ρ_0 increases. The B—matrix is singular and cannot be inverted if the fluid pressure cannot be prescribed, e.g. on a free surface.

Studying Eq. (3.43) we get, for a *hyperflexible* structure ($\mathbf{K}_s = 0$), the following equations expressed in the fluid displacement potential

$$\frac{\rho_0}{c^2} \mathbf{M}_f \ddot{\Psi} + (\rho_0 \mathbf{B}^T + \rho_0^2 \mathbf{M}_c^T \mathbf{M}_s^{-1} \mathbf{M}_c) \Psi = -\rho_0 \mathbf{f}_q - \rho_0 \mathbf{M}_c^T \mathbf{M}_s^{-1} \overset{**}{\mathbf{f}}_s^e \tag{3.61}$$

The fluid stiffness matrix (since $\mathbf{B} = \mathbf{K}_f$ for the case of identical fluid shape functions) is increased with an "added rigidity" matrix whose influence increases with fluid density and decreases with structural mass. For a very heavy (although flexible) structure the fluid eigenvalues thus approach the rigid wall values.

Finally, Eq. (3.45) can be simplified for cases with a *hyperlight* structure ($\mathbf{M}_s = 0$) to yield

$$(\frac{\rho_0}{c^2} \mathbf{M}_f + \rho_0^2 \mathbf{M}_c^T \mathbf{K}_s^{-1} \mathbf{M}_c) \ddot{\Psi} + \rho_0 \mathbf{B} \Psi = -\rho_0 \mathbf{f}_q + \rho_0 \mathbf{M}_c^T \mathbf{K}_s^{-1} \mathbf{f}_s^e \tag{3.62}$$

In these cases, the fluid mass matrix $\mathbf{M}_f$ is increased with an "added compressibility" matrix, whose influence increases with fluid density and decreases with structural stiffness. For a light but very stiff structure the fluid eigenvalues are close to the rigid wall values.

3.5   Transient equations for damped coupled systems

3.5.1   Introduction

In Section 3.3 and 3.4 eleven formally equivalent symmetric and unsymmetric systems of equations were found for the undamped coupled structure—acoustic problem. The three—field formulation Eq. (3.30) and the corresponding statically condensed two—field formulation Eq. (3.39) were found superior to the alternative symmetric forms in a coupled analysis.

In this section we introduce the porous medium in the symmetric fluid domain. Damped discrete mechanical devices applied to the structure and damped locally reacting surfaces are also introduced implicitly in the derivations below. We could have introduced these damping effects also in the unsymmetric system of equations and those forms would have been easily established by weak formulations of Eq. (2.128) or Eq. (2.132). However, the resulting unsymmetric non—proportionally damped systems of equations may not be reduced by the methods applied in Chapter 4 and we will concentrate here on the symmetric forms.

3.5.2   Symmetric forms

The linear damped fluid equations (2.124–125) derived in Chapter 2 are discretized below. For brevity we will use ' $\cdot$ ' for time derivatives $\partial\backslash\partial t$. The governing equations thus read

$$\rho_{\mathrm{e}}\nabla\ddot{\psi} + r\nabla\dot{\psi} + \nabla p_{\mathrm{d}} = 0 \tag{3.63}$$

$$\Omega_{\mathrm{v}}\frac{1}{\rho_{0}\mathrm{c}^2}\,p_{\mathrm{d}} + \nabla^2\psi = \frac{1}{\rho_0}\,Q \tag{3.64}$$

Following the same procedure as in Section 3.3.2 we derive the weak forms of these equations, viz.

$$\int\limits_{V}\rho_{\mathrm{e}}\nabla w\cdot\nabla\ddot{\psi}\,\mathrm{d}V + \int\limits_{V}r\nabla w\cdot\nabla\dot{\psi}\,\mathrm{d}V + \int\limits_{V}\nabla w\cdot\nabla p_{\mathrm{d}}\,\mathrm{d}V = 0 \tag{3.65}$$

and

$$\int\limits_{V}\frac{\Omega_{\mathrm{v}}}{\rho_0\mathrm{c}^2}\,wp_{\mathrm{d}}\,\mathrm{d}V - \int\limits_{V}\nabla w\cdot\nabla\psi\,\mathrm{d}V + \int\limits_{S}w\nabla\psi\cdot\mathrm{n}\,\mathrm{d}S = \int\limits_{V}\frac{1}{\rho_0}w\,Q\,\mathrm{d}V \tag{3.66}$$

3.22

Continuity in volume displacement across boundaries of adjacent domains with different porosity, Ω_v, is automatically fulfilled by the finite element formulation. The porous solid was assumed rigid in Section 2.6.2 and therefore we assume that no porous material is attached to the flexible wall, see Fig. 1.1. If that were the case the frictional retardation expressed by Eq. (2.119) would be different. Actually, the dragforce would be related to the difference between the fluid velocity and the velocity of the porous material, which is equal to the velocity of the flexible wall.

We expand p_d and ψ in shape functions according to Eqs. (3.18–19) and make the same choice of weighting functions as in Eq. (3.20–21). In order to show the structure of the final matrix equations we keep the material properties outside the volume integrals in Eq. (3.66). Of course, in programming of the element routines these properties may, although assumed constant within each element, be different for different elements.

The weak forms thus read

$$\rho_e \, \mathbf{K_f} \, \ddot{\boldsymbol\Psi} + r \, \mathbf{K_f} \, \dot{\boldsymbol\Psi} + \mathbf{B} \, \mathbf{p} = 0 \tag{3.67}$$

$$\frac{\Omega_v}{\rho_0 c^2} \, \mathbf{M_f} \, \mathbf{p} - \mathbf{B}^T \, \boldsymbol\Psi + \mathbf{M_c^T u_s} = \mathbf{f_q} \tag{3.68}$$

where

$$(\mathbf{M_f})_{ij} = \int_V N_p^i \, N_p^j \, dV \tag{3.69}$$

$$(\mathbf{K_f})_{ij} = \int_V \nabla N_\psi^i \cdot \nabla N_\psi^j \, dV \tag{3.70}$$

$$(\mathbf{M_c})_{ij} = \int_{S_{fs}} N_s^i \cdot \mathbf{n} \, N_p^j \, dS \tag{3.71}$$

$$(\mathbf{B})_{ij} = \int_V \nabla N_\psi^i \cdot \nabla N_p^j \, dV \tag{3.72}$$

$$(\mathbf{f_q})_i = \frac{1}{\rho_0} \int_V N_p^i \, Q \, dV \tag{3.73}$$

(i = row index, j = column index).

The coupling integral between structure and fluid is thus evaluated according to

$$\int_S w\nabla\psi \cdot \mathbf{n} \, dS = \int_S N_P \nabla\psi \cdot \mathbf{n} \, dS = \int_{S_{fs}} N_P \mathbf{u}_s \cdot \mathbf{n} \, dS + \int_{S-S_{fs}} N_P \nabla\psi \cdot \mathbf{n} \, dS$$

$$= \int_{S_{fs}} N_P N_s \cdot \mathbf{n} \, dS \, \mathbf{u}_s + \int_{S-S_{fs}} N_P \nabla\psi \cdot \mathbf{n} \, dS \qquad (3.74)$$

where the last integral vanishes at interelement boundaries. By the generally damped structural equations of motion Eq. (3.4) and Eq.(3.9), respectively, and by using (3.71) in Eq. (3.5) we get together with the fluid equations Eqs. (3.67–68) the following coupled system of equations

$$\begin{bmatrix} \mathbf{M}_s & 0 & 0 \\ 0 & \rho_e \mathbf{K}_f & 0 \\ 0 & 0 & 0 \end{bmatrix} \begin{bmatrix} \ddot{\mathbf{u}}_s \\ \ddot{\boldsymbol{\Psi}} \\ \ddot{\mathbf{p}} \end{bmatrix} + \begin{bmatrix} \mathbf{C}_s & 0 & 0 \\ 0 & r\mathbf{K}_f & 0 \\ 0 & 0 & 0 \end{bmatrix} \begin{bmatrix} \dot{\mathbf{u}}_s \\ \dot{\boldsymbol{\Psi}} \\ \dot{\mathbf{p}} \end{bmatrix}$$

$$+ \begin{bmatrix} \mathbf{K}_s & 0 & -\mathbf{M}_c \\ 0 & 0 & \mathbf{B} \\ -\mathbf{M}_c^T & \mathbf{B}^T & \frac{-\Omega_v}{\rho_o c^2}\mathbf{M}_f \end{bmatrix} \begin{bmatrix} \mathbf{u}_s \\ \boldsymbol{\Psi} \\ \mathbf{p} \end{bmatrix} = \begin{bmatrix} \mathbf{f}_s^e \\ 0 \\ \mathbf{f}_q \end{bmatrix} \qquad (3.75)$$

We observe that the symmetry of Eq. (3.30) in the undamped case is preserved when damping is introduced. Further, this system may be condensed to a two–field form similar to Eq. (3.39). The last matrix equation gives

$$\mathbf{p} = \frac{-\rho_o c^2}{\Omega_v} \mathbf{M}_f^{-1} [\mathbf{M}_c^T \mathbf{u}_s - \mathbf{B}^T - \mathbf{f}_q] \qquad (3.76)$$

and after substituting this equation in Eq. (3.75) one obtains

$$\begin{bmatrix} \mathbf{M}_s & 0 \\ 0 & \rho_e \mathbf{K}_f \end{bmatrix} \begin{bmatrix} \ddot{\mathbf{u}}_s \\ \ddot{\boldsymbol{\Psi}} \end{bmatrix} + \begin{bmatrix} \mathbf{C}_s & 0 \\ 0 & r\mathbf{K}_f \end{bmatrix} \begin{bmatrix} \dot{\mathbf{u}}_s \\ \dot{\boldsymbol{\Psi}} \end{bmatrix}$$

$$+ \begin{bmatrix} \mathbf{K}_s + \frac{\rho_o c^2}{\Omega_v}\mathbf{M}_c \mathbf{M}_f^{-1}\mathbf{M}_i^T & -\frac{1}{\Omega_v}\rho_o c^2 \mathbf{M}_c \mathbf{M}_f^{-1}\mathbf{B}^T \\ -\frac{1}{\Omega_v}\rho_o c^2 \, \mathbf{B}\mathbf{M}_f^{-1} \mathbf{M}_c^T & \frac{1}{\Omega_v}\rho_o c^2 \, \mathbf{B}\mathbf{M}_f^{-1}\mathbf{B}^T \end{bmatrix} \begin{bmatrix} \mathbf{u}_s \\ \boldsymbol{\Psi} \end{bmatrix} = \begin{bmatrix} \mathbf{f}_s^e + \frac{1}{\Omega_v}\rho_o c^2 \mathbf{M}_c \mathbf{M}_f^{-1}\mathbf{f}_q \\ -\frac{1}{\Omega_v}\,\rho_o c^2 \, \mathbf{B}\mathbf{M}_f^{-1}\mathbf{f}_q \end{bmatrix} \quad (3.77)$$

These symmetric non–proportionally damped systems of equations may be programmed for the general case including fluid elements with and without a porous solid.

4 REDUCED BASE TECHNIQUES

4.1 Introduction

4.1.1 Background

A finite element method was used in Chapter 3 to discretize the governing equations for structure—acoustic systems. The accuracy in the response improves as the model is refined by increasing the number of parameters (nodes in the finite element model). This refinement has three different effects. First, it improves the description of the lower modes of vibration in the discrete model. Second, it brings in crude approximations to higher modes that were not present in the coarser model and third, the computational time is increased as the number of equations is increased. By introducing global vectors that retain the improved description of the lower modes while keeping out the crude approximations to the higher modes, the computational effort will be reduced.

The mode superposition procedure is frequently used in this context in the dynamic analysis of linear structures. In this method an approximate solution of the original system of equations is sought by an orthogonal projection into the space spanned by the complete eigenvectors. The eigenvectors are first found by an eigenvalue analysis of the associated eigenvalue problem and then used to transform the coupled equations of motion into an equivalent set of decoupled equations, [5]. In practice, only a subset of the complete set of the eigenvectors is needed to find a satisfactory approximation, enhancing the computational efficiency by modal truncation.

An alternative approach to form a reduced base (or subspace) was proposed in [78] using a set of load—dependent Ritz vectors to solve a class of problems where the applied load $f(t)$ is of the form

$$f(t) = \hat{f} \, \gamma(t) \tag{4.1}$$

in which $\hat{f}$ is a space vector and $\gamma(t)$ is a time function. The Ritz vectors were generated using a static deflection vector as starting vector and found to produce better approximation than the same number of eigenvectors. In addition, the Ritz vectors were less expensive to generate than the eigenvectors.

The procedure used above to generate a set of orthogonal Ritz vectors was later shown to be identical to the Lanczos algorithm applied with full reorthogonalization [50]. In that work, the reduction of the original system of equations to tridiagonal form using Lanczos vectors as reduced base vectors was shown. The equivalence is due to the fact that they span the same subspace, a Krylov subspace. Krylov subspace methods are commonly used methods for solving large linear systems of equations and eigenvalue problems [34]; however, the direct application to the dynamic equilibrium equation is new.

The Lanczos process has been applied recently to the symmetric fluid—structure interaction problem [11, 58] using a dynamic deflection vector as starting vector. In addition, a procedure based on the Arnoldi algorithm for application to unsymmetric systems of equations was developed and preliminary results shown in [12].

In this chapter an introduction to reduced base techniques is given and Krylov subspace methods are discussed. Algorithms for reduction of symmetric and unsymmetric systems of equations are developed. Further, a slightly modified Lanczos algorithm is derived in order to reduce non—proportionally damped symmetric systems of equations.

4.1.2   Reduction by orthogonal projections

The semidiscrete dynamic equilibrium equations derived for the fluid—structure problem can be expressed symbolically as

$$\mathbf{M}\ \ddot{\mathbf{u}}(t) + \mathbf{C}\ \dot{\mathbf{u}}(t) + \mathbf{K}\ \mathbf{u}(t) = \mathbf{f}(t) \tag{4.2}$$

where $\mathbf{M}$, $\mathbf{C}$ and $\mathbf{K}$ are real $n \times n$ system mass, damping and stiffness matrices, respectively. $\mathbf{u}(t)$ is the $n \times 1$ state vector and $\dot{\mathbf{u}}(t)$ and $\ddot{\mathbf{u}}(t)$ are the first and second time derivatives of $\mathbf{u}(t)$. $\mathbf{f}(t)$ is the $n \times 1$ loading vector.

The exact solution to Eq. (4.2) can be expressed as

$$\mathbf{u}(t) = \sum_{j=1}^{n} \mathbf{y}_j\ x_j(t) = \mathbf{Y}\ \mathbf{x}(t) \tag{4.3}$$

where $\mathbf{Y} = [\mathbf{y_1},\ \mathbf{y_2},\ ...,\ \mathbf{y_n}]$ is a set of n linearly independent vectors and $\mathbf{x}(t)$ is a vector containing the generalized coordinates. Theoretically, for a system of size n, any set of n linearly independent vector can be chosen as a base for expressing the solution $\mathbf{u}(t)$. In practice, however, it is convenient to use an orthonormal set of vectors in $\mathbf{Y}$, satisfying $\mathbf{Y^TY} = \mathbf{I}$, where $\mathbf{I}$ is the $n \times n$ identity matrix. We seek approximate solutions $\mathbf{u_m}(t)$ to equation (4.2) that can be expressed as

$$\mathbf{u_m}(t) = \sum_{j=1}^{m} \mathbf{y_j}\, x_j(t) = \mathbf{Y_m}\, \mathbf{x_m}(t) \tag{4.4}$$

where the subscript m indicates the numbers of vectors used in the reduced base $\mathbf{Y_m}$. Thus, $\mathbf{u_m}(t)$ is the projection of $\mathbf{u}(t)$ onto the subspace $span\{\mathbf{Y_m}\}$.

The residual vector $\mathbf{d_m}(t)$ resulting from the approximate solution $\mathbf{u_m}(t)$ is

$$\mathbf{d_m}(t) = \mathbf{M}\,\ddot{\mathbf{u}}_m(t) + \mathbf{C}\,\dot{\mathbf{u}}_m(t) + \mathbf{K}\,\mathbf{u_m}(t) - \mathbf{f}(t) \tag{4.5}$$

We seek an approximation $\mathbf{u_m}(t)$ to Eq. (4.2) by forcing the residual $\mathbf{d_m}(t)$ to be orthogonal to the reduced base $\mathbf{Y_m}$, i.e. we apply the following Galerkin condition

$$\mathbf{Y_m}^T\,\mathbf{d_m}(t) = \mathbf{0} \tag{4.6}$$

An orthogonal projection method may thus be summarized by the following conditions

$$\begin{cases} \mathbf{u_m}(t) \in span\{\mathbf{Y_m}\} & (4.7a) \\ \mathbf{d_m} \perp span\{\mathbf{Y_m}\} & (4.7b) \end{cases}$$

By substituting Eq. (4.4) and Eq. (4.5) in Eq. (4.6) we obtain a reduced system of equation expressed in generalized coordinates $\mathbf{x_m}(t)$ as

$$\mathbf{M_m}\,\ddot{\mathbf{x}}_m(t) + \mathbf{C_m}\,\dot{\mathbf{x}}_m(t) + \mathbf{K_m}\,\mathbf{x_m}(t) = \mathbf{f_m}(t) \tag{4.8}$$

where the projected $m \times m$ mass, damping and stiffness matrices and the $m \times 1$ force vector are given by

$$M_m = Y_m^T M Y_m \tag{4.9a}$$

$$C_m = Y_m^T C Y_m \tag{4.9b}$$

$$K_m = Y_m^T K Y_m \tag{4.9c}$$

$$f_m(t) = Y_m^T f(t) \tag{4.9d}$$

We note that, for a given system of equations, the reduced system of equation (4.8) is determined entirely by the chosen vector base Y_m and that the quality of the approximate solution found through Eq. (4.4) therefore depends entirely on the quality of Y_m. From a computational point of view the size of system (4.8) is reduced from size n to m.

4.1.3   Projection onto a subset of eigenvectors

For **M** and **K** being real symmetric and positive definite or positive semidefinite matrices it is always possible to diagonalize **M** and **K** by the eigenvectors found as the solution to the general linear eigenvalue problem [60]

$$[K - \lambda_i M] z_i = 0 \tag{4.10}$$

where (λ_i, z_i) is the i:th eigenvalue and eigenvector, respectively, to the matrix pencil (K, M). However, it has been shown that several formulations for the fluid–structure interaction problem derived in Chapter 3 have a singular system stiffness matrix caused by a constant fluid potential mode (CPM). Additionally, we would like to analyze unconstrained or partially constrained structures with respect to rigid–body displacements. Most commonly used methods for solving the eigenvalue problem Eq. (4.10) for large sparse systems of equations make use of the inverted stiffness matrix [37]. This is valid also for the reduced base techniques studied in this chapter.

To avoid the singularity of the stiffness matrix we work with the spectrally transformed problem. Introducing a real shift σ we define the shifted stiffness matrix K_σ as [17]

$$K_\sigma = K - \sigma M \tag{4.11}$$

which transforms the eigenvalue problem in Eq. (4.10) to

$$[K_\sigma - \mu_i^2 M] z_i = 0 \tag{4.12}$$

where we have introduced

$$\mu_i^2 = (\lambda_i - \sigma) \tag{4.13}$$

Although the eigenvalues of Eq. (4.10) are uniformly changed (decreased) by the shift σ, the eigenvectors are unchanged by this transformation, which follows directly by substitution.

The eigenvectors of Eq. (4.12) are M-orthogonal and K_σ-orthogonal and are conveniently scaled such that

$$z_i^T M z_j = \delta_{ij} \tag{4.14}$$
$$z_i^T K_\sigma z_j = \mu_i^2 \delta_{ij} \tag{4.15}$$

where δ_{ij} is the Kronecker delta.

Considering proportional damping of Rayleigh type [17], viz.

$$C = a_0 M + a_1 K \tag{4.16}$$

where a_0 and a_1 are the Rayleigh constants, the eigenvectors will also be C-orthogonal and the damping matrix C thus shares the same eigenspace as K_σ and M and thus

$$z_i^T C z_j = (a_0 + a_1(\mu_i^2 + \sigma))\delta_{ij} \tag{4.17}$$

The orthogonal projection process will now be applied to the spectrally transformed system of equations, viz.

$$M \ddot{u}(t) + C \dot{u}(t) + (K_\sigma + \sigma M)u(t) = f(t) \tag{4.18}$$

An approximate solution $u_m(t)$ may be expressed in a subset of the complete eigenvectors to the pencil (K_σ, M) such as

$$u_m(t) = Z_m \, x_m(t) \tag{4.19}$$

where $Z_m = [z_1, z_2, ..., z_m]$. If eq. (4.19) is substituted in Eq. (4.18) and the Galerkin condition in Eq. (4.6) is applied we get

$$Z_m^T \left(M \, Z_m \, \ddot{x}_m(t) + C \, Z_m \, \dot{x}_m(t) + (K_\sigma + \sigma \, M) \, Z_m \, x_m(t) - f(t) \right) = 0 \tag{4.20}$$

By Eqs. (4.14–4.17) we get a reduced set of m uncoupled (proportional damping is assumed) equations to be solved. By introducing $\tilde{\mu}_i^2$ for $(\mu_i^2 + \sigma)$ and $2\xi_i \tilde{\mu}_i$ for $(a_0 + a_1\tilde{\mu}_i^2)$, the i:th equation reads

$$\ddot{x}_i(t) + 2\xi_i \, \tilde{\mu}_i \, \dot{x}(t) + \tilde{\mu}_i^2 \, x_i(t) = z_i^T \, f(t) \tag{4.21}$$

where the right hand side is the projection of the force vector on the i:th eigenvector. For a force of the type Eq.(4.1) the right hand side will be

$$z_i^T \, f(t) = z_i^T \, \hat{f} \, \gamma(t) = p_i \, \gamma(t) \tag{4.22}$$

where p_i is the participation factor, generally used to measure the extent to which z_i participates in synthesizing the total load on the system. The solution to Eq. (4.21) may be expressed by Duhamel's integral [17]

$$x_i(t) = \frac{p_i}{\bar{\mu}_i} \int_0^t \gamma(\tau) e^{-\xi_i \, \tilde{\mu}_i(t-\tau)} \, \sin \bar{\mu}_i(t-\tau) d\tau \tag{4.23}$$

where $\bar{\mu}_i = \tilde{\mu}_i(1-\xi_i)^{\frac{1}{2}}$ and where we have assumed $u(0) = \dot{u}(0) = 0$.

From Eq. (4.23) it is observed that the modal response is influenced by the participation factor p_i defined by Eq. (4.22). Moreover, modes corresponding to eigenvalues far from the shift point σ will have a lower weight because of the factor $1/\mu_i$. For a zero shift strategy these are the higher modes.

The method of orthogonal projection has been used above to derive the standard procedure of mode superposition. For proportional damping we have projected the solution u(t) onto a subset of the complete eigenvectors to the matrix pencil (K_σ, M). The decoupled equations may be conveniently solved for different types of load functions $\gamma(t)$, without changing the base and the approximate solution found by Eq. (4.23) and Eq. (4.19). The problems associated with the traditional mode superposition are numerous [44]. Firstly, the generation of eigenvectors for large systems is very time consuming. Secondly, it is difficult to automatically select the required number of eigenmodes *a priori* for satisfactory convergence. Normally, the eigenvectors are calculated first and the participation factors estimated afterwards. When the loading vector is sufficiently represented in the eigenbase the eigensolution is halted. Thirdly, the eigenbase ignores the information of the loading situation related to specified loading characteristics such as spatial distribution.

For non—proportional damping, a projection onto the eigenspace will not diagonalize the damping matrix C as in Eq. (4.17) and consequently the reduced system of equations will be coupled through the projected damping matrix C_m. This coupled system of equations may be solved by an iterative technique where the off—diagonal damping terms are moved to the right—hand side, as proposed in [39, 40]. The undamped modes are thus used as a reduced base in this case. A solution strategy for the non—proportionally damped system of equations, where the damping terms will be used in the construction of the reduced base, will be discussed in Section 4.2.

4.1.4   Krylov subspace methods

The reduced base techniques that will be introduced in Section 4.2 and 4.3 are examples of Krylov subspace methods. By Krylov subspace methods we will refer to orthogonal projection methods where the reduced base in Eq. (4.4) is chosen to be a set of orthogonalized Krylov vectors. To illustrate the reduction procedures used later we will first emphasize some basic properties of the Krylov vectors. A more detailed discussion is given in [60].

The Krylov vectors are the sequence of m column vectors in the Krylov matrix $\mathcal{K}^m$ defined by a matrix D and a single nonzero starting vector r_0 [60],

$$\mathcal{K}^m(D, r_0) = [r_0, \, D\,r_0, \, ..., \, D^{m-1}\,r_0] \tag{4.24}$$

The Krylov sequence generally converges to the eigenvector of D corresponding to the largest eigenvalue of D, a property used for example in the power method where each column vector

in Eq. (4.24) is overwritten by its predecessor and only the latest vector is retained. However, in the following we will save all the Krylov vectors generated and use them as a base for the Krylov subspace defined by

$$\mathcal{K}^m(D, r_0) = span\{\mathcal{K}^m(D, r_0)\} \tag{4.25}$$

The Krylov vectors are assumed to be linearly independent and thus the Krylov subspace has the dimension m according to

$$dim(\mathcal{K}^m) = m \tag{4.26}$$

Consider the spectrally transformed eigenvalue problem of Eq. (4.12), viz.

$$[K_\sigma - (\lambda_i - \sigma)M]z_i = 0 \tag{4.27}$$

By premultiplying with K_σ^{-1} we get

$$[I - (\lambda_i - \sigma)K_\sigma^{-1}M]z_i = 0 \tag{4.28}$$

or

$$[K_\sigma^{-1}M - \theta_i^2 I]z_i = 0 \tag{4.29}$$

where I is the $n \times n$ identity matrix and

$$\theta_i^2 = \frac{1}{\lambda_i - \sigma} \tag{4.30}$$

and thus

$$\lambda_i = \sigma + \frac{1}{\theta_i^2} \tag{4.31}$$

Applying the power method to the eigenvalue problem Eq. (4.29) will thus produce a set of Krylov vectors defined by the dynamic matrix $K_\sigma^{-1}M$, see [17], and a starting vector r_0.

Substituting

$$D = K_\sigma^{-1} M \tag{4.32}$$

in Eq. (4.24) yields the Krylov matrix

$$\mathcal{K}^m(K_\sigma^{-1} M, r_0) = [r_0, K_\sigma^{-1} M\, r_0, ..., (K_\sigma^{-1} M)^{m-1}\, r_0] \tag{4.33}$$

This sequence of vectors will converge to the eigenvector, non—orthogonal to r_0, corresponding to the largest eigenvalue θ_i^2 of $K_\sigma^{-1} M$. By Eq. (4.30) it follows that this eigenvalue of the inverted problem corresponds to the eigenvalue of the original problem, closest to the shift point σ, i.e. the smallest eigenvalue of the matrix pencil (K, M). The eigenvalues λ_i of the original system (K, M) are related to θ_i^2 through Eq. (4.31).

If r_0 is orthogonal to an eigenspace, such an eigenspace is also orthogonal to the space $span\{\mathcal{K}^m(D, r_0)\}$ for all m [60]. This property of the Krylov vectors may require a restart of the iteration with a new starting vector in eigenvalue solvers based on the Krylov subspace, e.g. the Lanczos method [34]. However, this limitation in using the Krylov subspace when we want to find all the eigenvectors (possibly within a specific frequency range) to a matrix, is turned into an important feature in the load—dependent vector—algorithms discussed later, where we want to find a set of base vectors non—orthogonal to the actual loading configuration.

4.2   Tridiagonalization by Lanczos vectors

4.2.1   Introduction

The Lanczos method, proposed in 1950 [43], was intended for computing a few of the extreme eigenvalues and corresponding eigenvectors of a general matrix. The eigenvectors are constructed by forming a linear combination of a set of vectors, known as Lanczos vectors, computed in the course of the algorithm. These Lanczos vectors were used to transform the original problem to tridiagonal form. Intensive research in the past ten years has resolved a number of difficulties concerning the stability of the Lanczos process [24, 52, 53, 69] and the algorithm has been extended to symmetric generalized eigenproblems. It is now widely accepted as the method of choice for determining a few eigenpairs of large sparse problems [37, 49]. In [49] it was demonstrated that the Lanczos algorithm is more efficient than the subspace iteration for the generalized eigenvalue problem.

As suggested in Section 4.1.3 the eigenvectors found for the generalized eigenvalue problem may be used as base vectors in a modal analysis. However, recently it has been shown that for a given level of accuracy the reduced system obtained using Lanczos vectors is smaller than that using vibration modes [40, 44, 50, 78]. In other words, the Lanczos vectors do a better job at capturing the characteristics of the response than the mode shapes. This approach has been used in dynamic analysis of structures [6, 40, 44, 50, 51, 55, 56, 78], in transient heat conduction analysis [54] and in uncoupled acoustic analysis [18].

The direct use of Lanczos vectors in the dynamic system of equations is described in this chapter for proportionally and non—proportionally damped systems. For proportionally damped systems the Lanczos process is applied to the original second—order system of equations, whereas in the case of non—proportional damping the original equations are first transformed to an equivalent first—order system.

In both cases we use Lanczos iterations to generate a set of Lanczos vectors $\mathbf{Q}_m$ for use in a reduced base procedure. An approximate solution to $\mathbf{u}(t)$ is constructed through

$$\mathbf{u}(t) \simeq \mathbf{u}_m(t) = \mathbf{Q}_m\, \mathbf{x}_m(t) \tag{4.34}$$

in which the components of $\mathbf{x}_m$ are the generalized Lanczos coordinates. As before, index m indicates the number of vectors used in the base.

4.2.2 Symmetric definite matrix pencil

Considering proportional damping, the coupled vibration problem expressed by the three–field form Eq. (3.32) or by the two–field form Eq. (3.39) will be reduced to tridiagonal form. Symbolically, we write these coupled systems of equations as

$$\mathbf{M}\,\ddot{\mathbf{u}} + \mathbf{C}\,\dot{\mathbf{u}} + \mathbf{K}\,\mathbf{u} = \mathbf{f}(t) \tag{4.35}$$

where $\mathbf{M}$, $\mathbf{C}$, and $\mathbf{K}$ are symmetric $n \times n$ matrices and $\mathbf{u}$ is the state vector consisting of different numbers of subvectors depending on the formulation used. The stiffness matrix in the three–field form Eq. (3.32) is singular. However, by using the shifted stiffness matrix $\mathbf{K}_\sigma = \mathbf{K} - \sigma \mathbf{M}$ in the reduction procedure this form has what we will call a symmetric definite matrix pencil $(\mathbf{K}_\sigma, \mathbf{M})$. Considering the two–field form, it has a symmetric definite pencil also for a zero shift. The matrix $\mathbf{M}$ may be positive definite or positive semidefinite in the derivations below.

Orthogonalization of Krylov vectors

In the following we will work with the transformed problem

$$\mathbf{K}_\sigma^{-1}\,\mathbf{M}\,\ddot{\mathbf{u}} + \mathbf{K}_\sigma^{-1}\,\mathbf{C}\,\dot{\mathbf{u}} + (\mathbf{I} + \sigma\,\mathbf{K}_\sigma^{-1}\,\mathbf{M})\,\mathbf{u} = \mathbf{K}_\sigma^{-1}\,\mathbf{f}(t) \tag{4.36}$$

where we have implicitly multiplied Eq. (4.35) by $\mathbf{K}_\sigma^{-1}$.

Given the dynamic matrix $\mathbf{K}_\sigma^{-1}\mathbf{M}$, the mass matrix $\mathbf{M}$ and a starting vector r_0, the Lanczos process generates an $\mathbf{M}$–orthonormal base for the Krylov subspace

$$\mathcal{K}_m(\mathbf{K}_\sigma^{-1}\mathbf{M}, r_0) \equiv span\{r_0,\ \mathbf{K}_\sigma^{-1}\mathbf{M}\,r_0,\ ...,\ (\mathbf{K}_\sigma^{-1}\mathbf{M})^{m-1}\,r_0\} \tag{4.37}$$

At a typical step, the algorithm orthogonalizes the next vector in the Krylov sequence and $\mathbf{M}$–normalizes the resulting vector; see [53] for details. The process is summarized in the three–form recurrence formula

$$r_j = \beta_{j+1}q_{j+1} = \mathbf{K}_\sigma^{-1}\mathbf{M}q_j - q_j\alpha_j - q_{j-1}\beta_j \tag{4.38}$$

where

$$\alpha_j = \mathbf{q}_j^T \mathbf{M} \mathbf{K}_\sigma^{-1} \mathbf{M} \mathbf{q}_j \qquad (4.39)$$

$$\beta_j = \mathbf{q}_{j-1}^T \mathbf{M} \mathbf{K}_\sigma^{-1} \mathbf{M} \mathbf{q}_j \qquad (4.40)$$

where β_j may also be determined by

$$\beta_{j+1} = (\mathbf{r}_j \mathbf{M} \mathbf{r}_j)^{\frac{1}{2}} \qquad (4.41)$$

After m steps in the algorithm the quantities obtained so far can be arranged in matrix form as

$$\mathbf{K}_\sigma^{-1} \mathbf{M} \mathbf{Q}_m = \mathbf{Q}_m \mathbf{T}_m + \mathbf{r}_m \mathbf{e}_m^T \qquad (4.42)$$

where $\mathbf{r}_m$ is the residual vector, $\mathbf{e}_m = [0, 0, ..., 1]^T$, $\mathbf{Q}_m$ an $n \times m$ matrix containing the Lanczos vectors $\mathbf{q}_i$, $i=1,2,...,m$ as column vectors and $\mathbf{T}_m$ is a $m \times m$ tridiagonal matrix of the form

$$\mathbf{T}_m = \begin{bmatrix} \alpha_1 & \beta_2 & & & & \\ \beta_2 & \alpha_2 & \beta_3 & & & \\ & \beta_3 & \cdot & \cdot & & \\ & & \cdot & \cdot & \cdot & \\ & & & \cdot & \cdot & \cdot \\ & & & & \cdot & \beta_m \\ & & & & \beta_m & \alpha_m \end{bmatrix} \qquad (4.43)$$

The matrix form of the three—term recurrence formula is illustrated in Fig. 4.1.

$$\mathbf{r}_m \mathbf{e}_m^T$$

Fig. 4.1   The matrix form of the three—term recurrence formula for the generalized symmetric definite problem.

The Lanczos vectors obtained in this way are M–orthonormal, i.e. $Q_m^T M Q_m = I_m$ and this can be used in Eq. (4.42). After pre–multiplying with $Q_m^T M$ we obtain

$$Q_m^T M K_\sigma^{-1} M Q_m = T_m \qquad (4.44)$$

A pedagogical discussion of the Lanczos process applied to the symmetric generalized eigenvalue problem is given in [53] and the three–term recurrence formula is derived. For brevity, we will spare the derivation of this formula until we look at the indefinite matrix pencil in the next section. Here it is sufficient to observe that the matrix $M K_\sigma^{-1} M$ is symmetric, when K_σ and M symmetric, and hence a tridiagonal form may be obtained by projection on an orthogonal matrix [60].

Reduction of system of equations to tridiagonal form

To continue with the dynamic problem we use the approximate solution in terms of the Lanczos vectors defined by Eq. (4.34) in the transformed equations of motion Eq. (4.36) and form the residual $d_m(t)$ as

$$d_m(t) = K_\sigma^{-1} M Q_m \ddot{x}_m + K_\sigma^{-1} C Q_m \dot{x}_m + (I_m + \sigma K_\sigma^{-1} M) Q_m x_m - K_\sigma^{-1} f(t) \qquad (4.45)$$

To take advantage of symmetry we will multiply the residual with M and require the resulting vector to be orthogonal to the set of Lanczos vectors

$$Q_m^T M d_m = 0 \qquad (4.46)$$

Actually, in this manner the residual is M–orthogonal and we get

$$Q_m^T M K_\sigma^{-1} M Q_m \ddot{x}_m + Q_m^T M K_\sigma^{-1} C Q_m \dot{x}_m + (Q_m^T M Q_m + \sigma Q_m^T M K_\sigma^{-1} M Q_m) x_m =$$
$$= Q_m^T M K_\sigma^{-1} f(t) \qquad (4.47)$$

Although we eventually multiply by a singular matrix M, as in the case of using Eq. (3.32), equation (4.47) is still valid, see [50].

The damping matrix in the reduced problem $Q_m^T M K_\sigma^{-1} C Q_m$ is generally not symmetric. If Rayleigh damping is assumed such as

$$C = a_0 M + a_1 K \tag{4.48}$$

then we can rewrite this term as

$$Q_m^T M K_\sigma^{-1} C Q_m = Q_m^T M K_\sigma^{-1}(a_0 M + a_1(K_\sigma + \sigma M))Q_m =$$

$$= a_0 Q_m^T M K_\sigma^{-1} M Q_m + a_1 Q_m^T M Q_m + a_1 \sigma Q_m^T M K_\sigma^{-1} M Q_m \tag{4.49}$$

By the M–orthonormality and the expression for T_m in Eq. (4.44), (4.47) reduces to the tridiagonal form

$$T_m \ddot{x}_m + [(a_0 + a_1\sigma)T_m + a_1 I_m]\dot{x}_m + (I_m + \sigma T_m)x_m = f_m(t) \tag{4.50}$$

where

$$f_m(t) = Q_m^T M K_\sigma^{-1} f(t) \tag{4.51}$$

The starting vector r_0 can be chosen arbitrarily. Indeed, when computing the eigensolution a random starting vector is often the best choice. When the starting vector is orthogonal to an eigenvector all the generated Lanczos vectors will also be orthogonal to that eigenvector. This is an important and desirable property of the Krylov subspace methods. When the right–hand vector of the equations of motion has no component along an eigenvector, the response of the system will also be orthogonal to the same eigenvector. Thus, the choice for this starting vector that produces the best solution with minimum computational efforts is the right–hand side. Accordingly,

$$r_0 = K_\sigma^{-1} \hat{f} \tag{4.52}$$

where we assumed that the applied load is of the form

$$f(t) = \hat{f}\gamma(t) \tag{4.53}$$

$\hat{f}$ is a normalized vector representing the spatial distribution of the load and is independent of time, while $\gamma(t)$ is the scalar time dependent amplitude of the applied load vector. This choice for the starting vector simplifies the right–hand side of Eq. (4.50) to

$$
\begin{aligned}
f_m(t) &= Q_m^T M K_\sigma^{-1} \hat{f} \gamma(t) \\
&= Q_m^T M r_0 \gamma(t) \\
&= Q_m^T M q_1 \beta_1 \gamma(t) \\
&= Q_m^T M Q_m e_1 \beta_1 \gamma(t) \\
&= e_1 \beta_1 \gamma(t)
\end{aligned}
\tag{4.54}
$$

where $e_1 = [1, 0, ..., 0]^T$. Finally, Eq. (4.50) takes the form

$$
T_m \ddot{x}_m + [(a_0 + a_1 \sigma) T_m + a_1 I_m] \dot{x}_m + (I_m + \sigma T_m) x_m = e_1 \beta_1 \gamma(t)
\tag{4.55}
$$

When the starting vector differs from that in Eq. (4.52), then the Lanczos algorithm is less than optimum and Eq. (4.51) must be used to evaluate f_m. Such a case arises when the same problem needs to be solved with a new forcing function, i.e. the spatial distribution is changed.

The tridiagonal system of equations in the transient case might be solved either by step–by–step integration methods such as the Newmark method, or the eigenvectors of T_m can be calculated to be used in the mode superposition procedure as discussed below. Due to the fact that the system is only slightly coupled by its tridiagonal form, the computational cost of either of these methods is small compared to the factorization of K_σ. If an implicit method is used, a direct solution with a symmetric tridiagonal coefficient matrix requires $8m$ flops in each time step, in comparison to the number of operations of order n^3 to factorize K_σ.

In the harmonic case $\gamma(t)$ is of the form $e^{i\bar{\omega}t}$, where $\bar{\omega}$ is the loading frequency. Equation (4.55) can then be written as

$$
[I_m + (\sigma - \bar{\omega}^2) T_m + ((a_0 + a_1 \sigma) T_m + a_1 I_m) i] \hat{x}_m(\bar{\omega}) = \beta_1 e_1
\tag{4.56}
$$

where $i = \sqrt{-1}$ and $\hat{x}_m$ is the frequency dependent response function expressed in Lanczos coordinates. From Eq. (4.56) it is clear that the choice of σ affects the required number of Lanczos vectors for evaluating the harmonic response. Studying the response at a single

frequency $\bar{\omega}_i$, the exact solution for the undamped case is $\hat{u} = (K - \bar{\omega}_i^2 M)^{-1} \hat{f}$. Choosing σ to be $\bar{\omega}_i^2$ in Eq. (4.56) gives the exact solution using only one Lanczos vector, $m = 1$, since the elements in $\hat{x}$ will be zero for $m > 1$. If σ differs from $\bar{\omega}^2$, as in a frequency sweep, more Lanczos vectors will be required to express the response function accurately within the frequency interval of the sweep.

Ritz vector base

In order to study the characteristics of the reduced system of equations we return to the transformed eigenvalue problem in Eq. (4.29), viz.

$$[K_\sigma^{-1} M - \theta_i^2 I] z_i = 0 \tag{4.57}$$

We are seeking approximate eigenvectors, or Ritz vectors $z_{i,m}$ to the exact eigenvectors z_i, that may be expressed as linear combinations of Lanczos vectors, viz.

$$z_{i,m} = Q_m s_{i,m} \tag{4.58}$$

where $s_{i,m}$ contains the generalized coordinates in the base Q_m.

We will now look for the properties of $s_{i,m}$. Substituting Eq. (4.58) in Eq. (4.57) we may form the residual

$$d_{i,m} = K_\sigma^{-1} M Q_m s_{i,m} - \theta_{i,m}^2 Q_m s_{i,m} \tag{4.59}$$

where $\theta_{i,m}^2$ is an approximate eigenvalue, or Ritz value, to the matrix $K_\sigma^{-1} M$, associated with m Lanczos vectors in the reduced base. We multiply by M in order to take advantage of symmetry and apply the Galerkin condition Eq. (4.6) to obtain

$$Q_m^T M d_{i,m} = 0 \tag{4.60}$$

and by Eq. (4.59)

$$Q_m^T M K_\sigma^{-1} M Q_m s_{i,m} - \theta_{i,m}^2 Q_m^T M Q_m s_{i,m} = 0 \tag{4.61}$$

or equivalently

$$[T_m - \theta_{i,m}^2 \, I_m] s_{i,m} = 0 \tag{4.62}$$

Thus, the coefficients in the eigenvector to the tridiagonal matrix T_m, are the generalized coordinates in Eq. (4.58). Thus, by solving the tridiagonal eigenvalue problem Eq. (4.62) we obtain approximate eigenpairs $(\theta_{i,m}^2, \, z_{i,m})$ to the inverted (and spectrally transformed) eigenproblem of Eq. (4.29). Approximate eigenvalues, or Ritz values to the general eigenvalue problem Eq. (4.10) are found by the relation

$$\lambda_{i,m} = \sigma + \frac{1}{\theta_{i,m}^2} \tag{4.63}$$

and approximate eigenvectors by Eq. (4.58). It should be observed that when m gets larger the eigenvalues of T_m converge to the eigenvalues θ_i^2, of $K_\sigma^{-1}M$ and that the eigenvalues λ of the original system can be recovered by the inverse transformation in Eq. (4.63), see [34]. If the starting vector is chosen according to Eq. (4.52), only eigenvalues corresponding to eigenmodes that are non—orthogonal to the loading distribution are found. The eigenvalue closest to the shift point σ converges first.

Diagonalization by Ritz vectors

The tridiagonal system of equations derived in the transient case, Eq. (4.50) will now be decoupled. The Ritz vectors expressed as $Z_m = Q_m S_m$ satisify M—orthonormality and $MK_\sigma^{-1}M$—orthogonality, viz.

$$Z_m^T M Z_m = S_m^T Q_m^T M Q_m S_m = S_m^T S_m = I_m \tag{4.64}$$

$$Z_m^T M K_\sigma^{-1} M Z_m^T = S_m^T Q_m^T M K_\sigma^{-1} M Q_m S_m = S_m^T T_m S_m = \theta_m \tag{4.65}$$

where the last equation results from Eq. (4.62). It is easy to verify that either we express the approximate solution to the transformed problem Eq. (4.36) by the Ritz vectors

$$u_m(t) \simeq Z_m \, y_m(t) = Q_m S_m y_m(t) \tag{4.66}$$

or we use the eigenvectors S_m of the tridiagonal matrix T_m to diagonalize Eq. (4.50) and we obtain

$$\theta_m^2 \, \ddot{y}_m(t) + [(a_0+a_1\sigma)\theta_m^2 + a_1 I_m]\dot{y}_m(t) + (I_m + \sigma\theta_m^2)y_m(t) = S_m^T Q_m^T M \, K_\sigma^{-1} \, \hat{f}\gamma(t) \quad (4.67)$$

With a starting vector according to Eq. (4.52) the right–hand side reads, by use of Eq. (4.54),

$$S_m^T Q_m^T M \, K_\sigma^{-1} \, \hat{f}\gamma(t) = S_m^T e_1 \beta_1 \gamma(t) = s_{1,m}\beta_1 \gamma(t) \qquad (4.68)$$

where $s_{1,m}$ is the first row vector in S_m. Solving the j:th equation in Eq. (4.67) gives

$$\ddot{y}_{j,m}(t) + [a_0 + a_1\,(\sigma + \theta_{j,m}^{-2})]\dot{y}_{j,m}(t) + (\theta_{j,m}^{-2} + \sigma)y_{j,m}(t)$$
$$= \theta_{j,m}^{-2}\,s_{j,1,m}\,\beta_1\gamma(t) \qquad (4.69)$$

The indices m is used to emphasize that these equations will change if more Ritz vectors are appended to the Krylov space, and thus m is increased, which is different from the modal equations Eq. (4.21). Further, if we introduce $\tilde{\theta}_{j,m}^{-2}$ for $(\theta_{j,m}^{-2} + \sigma)$ and $2\xi_{j,m}\tilde{\theta}_{j,m}^{-1}$ for $(a_0+a_1\tilde{\theta}_{j,m}^{-2})$ we rewrite Eq. (4.69) as

$$\ddot{y}_{j,m}(t) + 2\xi_{j,m}\,\tilde{\theta}_{j,m}^{-1}\,\dot{y}_{j,m}(t) + \tilde{\theta}_{j,m}^{-2}\,y_{j,m} = \theta_{j,m}^{-2}\,s_{j,1,m}\beta_1\gamma(t) \qquad (4.70)$$

By direct use of Duhamel's integral in Eq. (4.23) we obtain a solution to Eq. (4.70)

$$y_{j,m}(t) = \frac{\theta_{j,m}^{-2}s_{j,1,m}\beta_1}{\bar{\theta}_{j,m}^{-2}} \int_0^t \gamma(t)e^{-\xi_{j,m}\tilde{\theta}_{j,m}^{-1}(t-\tau)}\sin\bar{\theta}_{j,m}^{-1}(t-\tau)d\tau \qquad (4.71)$$

where $\bar{\theta}_{j,m}^2 = \tilde{\theta}_{j,m}^2(1-\xi_{j,m}^2)$, and where we observe the factor $\theta_{j,m}^{-2}/\bar{\theta}_{j,m}^{-2}$. For a zero shift $\sigma=0$ this factor is equal to one and hence contrary to the modal equations the higher modes have equal weight as the lower modes. By this result we may expect high–frequency oscillations in the response due to unconverged Ritz vectors. This is equally true when using the Lanczos vectors since the Lanczos vectors and the Ritz vectors span the same subspace.

Comparing with a reduced base where a subset of eigenvectors is used the mechanism is quite different when approximating the dynamic solution by Lanczos (or Ritz) vectors. The conventional criterion for deciding how many vectors to be used by studying the representation of the loading vector has no meaning when using Lanczos vectors. Although the load vector in the transformed problem Eq. (4.36) is completely represented in the Lanczos space (actually it is parallel to the first Lanczos vector), it does not follow that the exact solution is obtained in this base. A termination criteria when using a Ritz vector base is discussed in [41]. An alternative measure is given below for a Lanczos vector base.

Error Estimate

The time–dependent residual vector $d_m(t)$ in Eq. (4.55) may be used to get an indication of the error in the approximate solution $u_m(t)$. We substitute the Lanczos relation Eq. (4.42) in Eq. (4.45) and yield

$$d_m(t) = (Q_m T_m + r_m e_m^T)\ddot{x}_m + K_\sigma^{-1}CQ_m\dot{x}_m + Q_m x_m + \sigma(Q_m T_m + r_m e_m^T)x_m - K_\sigma^{-1}\hat{f}\gamma(t) \tag{4.72}$$

For Rayleigh damping according to Eq. (4.48) the damping force reads

$$K_\sigma^{-1}CQ_m\dot{x}_m = (a_0+a_1\sigma)K_\sigma^{-1}MQ_m\dot{x}_m + a_1Q_m\dot{x}_m =$$
$$= (a_0+a_1\sigma)(Q_m T_m+r_m e_m^T)\dot{x}_m + a_1Q_m\dot{x}_m \tag{4.73}$$

Substituting the last expression in Eq. (4.72) gives

$$d_m(t) = r_m^T e_m^T \ddot{x}_m + (a_0+a_1\sigma)r_m^T e_m^T \dot{x}_m + \sigma r_m^T e_m^T \ddot{x}_m +$$
$$Q_m[T_m\ddot{x}_m + ((a_0+a_1\sigma)T_m+a_1 I_m)\dot{x}_m+(I_m+\sigma T_m)x_m - e_1\beta_1\gamma(t)] \tag{4.74}$$

where we have used $K_\sigma^{-1}\hat{f}\gamma(t) = r_0\gamma(t) = Q_m e_1\beta_1\gamma(t)$.

The term inside the square brackets becomes identically zero, cf. Eq. (4.55) and hence

$$d_m(t) = r_m e_m^T(\ddot{x}_m + (a_0+a_1\sigma)\dot{x}_m + \sigma x_m) \tag{4.75}$$

Computing the **M**—norm of this residual results in

$$\|d_m(t)\|_{\mathbf{M}} = \|r_m\|_{\mathbf{M}} \, | \ddot{\chi}_m + (a_0 + a_1\sigma)\dot{\chi}_m + \sigma\chi_m) | \tag{4.76}$$

where $\ddot{\chi}_m$, $\dot{\chi}_m$ and χ_m are the bottom elements of $\ddot{x}_m$, $\dot{x}_m$ and x_m, respectively and $\|r_m\|_{\mathbf{M}} = \beta_{m+1}$. This error is a measure of the unbalance force, during the course of time integrating, due to the reduced base introduced in Eq. (4.36).

We define an error function $e(t)$, see [54], relating the norm of the residual to the norm of the loading function in the transformed equation such as

$$e(t) = \frac{\|d_m\|_{\mathbf{M}}}{\|r_0 \gamma(t)\|_{\mathbf{M}}} = \frac{\beta_{m+1}}{\beta_1} \frac{|\ddot{\chi}_m + (a_0 + a_1\sigma)\dot{\chi}_m + \sigma\chi_m|}{|\gamma(t)|} \tag{4.77}$$

When the solution vector is completely represented in the current space spanned by the m Lanczos vectors, the residual β_{m+1} vanishes and the error function will be zero. The residual in Eq. (4.76) may also be used as a termination criterion during the Lanczos iterations, as shown in [54].

In summary, the Lanczos vectors are load—dependent and are generated directly from the right-hand side force vector. The components of the first residual vector are the actual right-hand side forces in the transformed problem Eq. (4.36) and the first Lanczos vector is the normalized dynamic deflection due to this force vector. The following Lanczos vectors are a sequence of normalized dynamic deflections associated with a residual force vector. These residual vectors are the unbalance forces in the governing equations associated with the approximation achieved from the previous set of Lanczos vectors. At any given step j, the Lanczos algorithm computes a vector that is parallel to the residual vector associated with the approximate solution using the current m Lanczos vectors as its bases. This residual vector is then used to obtain the next Lanczos vector, and hence the the Lanczos algorithm may be viewed as implicitly performing a sequence of orthogonal projections onto a growing subspace. At the end of each step a new Lanczos vector is appended to the current subspace. An important property of the Lanczos algorithm is that the reduced matrix has a tridiagonal structure. Typically, the number of Lanczos vectors and hence the size of this tridiagonal matrix, m, is considerably smaller than n.

4.2.3 Symmetric indefinite matrix pencil

Non—proportional damping was introduced in the finite element models in Chapter 3.5. In order to reduce the size of these systems of equations we will apply a modified Lanczos algorithm for symmetric indefinite matrix pencils [13, 40]. The eigenvectors to these pencils are generally complex. However, the Lanczos vectors derived below are real. Therefore we will use the same notation for these vectors as for the Lanczos vectors generated in the case of a definite matrix pencil, although the Lanczos vectors derived below have length $2n$.

By introducing a new variable

$$\mathbf{v} = \dot{\mathbf{u}} \qquad (4.78)$$

we rewrite the equation of motion to

$$\mathbf{M}\,\dot{\mathbf{v}} + \mathbf{C}\,\mathbf{v} + \mathbf{K}\,\mathbf{u} = \mathbf{f}(t) \qquad (4.79)$$

By adding the trivial equation, $\mathbf{K}\,\dot{\mathbf{u}} = \mathbf{K}\,\mathbf{v}$ to Eq. (4.79), we obtain

$$\begin{bmatrix} \mathbf{M} & 0 \\ 0 & -\mathbf{K} \end{bmatrix} \begin{bmatrix} \dot{\mathbf{v}} \\ \dot{\mathbf{u}} \end{bmatrix} + \begin{bmatrix} \mathbf{C} & \mathbf{K} \\ \mathbf{K} & 0 \end{bmatrix} \begin{bmatrix} \mathbf{v} \\ \mathbf{u} \end{bmatrix} = \begin{bmatrix} \mathbf{f}(t) \\ 0 \end{bmatrix} \qquad (4.80)$$

Alternatively by substitution for $\dot{\mathbf{u}}$ and adding $\mathbf{M}\dot{\mathbf{u}} = \mathbf{M}\mathbf{v}$ we get

$$\begin{bmatrix} \mathbf{C} & \mathbf{M} \\ \mathbf{M} & 0 \end{bmatrix} \begin{bmatrix} \dot{\mathbf{u}} \\ \dot{\mathbf{v}} \end{bmatrix} + \begin{bmatrix} \mathbf{K} & 0 \\ 0 & -\mathbf{M} \end{bmatrix} \begin{bmatrix} \mathbf{u} \\ \mathbf{v} \end{bmatrix} = \begin{bmatrix} \mathbf{f}(t) \\ 0 \end{bmatrix} \qquad (4.81)$$

Symbolically, both systems are of first—order and have the form

$$\mathbf{A}\,\dot{\mathbf{y}} + \mathbf{B}\,\mathbf{y} = \mathbf{g}(t) \qquad (4.82)$$

This system has $2n$ unknowns as compared with n unknowns in the second—order system. The $\mathbf{M}$, $\mathbf{C}$ and $\mathbf{K}$ matrices are symmetric and hence the matrices $\mathbf{A}$ and $\mathbf{B}$ are also symmetric although neither is definite, i.e. the pencil $(\mathbf{B}_\sigma, \mathbf{A})$ is indefinite. Depending on the properties of the $\mathbf{M}$, $\mathbf{C}$ and $\mathbf{K}$ matrices we may choose a suitable form. The only assumption we make beside symmetry is that a linear combination of $\mathbf{M}$, $\mathbf{C}$ and $\mathbf{K}$ is nonsingular.

Orthogonalization of Krylov vectors

We first transform Eq. (4.82) by multiplying by B_σ^{-1} and yield

$$B_\sigma^{-1}A\,\dot{y} + (I + \sigma B_\sigma^{-1}A)y = B_\sigma^{-1}g(t) \tag{4.83}$$

where $B_\sigma = B - \sigma A$. We will now use a Krylov subspace method to find an approximative solution to Eq. (4.83). The technique follows closely the one used for the definite problem above.

Given the dynamic matrix $B_\sigma^{-1}A$, the A matrix and a starting vector r_0, the Lanczos process generates an A—orthonormal base for the Krylov subspace

$$\mathcal{K}^m(B_\sigma^{-1}A,\, r_0) \equiv span \left\{r_0,\, B_\sigma^{-1}r_0,\, ...,\, (B_\sigma^{-1}A)^{m-1}r_0\right\} \tag{4.84}$$

Next we will derive the Lanczos algorithm for indefinite problems. Assume that the first j Lanczos vectors (q_1, q_2, ..., q_j) have been found and that they satisfy A—orthogonality in the sense that $q_i^T A q_j = \pm 1 \delta_{ij}$, as a consequence of A being an indefinite matrix. The next Lanczos vector q_{j+1} will be obtained by computing a preliminary vector $\bar{r}_j$ from the previous vector in the Krylov sequence

$$\bar{r}_j = B_\sigma^{-1}A\,q_j \tag{4.85}$$

This vector may be expressed as a linear combination of all the previous Lanczos vectors and a residual vector r_j orthogonal to all previous Lanczos vectors

$$\bar{r}_j = r_j + \alpha_j q_j + \beta_j q_{j-1} + \gamma_j q_{j-2} + ... \tag{4.86}$$

The amplitudes α_j, β_j, γ_j, ... are evaluated by imposing A—orthogonality, i.e. we premultiply Eq. (4.86) by $q_j^T A$ and get

$$q_j^T A\,\bar{r} = q_j^T A\,r_j + \alpha_j q_j^T A q_j + \beta_j q_j^T A q_{j-1} + \gamma_j\,q_j^T A q_{j-2} + ... \tag{4.87}$$

The first term on the right—hand side vanishes by definition and all terms after the second vanish due to A—orthogonality. We are now ready to estimate the component of q_j built up along $\bar{r}$ by

$$\alpha_j = \frac{q_j^T A \bar{r}_j}{q_j^T A q_j} \tag{4.88}$$

The component of q_{j-1} along $\bar{r}_j$ may be found in a similar way by premultiplying Eq. (4.86) by $q_{j-1}^T A$. In this case we get

$$\beta_j = \frac{q_{j-1}^T A \bar{r}_j}{q_{j-1}^T A q_{j-1}} \tag{4.89}$$

Similarly, the component of q_{j-2} along $\bar{r}_j$ is obtained by

$$\gamma_j = \frac{q_{j-2}^T A \bar{r}_j}{q_{j-2}^T A q_{j-2}} \tag{4.90}$$

However, by Eq. (4.85) the nominator reads

$$q_{j-2}^T A \, \bar{r}_j = q_{j-2}^T A \, B_\sigma^{-1} A q_j = q_j^T A \, (B_\sigma^{-1} A q_{j-2}) = q_j^T A \, \bar{r}_{j-2} \tag{4.91}$$

where we have used the symmetry of the matrices A and B. Expanding the result in Eq. (4.67) according to Eq. (4.85) we get

$$q_j^T A \, \bar{r}_{j-2} = q_j^T A \, (r_{j-2} + \alpha_{j-2} \, q_{j-2} + \beta_{j-2} \, q_{j-3} + \gamma_{j-2} \, q_{j-4} + \ldots) \tag{4.92}$$

where all forms on the right—hand side vanish due to A—orthogonality.

It can be shown [53] that all further terms in Eq. (4.86) will vanish and hence $\bar{r}_j$ can be expressed as a combination of the previous two Lanczos vectors and the residual vector r_j.

This condition leads to the three–form recurrence formula for the indefinite matrix pencil (B_σ, A)

$$r_j = \delta_{j+1}^{-1} \, \beta_{j+1} \, q_{j+1} = B_\sigma^{-1} A \, q_j - q_j \, \alpha_j - q_{j-1} \, \beta_j \tag{4.93}$$

where

$$\alpha_j = \delta_j^{-1} \, q_j^T A \, B_\sigma^{-1} A \, q_j \tag{4.94}$$

$$\beta_j = \delta_{j-1}^{-1} \, q_{j-1}^T A \, B_\sigma^{-1} A \, q_j \tag{4.95}$$

$$\beta_{j+1} = | r_j^T A \, r_j |^{\frac{1}{2}} \tag{4.96}$$

$$\delta_{j+1} = \text{sign} \, (r_j^T A \, r_j) \tag{4.97}$$

After m steps in the algorithm all the quantities obtained so far can be arranged in a single matrix equation of the form

$$B_\sigma^{-1} A \, Q_m = Q_m \, D_m^{-1} \, T_m + r_m \, e_m^T \tag{4.98}$$

where T_m is a symmetric tridiagonal matrix according to Eq. (4.43) and $D_m = \text{diag}(\delta_1, \delta_2, ..., \delta_m)$ with values $+1$ or -1, see Fig. 4.2.
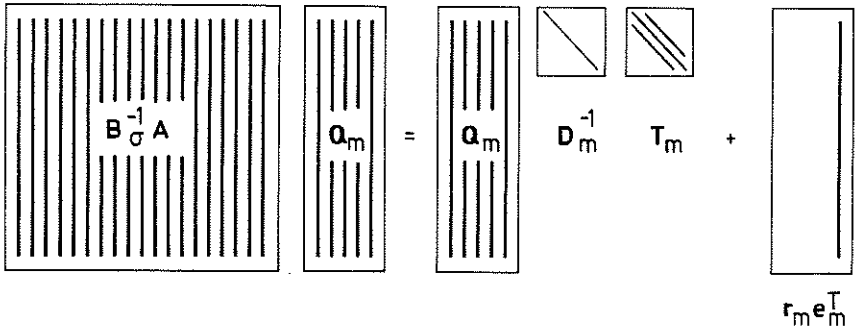
Fig. 4.2   The matrix form of the three–term recurrence formula for the generalized symmetric indefinite problem.

The Lanczos vectors stored in Q_m are A–orthonormal in the sense that

$$Q_m^T A \, Q_m = D_m \tag{4.99}$$

Premultiplying Eq. (4.98) by $Q_m^T A$ results in

$$Q_m^T A \, B_\sigma^{-1} A \, Q_m = Q_m^T A \, Q_m \, D_m^{-1} \, T_m \qquad (4.100)$$

and thus by Eq. (4.99)

$$T_m = Q_m^T A \, B_\sigma^{-1} A \, Q_m \qquad (4.101)$$

Reduction of system of equations to tridiagonal form

We express the approximate solution to Eq. (4.82) by Eq. (4.34) and form the residual $d_m(t)$ as

$$d_m(t) = B_\sigma^{-1} A \, Q_m \dot{x}_m + (I_m + \sigma B_\sigma^{-1} A) Q_m \, x_m - B_\sigma^{-1} g(t) \qquad (4.102)$$

We multiply by A and apply the Galerkin condition Eq. (4.6), i.e.

$$Q_m^T \, A \, d_m(t) = 0 \qquad (4.103)$$

We combine Eq. (4.102) and Eq. (4.103) and obtain

$$Q_m^T B_\sigma^{-1} A \, Q_m \dot{x}_m + (Q_m^T A Q_m + \sigma Q_m^T A B_\sigma^{-1} A Q_m) x_m - Q_m^T A B_\sigma^{-1} g(t) = 0 \qquad (4.104)$$

By the expressions in Eqs. (4.99) and (4.101) we get the tridiagonal form

$$T_m \dot{x}_m + (D_m + \sigma T_m) x_m = g_m(t) \qquad (4.105)$$

where

$$g_m(t) = Q_m^T A B_\sigma^{-1} g(t) \qquad (4.106)$$

If the loading function is of the form

$$g(t) = \hat{g} \, \gamma(\tau) \qquad (4.107)$$

we choose the starting vector r_0 in the direction of $B_\sigma^{-1}\hat{g}$ and thus

$$
\begin{aligned}
g_m(t) &= Q_m^T A B_\sigma^{-1}\hat{g}\gamma(t) \\
&= Q_m^T A r_0 \gamma(t) \\
&= Q_m^T A q_1 \delta_1^{-1}\beta_1\gamma(t) \\
&= Q_m^T A Q_m e_1 \delta_1^{-1}\beta_1\gamma(t) \\
&= D_m e_1 \delta_1^{-1}\beta_1\gamma(t) \\
&= e_1\beta_1\gamma(t)
\end{aligned}
\tag{4.108}
$$

and finally we obtain

$$
T_m\dot{x}_m + (D_m + \sigma T_m)x_m = e_1\beta_1\gamma(t) \tag{4.109}
$$

In comparison with the Lanczos procedure for definite systems we only need to define an extra array $D_m = \mathrm{diag}(\delta_1,\delta_2,...,\delta_m)$ of length $2n$ to store the sign of the indefinite norm $q_i^T A q_i$. The algorithm works equally well for symmetric definite matrices, in which case $D_m = I_m$.

Real and complex Ritz vector bases

All matrix and vector operations in the suggested reduction method are done in real arithmetic and the resulting matrices are all real. Complex arithmetic need only be used in the case where we want to diagonalize the tridiagonal system of equations resulting from the reduction of non—proportionally damped systems [45]. A diagonal form of the reduced equations may be preferable for certain types of loading functions, like piecewise linear functions for which an analytical solution is obtainable for each generalized coordinate. However, the accuracy of the approximate solution is determined by the first step; the reduction to tridiagonal form.

A corresponding eigenvalue solver would use a random starting vector, and generate the T_m and D_m matrices respectively and solve the complex eigenvalue problem. This approach has been used in [13] where the Lanczos algorithm was found considerably more efficient than the subspace iteration algorithm.

4.2.4   Numerical implementations

The load–dependent Lanczos algorithm for a definite matrix pencil is summarized in Table 4.1 for the spectrally transformed problem. The computational effort in each step involves a matrix–vector multiplication by **M**, the solution of a system of equations with $\mathbf{K}_\sigma$ as the coefficient matrix, two vector–vector (inner) products and four saxpy operations, where saxpy stands for a scalar times a vector x plus a vector y. The algorithm requires storage for $\mathbf{K}_\sigma$ and **M**, and four vectors of length n, to store $\mathbf{r}_{j-1}$, $\bar{\mathbf{p}}_{j-1}$, $\bar{\mathbf{r}}_j$ and $\mathbf{q}_{j-1}$. The orthogonalization coefficients α and β are stored in an array of length $2m$ to be used in the solution of the reduced problem.

From Table 4.1 we note that the **M**–orthogonality imposed for the Lanczos vectors does not require additional multiplications by **M**. Instead an extra array **p** is introduced to compute the next vector both in the Krylov sequence by $\bar{\mathbf{r}}_j = \mathbf{K}_\sigma^{-1}\mathbf{M}\mathbf{q}_j = \mathbf{K}_\sigma^{-1}\mathbf{p}_j$ and in the orthogonalization procedure step 2.e and 2.h. The algorithm is similar to the one derived in [53] for the associated eigenvalue problem.

The linear equation solving within the algorithm may take advantage of the sparsity of the matrices $\mathbf{K}_\sigma$ and **M**. Profile–stored solvers for symmetric systems of equations are discussed in [28]. A discussion on substructuring techniques may be found in [27, 61].

A slightly different Lanczos algorithm derived in the previous section in order to tridiagonalize indefinite matrices is given in Table 4.2. This algorithm is a modified version of the algorithm derived in [53] and a similar algorithm is used in [13, 40].

From the operation count we note that the number of vector operations is increased from $12n$ to $24n$ in each iteration compared with the definite algorithm. The additional operations required to solve with $\mathbf{B}_\sigma$ and to compute **Ar**, compared to the first-order systems, will depend on to what extent the sparsity of $\mathbf{B}_\sigma$ and **A** can be exploited. Generally it will not be doubled as in the case of the vector operations. Considering the memory requirement we need an extra array of length m to store the values of $(\delta_1, \delta_2, \ldots, \delta_m)$.

Table 4.1   The load–dependent Lanczos algorithm for a symmetric *definite* matrix pencil (K_σ, M) with operation count in flop.

Given a load vector $\hat{f}$:   Op. count

1. initialize

    a. factorize K_σ $\zeta(K_\sigma)$[1]

    b. $q_0 = 0$

    c. $r_0 = K_\sigma^{-1}\hat{f}$ $\kappa(K_\sigma)$[2]

    d. $\bar{p}_0 = Mr_0$ $\mu(M)$[3]

    e. $\beta_1 = (r_0^T M r_0)^{\frac{1}{2}} = (\bar{p}_0^T r_0)^{\frac{1}{2}}$ $2n$

$$\Sigma\ \zeta(K_\sigma) + \kappa(K_\sigma) + \mu(M) + 2n$$

2. for $j = 1, 2, \ldots, m$:

    a. $q_j = r_{j-1}/\beta_j$ $2n$

    b. $p_j = \bar{p}_{j-1}/\beta_j$ $2n$

    c. $\bar{r}_j = K_\sigma^{-1} p_j$ $\kappa(K_\sigma)$[2]

    d. $\hat{r}_j = \bar{r}_j - q_{j-1}\beta_j$ $2n$

    e. $\alpha_j = q_j^T M \hat{r}_j = p_j^T \hat{r}_j$ $2n$

    f. $r_j = \hat{r}_j - q_j\alpha_j$ $2n$

    g. $\bar{p}_j = Mr_j$ $\mu(M)$[3]

    h. $\beta_{j+1} = (r_j^T M r_j)^{\frac{1}{2}} = (\bar{p}_j^T r_j)^{\frac{1}{2}}$ $2n$

$$\Sigma\ \kappa(K_\sigma) + \mu(M) + 12n$$

    end

---

[1] $\zeta(K_\sigma)$ represents number of operations to factorize K_σ

[2] $\kappa(K_\sigma)$ represents number of operations to solve with K_σ

[3] $\mu(M)$ represents number of operations to compute Mr

Table 4.2   The load–dependent Lanczos algorithm for a symmetric *indefinite* matrix pencil (B_σ, A) with operation count in flop.

Given a load vector $\hat{g}$:   Op. count

1. **initialize**

     a.   factorize B_σ $\zeta(B_\sigma)$[1]

     b. $q_0 = 0$

     c. $r_0 = B_\sigma^{-1}\hat{g}$ $\kappa(B_\sigma)$[2]

     d. $\bar{p}_0 = A r_0$ $\mu(A)$[3]

     e. $\beta_1 = |r_0^T A r_0|^{\frac{1}{2}} = |\bar{p}_0^T r_0|^{\frac{1}{2}}$ $4n$

     f. $\delta_1 = \text{sign}(\bar{p}_0^T r_0)$

$$\Sigma\ \zeta(B_\sigma) + \kappa(B_\sigma) + \mu(A) + 4n$$

2. **for $j = 1, 2,..., m$:**

     a. $q_j = r_{j-1}(\delta_j/\beta_j)$ $4n$

     b. $p_j = \bar{p}_{j-1}(\delta_j/\beta_j)$ $4n$

     c. $\bar{r}_j = B_\sigma^{-1} p_j$ $\kappa(B_\sigma)$[2]

     d. $\hat{r}_j = \bar{r}_j - q_{j-1}(\beta_j/\delta_{j-1})$ $4n$

     e. $\alpha_j = q_j^T A \hat{r}_j = p_j^T \hat{r}_j$ $4n$

     f. $r_j = \hat{r}_j - q_j(\alpha_j/\delta_j)$ $4n$

     g. $\bar{p}_j = A r_j$ $\mu(A)$[3]

     h. $\beta_{j+1} = |r_j^T A r_j|^{\frac{1}{2}} = |\bar{p}_j^T r_j|^{\frac{1}{2}}$ $4n$

     i. $\delta_{j+1} = \text{sign}(\bar{p}_j r_j)$

$$\Sigma\ \kappa(B_\sigma) + \mu(A) + 24n$$

     end

---

[1] $\zeta(B_\sigma)$ represents number of operations to factorize B_σ

[2] $\kappa(B_\sigma)$ represents number of operations to solve with B_σ

[3] $\mu(A)$ represents number of operations to compute $A r$

Some remarks should be made concerning the computer implementations of the algorithms in Table 4.1 and 4.2. In exact arithmetic (no round–off errors) the orthogonality between all the Lanczos vectors is obtained by orthogonalization with respect to the two preceding vectors at each step in the algorithm. However, due to the round–off errors introduced in finite precision, the orthogonality with respect to earlier vectors might be lost, and this is discussed next.

We define the unit round–off error ϵ as the smallest positive number recognized by the computer to satisfy the relation $1 + \epsilon > 1$. The value of ϵ is computer-dependent; however, a typical value in double precision is 10^{-14}.

We introduce a measure of orthogonality such that for the algorithm in Table 4.1 we define

$$h_{ij} = \mathbf{q}_i^T \, \mathbf{M} \, \mathbf{q}_j \qquad (4.110)$$

or in the case of an indefinite matrix in Table 4.2

$$h_{ij} = \mathbf{q}_i^T \, \mathbf{A} \, \mathbf{q}_j \qquad (4.111)$$

In exact arithmetic we expect the value of h_{ij} to be such as

$$| \, h_{ij} \, | = \delta_{ij} \qquad (4.112)$$

where δ_{ij} is the Kronecker delta. In finite precision arithmetic we would have

$$| \, h_{ij} \, | = \begin{cases} 1 & i = j \\ \leq n\epsilon & i \neq j \end{cases} \qquad (4.113)$$

However, due to accumulated round–off the output from the algorithm might be such as

$$| \, h_{ij} \, | = \begin{cases} 1 & i = j \\ > n\epsilon & i \neq j \end{cases} \qquad (4.114)$$

Various reorthogonalization schemes have been formulated to maintain near global orthogonality of the Lanczos vectors. A straightforward method to implement is a full reorthogonalization (FRO) at each step of the Lanczos iteration, i.e. the vector r_j, computed with the three–term recurrence, is explicitly orthogonalized with respect to all previous Lanczos vectors using a modified Gram–Schmidt process [34].

In the definite algorithm we apply a modified Gram—Schmidt process to force r_j orthogonal to the previous set of vectors q_1, ... q_j according to

for $i = 1, 2, 3, ..., j$
$$c_i = q_i^T M r_j = q_i^T \bar{p}_j$$
$$r_j = r_j - c_i q_i$$
end
$\qquad\qquad\qquad\qquad\qquad\qquad\qquad$ (4.115)

which in the algorithm for an indefinite matrix pencil will read

for $i = 1, 2, 3, ..., j$
$$c_i = q_i^T A r_j = q_i^T \bar{p}_j$$
$$r_j = r_j - (c_i/\delta_i) q_i$$
end
$\qquad\qquad\qquad\qquad\qquad\qquad\qquad$ (4.116)

In this way the Lanczos vectors are orthogonal up to round—off level according to Eq. (4.113).

These orthogonalization schemes are appended at the end of the algorithm in Table 4.1 and 4.2 (after step 2.h and 2.i) respectively. Each orthogonalization with respect to a single previous set of j vectors consists of j dot products and j saxpy operations, or in total $j(4n)$ floating point operations. The cumultative cost of a full reorthogonalization grows as the iteration number squared, viz. $(1 + 2 + ... + j)(4n) \simeq 2j^2 n$ and can be quite burdensome for large problems. For example, for $n = 10\ 000$ and $j = 100$, a full reorthogonlization will require 200 Mflop.

However, recent research shows that *semi—orthogonality* between Lanczos vectors is sufficient, i.e. maintaining the h's at $\sqrt{\epsilon}$ level [69]. By maintaining semi—orthogonality the resulting Ritz values, according to Eq. (4.63), are as accurate as with full reorthogonalization. Following this approach also for the load—dependent algorithms we thus require

$$| h_{ij} | = \begin{cases} 1 & i = j \\ \leq \sqrt{\epsilon} & i \neq j \end{cases}$$
$\qquad\qquad\qquad\qquad\qquad\qquad\qquad$ (4.117)

It has been observed that the growth of round—off errors follows a regular pattern in terms of h_{ij} and that we do not need to compute all these quantities explicitly. In fact at the end of iteration j we may check the orthogonality state between the previous set of j Lanczos vectors and the new Lanczos vector $q_{j+1} = r_j/\beta_{j+1}$, by a recurrence formula derived in [69]. For the definite problem we may define a $(j+1) \times (j+1)$ matrix such that

$$H_{j+1} = Q_{j+1}^T M Q_{j+1} - I_{j+1} \qquad (4.118)$$

where in exact arithmetic $H_{j+1} = 0$. We monitor the growth of round–off error during the course of the Lanczos process by

$$h_{j+1} \simeq \frac{1}{\beta_{j+1}} [T_{j-1} h_j - \alpha_j h_j - \beta_j h_{j-1}] \qquad (4.119)$$

where the orthogonality state given by coefficients in the vector h_{j+1} may be computed by the elements of T_{j-1} and the two previous columns in H, i.e. h_j and h_{j-1}, see [53, 69] for details.

In the present implementation we have adopted the partial reorthogonalization scheme similar to the one used in [69]. The reorthogonalization needs only to be performed with respect to those vectors q_i for which $(h_{j+1})_i$ indicates loss of semi–orthogonality. However, we will simply reorthogonalize q_{j+1} against *all* previous Lanczos vectors if any of the elements of h_{j+1} exceeds $\sqrt{\epsilon}$. Then the value of h_j and h_{j+1} is reset to $\epsilon\sqrt{n}$ and the Lanczos algorithm is continued. Full orthogonalization is performed again as round–off errors accumulated by equation (4.119) are built up to the level of $\sqrt{\epsilon}$. For more details, see [53, 69].

This scheme has been found to accurately compute the desired solution for the definite problem in our applications. By combining the semi–orthogonality condition and partial reorthogonalization (PRO) the resulting response is as accurate as the one obtained with the full reorthogonalization scheme (FRO). But a great many of the reorthogonalization steps are eliminated.

A similar relation to Eq. (4.119) may be found for the indefinite algorithm in Table 4.2 [13]. However, for simplicity we choose to use a full reorthogonalization (FRO) in this case.

4.3   Hessenberger reduction by Arnoldi vectors

4.3.1   Introduction

The symmetric systems of equations on generalized form derived in Chapter 3 were achieved at the cost of either a very sparse coefficient matrix with two fluid degrees—of—freedom per fluid node or a full coefficient matrix with one degree—of—freedom per fluid node, cf. Eqs. (3.32) and (3.39). The unsymmetric systems Eq. (3.46) and Eq. (3.47) have a sparse matrix structure with one single degree—of—freedom per node in the fluid domain, although unsymmetric.

In this chapter we will study the reduction of unsymmetric systems of equations. We will extend the method of Arnoldi [4, 34] to a generalized problem with unsymmetric matrices K and M. The resulting Arnoldi vectors are used to reduce the system of differential equations to a smaller set of equations of upper Hessenberg form. A similar method has been used recently for a convection—diffusion problem with a symmetric M and an unsymmetric K matrix, see [57]. Krylov subspace methods for solving unsymmetric linear systems of equations are discussed in [64, 65].

4.3.2   Unsymmetric definite matrix pencil

The unsymmetric systems of equation (3.46) and (3.47) may be written symbolically in the form

$$M\ \ddot{u} + K\ u = f(t) \tag{4.123}$$

in which M and K are $n \times n$ unsymmetric matrices and $f(t)$ is the time–dependent external load. The solution vector u thus includes the structure subvector u_s and either of the fluid vectors p or Ψ.

Orthogonalization of Krylov vectors

We transform the problem to

$$K_\sigma^{-1}\ M\ \ddot{u} + (I + \sigma K_\sigma^{-1}M)u = K_\sigma^{-1}f(t) \tag{4.124}$$

by multiplying with the inverse to $K_\sigma = K - \sigma M$.

The Arnoldi algorithm performs a sequence of matrix–vector operations using the unsymmetric dynamic matrix $K_\sigma^{-1}M$ and a starting vector r_0 to produce a set of orthonormal Arnoldi vectors as the base for the Krylov subspace

$$\mathcal{K}^m(K_\sigma^{-1}M, r_0) \equiv span\{r_0, K_\sigma^{-1}M\, r_0, ..., (K_\sigma^{-1}M)^{m-1}\, r_0\} \qquad (4.125)$$

The resulting Arnoldi vectors may then be used to approximate a solution $u(t)$ to Eq. (4.124) through

$$u(t) \approx u_m(t) = V_m x_m(t) \qquad (4.126)$$

in which x_m contains the generalized Arnoldi coordinates.

At a typical step j, the algorithm orthogonalizes the next vector in the Krylov sequence $K_\sigma^{-1}Mv_j$ against all the previous j Arnoldi vectors, thus

$$r_j = \eta_{j+1,j}\, v_{j+1} = K_\sigma^{-1}Mv_j - \sum_{i=1}^{j} \eta_{i,j}v_i \qquad (4.127)$$

where

$$\eta_{i,j} = v_i^T\, K_\sigma^{-1}Mv_j \qquad (4.128)$$
$$\eta_{j+1,j} = \|\, r_j\, \| \qquad (4.129)$$

After m steps in the Arnoldi algorithm we have obtained

$$K_\sigma^{-1}MV_m = V_m H_m + r_m e_m^T \qquad (4.130)$$

where $V_m = [v_1, v_2, ..., v_m]$ is a matrix holding the Arnoldi vectors and H_m is an upper Hessenberg matrix that holds all the coefficients in the orthogonalization procedure such that

$$H_m = \begin{bmatrix} \eta_{1,1} & \eta_{1,2} & \eta_{1,3} & \cdot & \cdot & \cdot & \eta_{1,m} \\ \eta_{2,1} & \eta_{2,2} & \eta_{2,3} & \cdot & \cdot & \cdot & \eta_{2,m} \\ & \eta_{3,2} & \eta_{3,3} & \cdot & \cdot & \cdot & \eta_{3,m} \\ & & \eta_{4,3} & & & & \\ & & & \cdot & & & \\ & & & & \cdot & & \\ & & & & \eta_{m,m-1} & \eta_{m,m} \end{bmatrix} \qquad (4.131)$$

$$r_m e_m^T$$
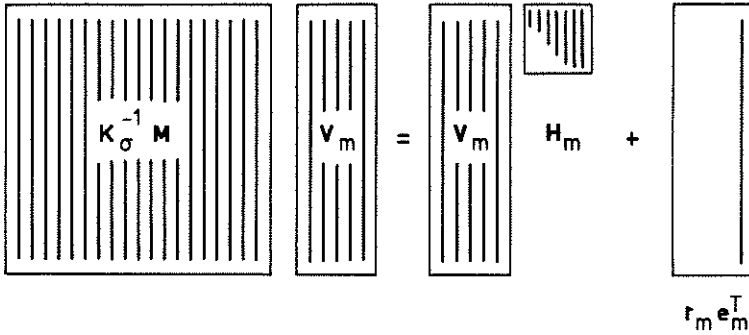
Fig. 4.3   The matrix form of the recurrence formula for the unsymmetric definite problem

The Arnoldi vectors satisfy the orthogonality condition

$$V_m^T V_m = I_m \tag{4.132}$$

We premultiply Eq. (4.130) by V_m^T and get

$$V_m^T K_\sigma^{-1} M V_m = V_m^T V_m H_m + 0 \tag{4.133}$$

and by Eq. (4.132) it follows that

$$H_m = V_m^T K_\sigma^{-1} M V_m \tag{4.134}$$

Reduction of system of equations to upper Hessenberg form

We express the approximate solution to the transformed equation by using the Arnoldi vectors according to Eq. (4.126). Substituting this approximate solution in Eq. (4.124) we form the residual as

$$d_m(t) = K_\sigma^{-1} M V_m \ddot{x}_m + (I + \sigma K_\sigma^{-1} M) V_m x_m - K_\sigma^{-1} f(t) \tag{4.135}$$

where the free parameter in x_m is calculated by applying the Galerkin condition in Eq. (4.6), i.e.

$$V_m^T d_m(t) = 0 \tag{4.136}$$

Substituting Eq. (4.135) in (4.136) results in

$$V_m^T K_\sigma^{-1} M V_m \ddot{x}_m + (V_m^T V_m + \sigma V_m^T K_\sigma^{-1} M V_m) \ddot{x}_m = V_m^T K_\sigma^{-1} f(t) \tag{4.137}$$

which by use of Eq. (4.132) and (4.134) can be rewritten as

$$H_x \ddot{x}_m + (I_m + \sigma H_m) x_m = f_m(t) \tag{4.138}$$

and hence the transformed equation (4.124) has been reduced to upper Hessenberger form.

To make optimum use of the information about the problem to be solved we start the Arnoldi algorithm with a vector in the direction of the right–hand side in Eq. (4.124), i.e.

$$r_0 = K_\sigma^{-1} \hat{f} \tag{4.139}$$

where $\hat{f}$ is the spatial variation of the load $f(t) = \hat{f} \gamma(t)$. In that case the right–hand side in the reduced system of equation Eq. (4.93) may be simplified as

$$\begin{aligned}
f_m(t) &= V_m^T K_\sigma^{-1} \hat{f}(t) \\
&= V_m^T K_\sigma^{-1} \hat{f} \gamma(t) \\
&= V_m^T r_0 \hat{f} \gamma(t) \\
&= V_m^T v_1 \eta_{1,0} \hat{f} \gamma(t) \\
&= V_m^T V_m e_1 \eta_{1,0} \hat{f} \gamma(t) \\
&= e_1 \eta_{1,0} \gamma(t)
\end{aligned} \tag{4.140}$$

where $\eta_{1,0}$ is the norm of the starting vector r_0 and e_1 is the first column in the identity matrix. Thus Eq. (4.138) takes the simple form

$$H_m \ddot{x}_m + (I_m + \sigma H_m) x_m = e_1 \eta_{1,0} \gamma(t) \tag{4.141}$$

This equation of size $m \times m$ may be solved by a suitable time integration scheme or through a modal decomposition. An implicit method requires the solution of a linear system of equations with an upper Hessenberg coefficient matrix.

Error estimate

The time–dependent residual vector $\mathbf{d}_m(t)$ in Eq. (4.135) may be used to derive an error estimate similar to the one given in [57]. By substituting Eq. (4.133) in Eq. (4.135) we obtain

$$
\begin{aligned}
\mathbf{d}_m(t) &= (\mathbf{V}_m\mathbf{H}_m + \mathbf{r}_m\mathbf{e}_m^T)\ddot{\mathbf{x}}_m + \mathbf{V}_m\mathbf{x}_m + \sigma(\mathbf{V}_m\mathbf{H}_m + \mathbf{r}_m\mathbf{e}_m^T)\mathbf{x}_m - \mathbf{K}_\sigma^{-1}\hat{\mathbf{f}}\gamma(t) = \\
&\mathbf{V}_m[\mathbf{H}_m\ddot{\mathbf{x}}_m + (\mathbf{I}_m + \sigma\mathbf{H}_m)\mathbf{x}_m - \mathbf{e}_1\eta_{1,0}\gamma(t)] + \mathbf{r}_m(\mathbf{e}_m^T\ddot{\mathbf{x}}_m + \sigma\mathbf{e}_m^T\mathbf{x}_m)
\end{aligned}
\tag{4.142}
$$

where we have used $\mathbf{K}_\sigma^{-1}\hat{\mathbf{f}}\gamma(t) = \mathbf{r}_0\gamma(t) = \mathbf{V}_m\mathbf{e}_1\eta_{1,0}\mathbf{r}\gamma(t)$

The Arnoldi coordinates kept in $\mathbf{x}_m$ were calculated to satisfy Eq. (4.141) and thus the term in the square brackets becomes identically zero. The Eq. (4.142) now reads

$$
\mathbf{d}_m(t) = \mathbf{r}_m\mathbf{e}_m^T(\ddot{\mathbf{x}}_m + \sigma\mathbf{x}_m)
\tag{4.143}
$$

We compute the norm of $\mathbf{d}_m(t)$ such as

$$
\|\mathbf{d}_m\| = \|\mathbf{r}_m\| \, |\ddot{\chi}_m + \sigma\chi_m| = \eta_{m+1,m}|\ddot{\chi}_m + \sigma\chi_m|
\tag{4.144}
$$

where $\ddot{\chi}_m$ and χ_m are the bottom elements of the vectors $\ddot{\mathbf{x}}_m$ and $\mathbf{x}_m$, respectively. Thus, the norm of the residual may be monitored in the course of the time integration. An error function relating the norm of the residual to the norm of the loading function in the transformed equation (4.124) would read

$$
e(t) = \frac{\|\mathbf{d}_m(t)\|}{\|\mathbf{r}_0\gamma(t)\|} = \frac{\eta_{m+1,m}}{\eta_{1,0}}\frac{|\ddot{\chi}_m + \sigma\chi|}{|\gamma(t)|}
\tag{4.145}
$$

This function may then be used to monitor the error in the transient response in the reduced system of equations, compared to the response expected from a direct solution of the original unreduced system of equations (with an identical time integrator). We observe that if the norm of the residual vector vanishes, i.e. goes towards the round–off level ϵ, the error in the solution will be zero, implying that the computed Arnoldi vector have spanned the whole solution space.

The term $|\gamma(t)|$ may be set at the maximum value max $(|\gamma(t)|)$ in order to ensure a proper error function also for $\gamma(t) = 0$. One solution strategy would be to generate a chosen number of Arnoldi vectors, solve the reduced problem Eq. (4.141) and monitor the value of $e(t)$. Once this value exceeds a given tolerance the Arnoldi algorithm is restarted to extend the subspace spanned by the Arnoldi vectors. After that more Arnoldi vectors are added to this space and the time integration is started over.

4.3.3   Numerical implementation

The load–dependent Arnoldi algorithm is shown in Table 4.3. The algorithm is provided with the matrices $\mathbf{M}$ and $\mathbf{K}_\sigma$ and a load vector $\hat{\mathbf{f}}$. After the initialization stop the Arnoldi vectors are computed. Typically, one matrix multiplication with $\mathbf{M}$ and one solution with $\mathbf{K}_\sigma$ as the coefficient matrix are performed in each iteration. These calculations may be performed by calls to subroutines that take full advantage of the structure of these matrices. In the unsymmetric formulations of structure–acoustic systems, see Eqs. (3.46) and (3.47), the unsymmetric terms are the coupling matrices whereas the main part of the system matrices is symmetric. Unsymmetric equation solvers are discussed in [76, 77, 79].

A modified Gram–Schmidt procedure is applied in order to orthogonalize the new Krylov vector in each iteration. Loss of orthogonality among the Arnoldi vectors is an issue also in this algorithm. We therefore suggest that the orthogonalization procedure in step 2.d and 2.e is performed twice in each iteration.

The Arnoldi method may be seen as an extension of the Lanczos algorithm for unsymmetric matrices. In the case of Lanczos, the symmetry of $\mathbf{M}\mathbf{K}_\sigma^{-1}\mathbf{M}$ resulted in the three–term recurrence formula. When $\mathbf{K}_\sigma$ and $\mathbf{M}$ are not symmetric one alternative to the Arnoldi method is to generate two subspaces, the left and right Krylov subspace, respectively. This approach, leading to the unsymmetric Lanczos method, has been used recently in structure–acoustic applications [63]. The unsymmetric Lanczos method requires two solve in each iteration and orthogonalization against two sets of vectors, the left and right Lanczos vectors, respectively, see [34] for details.

Table 4.3 The load–dependent Arnoldi algorithm for an unsymmetric *definite* matrix pencil (K_σ, M) with operation count in flop.

Given a load vector $\hat{f}$:   Op. count

1. **initialize**

   a. factorize K_σ $\zeta(K_\sigma)^{1)}$

   b. $v_0 = 0$

   c. $r_0 = K_\sigma^{-1}\hat{f}$ $\kappa(K_\sigma)^{2)}$

   d. $\eta_{1,0} = (r_0^T r_0)^{1/2}$ $2n$

   $$\Sigma\ \zeta(K_\sigma) + \kappa(K_\sigma) + 2n$$

2. **for** $j = 1, 2, ..., m$:

   a. $v_j = r_{j-1}/\eta_{j,j-1}$ $2n$

   b. $p_j = Mv_j$ $\mu(M)^{3)}$

   c. $r_j = K_\sigma^{-1} p_j$ $\kappa(K_\sigma)^{2)}$

   d. **for** $i = 1, 2, ..., j$ $j\,(4n)$

   $\quad\quad \eta_{i,j} = v_i^T r_j$

   $\quad\quad r_j = r_j - \eta_{i,j} v_i$

   $\quad$ **end**

   e. $\eta_{j+1,j} = (r_j^T r_j)^{1/2}$ $2n$

   $$\Sigma\ \mu(M) + \kappa(K_\sigma) + j\,(4n) + 4n$$

   end

---

[1] $\zeta(K_\sigma)$ represents number of operations to factorize K_σ

[2] $\kappa(K_\sigma)$ represents number of operations to solve with K_σ

[3] $\mu(M)$ represents number of operations to compute Mv

5 NUMERICAL EXAMPLES

5.1 Introduction

In this chapter we apply the reduced base techniques described in Chapter 4 to one— and two—dimensional structure—acoustic problems. The Lanczos process is applied to symmetric systems of equations with a positive definite matrix pencil (K_σ, M) or alternatively to systems with an indefinite matrix pencil (B_σ, A) in the case of non—proportional damping. The Arnoldi process is applied to unsymmetric systems of equations and a comparison with the Lanczos result is given with respect to accuracy and computational effort.

The numerical studies presented in this chapter have been performed utilizing the computer program CAMFEM (Computer Aided Modelling based the the Finite Element Method) [23]. CAMFEM is based on a command language, i.e. the computational procedure is defined by commands given by the user. The problem independent program structure includes commands for facilities needed in most computations. By supplementing the problem independent program structure with problem dependent program modules a special purpose program can be rapidly obtained.

Both transient and harmonic analysis are performed in order to show the characteristics and applicability of the reduced base techniques. In transient analysis the time integration can be performed with implicit, explicit or mixed implicit—explicit methods [37]. In this study we will use an implicit scheme of Newmark type for the second—order systems of equations and a central—difference scheme for the first-order systems. The fluid mass matrix is made diagonal in all calculations by a lumping technique proposed in [36].

The first numerical example is a fluid—filled pipe with spring supported piston for which an exact analytical solution can be obtained. This one—dimensional example has been used extensively in previous work for verification of eigenfrequencies and response functions obtained by a direct solution of the finite element equations [8, 9]. We will first refer to some results from these studies in order to illustrate the solution to a simple coupled structure—acoustic problem.

We consider a tube of length L and unit cross—sectional area A, terminated by a rigid, movable plug of mass m and supported by a spring with stiffness k see Fig. 5.1. The tube is filled with water.
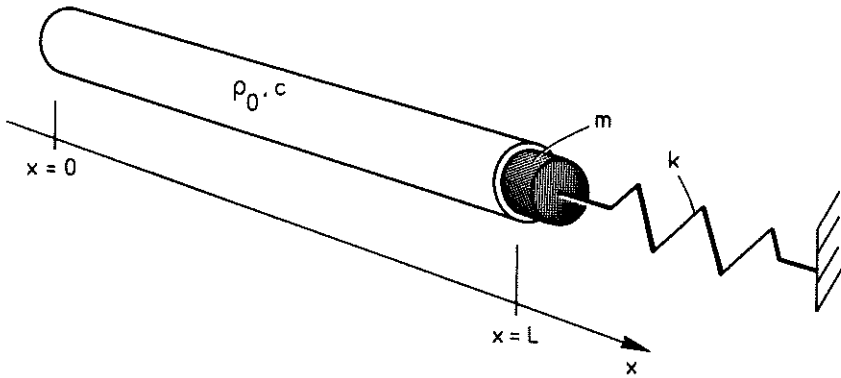
Fig. 5.1   Rigid wall cylinder filled with water and with a spring supported piston.
c = 1500 m/s, ρ_0 = 1000 kg/m³, L = 3 m, A = 1 m², m = 200 kg,
k = 493.48 MN/m

The eigenfrequencies of this system can be analytically determined by

$$\lambda_i^2 - [\, \frac{\rho_0 cA}{m} \cot (\, \frac{\lambda_i L}{c}\,)]\, \lambda_i - \frac{k}{m} = 0 \qquad\qquad (5.1)$$

with notations from Fig. 5.1, derived from [74].

With parameters chosen according to Fig. 5.1 we have a hard—coupled system with a very clear separation of eigenfrequencies, see Table 5.1.

Table 5.1   Analytical coupled and uncoupled eigenfrequencies in (Hz)

Uncoupled	Coupled
250.0[1)]	143.974
250.0[2)]	362.44
500.0[2)]	594.07
750.0[2)]	830.18

[1)] Structural mode

[2)] Fluid mode

Transfer functions that relate a harmonically varying force $f(t) = \hat{f} \sin\bar{\omega}t$, applied to the structure, and the resulting piston displacement or fluid pressure at the surface of the piston were derived in [9]. The transfer function H_u for the displacement of the piston is defined by

$$\hat{u}_s = H_u \hat{f} \tag{5.2}$$

where $\hat{u}$ is the piston displacement amplitude and

$$H_u = \left[\frac{1}{k - \bar{\omega}^2 m + \rho_0 cA\bar{\omega}\cot(\frac{\bar{\omega}L}{c})} \right] \tag{5.3}$$

The transfer function for the dynamic fluid pressure amplitude $\hat{p}$ at the piston surface is defined by

$$\hat{p} = H_p \hat{f} \tag{5.4}$$

where

$$H_p = \left[\frac{1}{\left[\frac{k - \bar{\omega}^2 m}{-\rho_0 cA\bar{\omega}\cot(\frac{\bar{\omega}L}{c})} \right]} \right] \tag{5.5}$$

Clearly, for a unit amplitude force $\hat{f} = 1$ it follows that $\hat{u}_s = H_u$ and $\hat{p} = H_p$.

The result from a frequency analysis with a resolution of 1 Hz is shown in Fig. 5.2 where a comparison with the analytical transfer function can also be made. The fluid domain was discretized in the finite element analysis by five one–dimensional three–node elements with quadratic shape functions approximating the fluid pressure. An unsymmetric (u_s, p)–formulation according to Eq. (3.46) was thus used in Fig. 5.2. Identical results were obtained by the symmetric (u_s, Ψ, p)–formulation Eq. (3.32) and by the symmetric (u_s, Ψ)–formulation according to Eq. (3.39). It is clear from Fig. 5.2 that the finite element approximation is very good both in frequency and in magnitude. Actually, with five fluid elements the four lowest eigenfrequencies were captured within an error of less than 1 percent compared to the analytical solution. For more details, see references [8, 9].
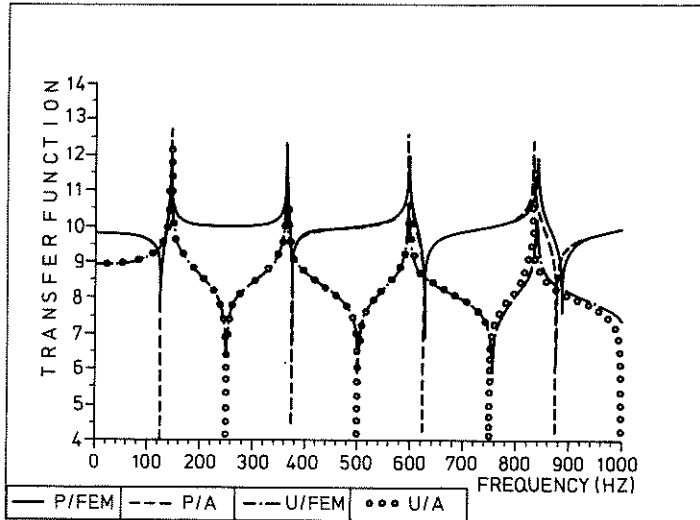
Fig. 5.2   Comparison between finite element (/FEM in the legend) and analytically (/A
in the legend) calculated transfer functions H_u Eq. (5.3) and H_P Eq. (5.5).
The data are adjusted along the y—axis in the following manner:
Pressure (P): $y = {}^{10}\log|H_P| + 10$
Displacement (U): $y = {}^{10}\log|H_u| + 18$

5.2   Fluid—filled pipe with spring supported piston

In this section we illustrate the use of Lanczos vectors in one—dimensional structure—acoustic
problems. For simplicity, all numerical examples are based on the same model, the rigid wall
cylinder shown in Fig. 5.3. The cylinder with a unit cross sectional area is filled with water
and closed by a spring supported piston at one end.

The fluid domains were discretized in the finite element analysis by one—dimensional fluid
elements with quadratic interpolation functions in both fluid pressure and fluid displacement—
potential. To capture the four lowest eigenfrequencies within an error of less than 1 percent
compared to the analytical solution, only five fluid elements are necessary, as shown above.
However, in the present study we are also interested in the high frequency content of the
solution and therefore we use a model with 50 fluid elements, see Fig. 5.4. This results in a
system of 201 degrees—of—freedom when Eq. (3.32) is used and 101 degrees—of—freedom

when Eq. (3.39) is used (after suppressing one degree–of–freedom in the displacement potential, i.e. setting $\Psi=0$ in any arbitrary chosen node in the fluid domain.)

We apply different loads to the system in Fig. 5.3. In the transient case we study the response to a structural load and to a fluid load, see Fig. 5.5. In the harmonic case we estimate the harmonic response function for a structural load in a certain frequency interval.
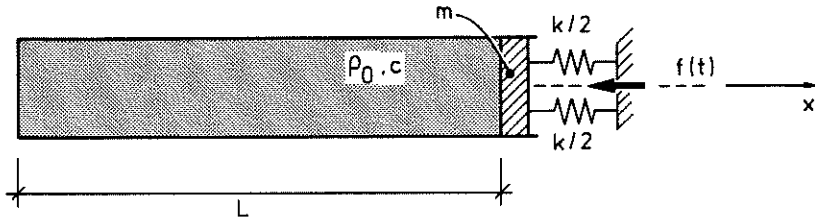
Fig. 5.3   Rigid wall cylinder with spring supported piston. $c = 1500$ m/s, $\rho_0 = 1000$ kg/m^3, $L = 3$ m, $A = 1$ m^2, $m = 200$ kg, $k = 493.48$ MN/m.
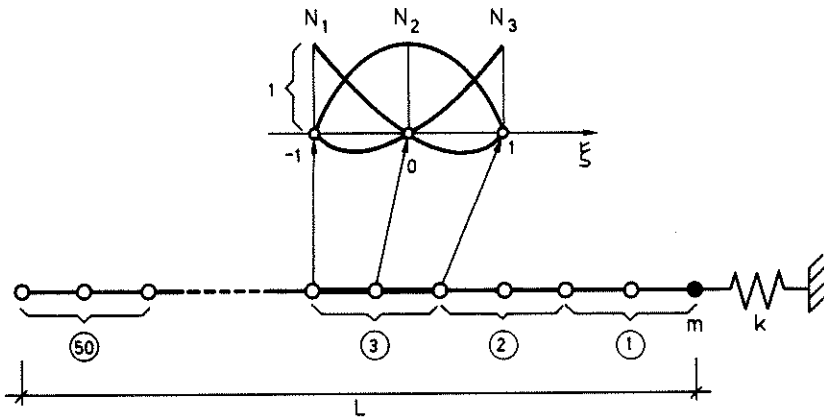
Fig. 5.4   The finite element mesh with 50 quadratic fluid elements.
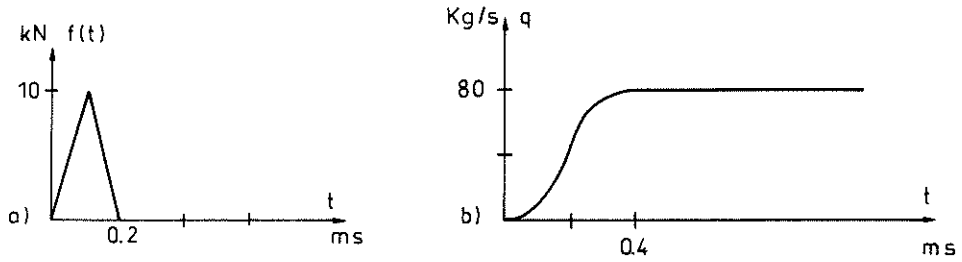
Fig. 5.5   a) Triangular pulse load applied to the piston. b) Fluid source function located at a distance 3L/4 from the piston end.

The time integration scheme in the transient case is the Newmark method [37] with $\beta=0.25$ and $\gamma=0.5$ (undamped) at the time step is 0.01 ms. The transient response curves are calculated in 600 time steps from 0–6 ms. In the harmonic case a resolution of 1.0 Hz is used to calculate the response function.

5.2.1   Impulsive structural load

A triangular pulse load is applied to the piston according to Fig. 5.5a. This is a typical wave propagation problem where a large number of vectors have to be used to trace the wave front accurately.

Fig. 5.6 compares the fluid pressure at the piston surface, obtained by direct solution of the two–field condensed system Eq. (3.39) with solution of the same system first reduced to the tridiagonal form (4.55), by using 25, 30, 35 Lanczos vectors respectively. No damping is considered and no frequency shift was used in this case $(\sigma=0)$. The pressure was recovered in both methods by a back–substitution in each step according to Eq. (3.38).

Fig. 5.6   Comparison of computed response due to structural load obtained by direct time integration of Eq. (3.39) [a) — c). Pressure at the piston surface (————), d) Piston displacement (————)] and the same quantities obtained by integration of the reduced system for different numbers of Lanczos vectors (— — — —).

We can readily follow the propagating wave in the system by studying the response in Fig. 5.6. The first peak at the piston is due to the impulsive load. This incident wave reaches the rigid end, is reflected, and returns at the "soft" end at 4.0 ms.

If we tridiagonalize the whole system of equations $(m=101)$ we get identical results comparing the direct method with the Lanczos method. From Fig. 5.6 we see that this is not necessary; in fact we obtain accurate results with only 35 Lanczos vectors $(m=35)$ in the pressure response. With 30 Lanczos vectors $(m=30)$ the error in the peak values is less than 10 %. With only 25 vectors $(m=25)$ the pressure response at the piston end shows some instability due to high—frequency oscillation of unconverged Ritz vectors, see Section 4.2.2. The corresponding displacement of the piston, see Fig. 5.6, is achieved accurately, however, for the same number of Lanczos vectors.

5.2.2   Impulsive fluid load

The excitation in this case is a sudden mass discharge in a section (we assume one–dimensional wave propagation) of the pipe located at a distance 3L/4 from the piston. The source function for this load is drawn in Fig. 5.5b. In this case the piston acts like a locally reacting surface with $\bar{m}$ and $\bar{k}$ given above and with $\bar{c} = 0$.

We use the uncondensed three–field form Eq. (3.32). We apply a frequency shift not too far from zero ($\sigma=200$ Hz) to remove the singularity of the original system of equations but allowing the fundamental modes to participate in the solution. The actual shift does not affect the solution as long as the same Lanczos vectors are obtained. A too large (positive) shift may cause the lowest modes to be missed, and these have in general a large participation factor in the superposed solution. The direct solution of Eq. (3.32) is compared to the results obtained when (3.32) is first reduced to tridiagonal form (4.55), by using 15, 20, 25 Lanczos vectors respectively. No damping is included.

In this case too we can readily follow the propagation of the disturbance through the pipe; see Fig. 5.7. The left–going wave hits the rigid end and is reflected. The direct right–going wave hits the piston after 1.5 ms followed by the once–reflected wave that arrives at 2.5 ms. Due to the direct wave and the once–reflected wave impinging on the piston after each other the piston displacement reaches its peak after 3.0 ms.

Only about 25 load–dependent Lanczos vectors are required to get the accurate pressure response. The accurate displacement response is captured with less than 15 Lanczos vectors.
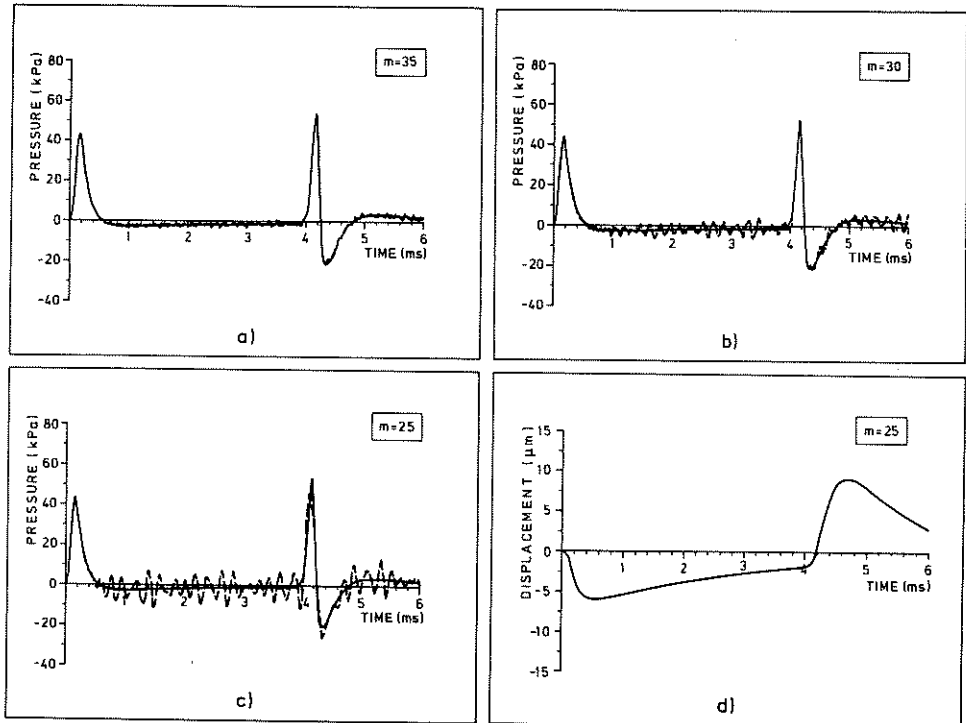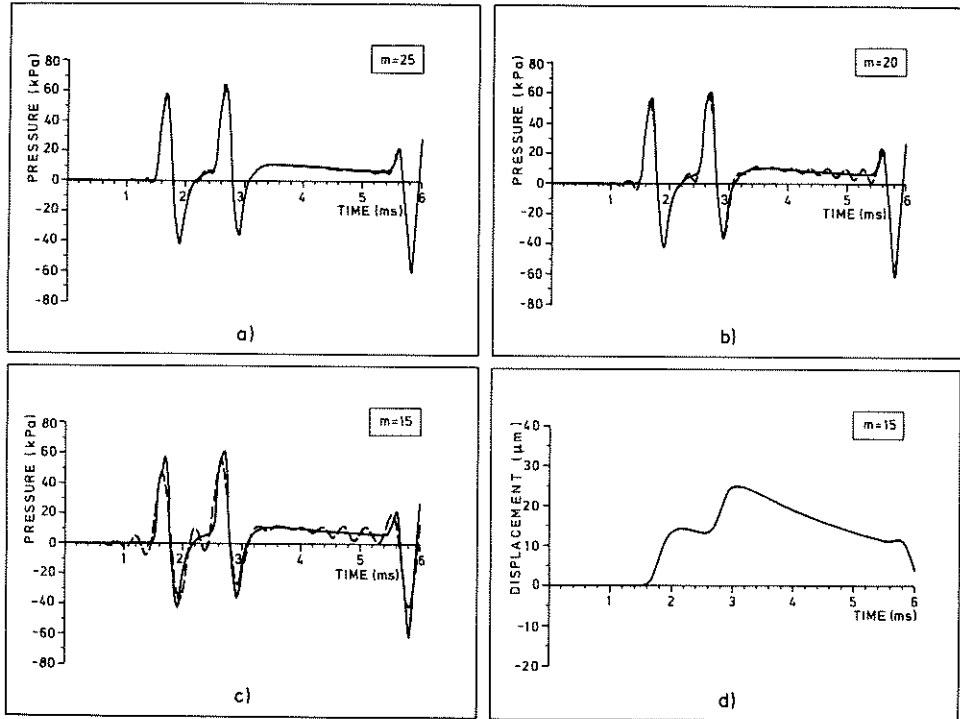
Fig. 5.7   Comparison of computed response due to fluid load obtained by direct time integration of Eq. (3.32) [a) – c). Pressure at piston surface (————), d) Piston displacement (————)] and the same quantities obtained by integration of the reduced system (4.55) for different numbers of Lanczos vectors (— — — —).

5.2.3   Harmonic structural load

We now make use of the simple form Eq. (4.56) to calculate the piston displacement versus frequency for an applied unit structural force. Let us assume that we are interested in the response in the frequency interval between 4.2 kHz and 5.2 kHz. We pick a shiftpoint inside the interval (actually the midpoint) $\sigma = 4.7$ kHz. Fig. 5.8 compares the direct harmonic solution of the condensed system Eq. (3.32) and the result obtained by Eq. (4.56) using only 5 Lanczos vectors ($m = 5$).

We see that the accurate response is achieved between 4.4 kHz and 4.9 kHz due to the two converged eigenvalues of T_m that can also be identified in the figure.

From Fig. 5.8 we can also identify the characteristics of the method. The eigenvalues closest to the shiftpoint converge first. With $m = 5$ we have five eigenvalues of the reduced system (4.56) (three of these can be found inside the interval shown above). Two of these eigenvalues of (4.56) have converged to the true eigenvalues of the (unreduced) system of equations (3.32). When m is increased the number of converged eigenvalues will also be increased.
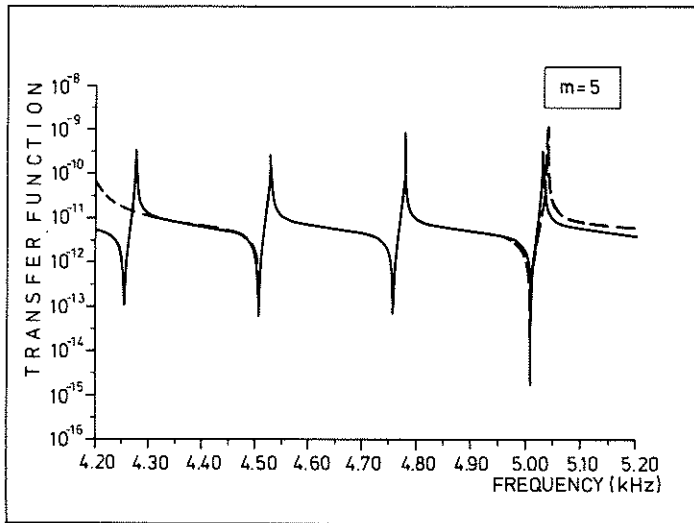
Fig. 5.8   Comparison of computed piston displacement versus frequency for an applied unit structural force obtained by the harmonic solution of Eq. (3.32) (————) and the solution of the reduced form Eq. (4.56) for five Lanczos vectors (— — — —).

5.3   Fluid–filled box with one flexible wall

In this section we apply the Lanczos process to a two–dimensional structure–acoustic problem. For simplicity, both transient and harmonic calculations are performed on the same model; the two–dimensional box shown in Fig. 5.9. The box is filled with water and has a flexible wall at the top. Taking advantage of symmetry of the box and the loading configuration, 5 beam elements with cubic interpolation and 75 fluid elements are used in the finite element calculation.

In this two–dimensional example, a Bernoulli–Euler beam theory is used modelling the flexible wall. Piecewise cubic Hermite shape functions are used to interpolate the structural displacements [37]. For the fluid elements quadratic interpolation functions in both fluid pressure and fluid displacement– potential are used. One–to–one element coupling is used and the coupling matrix M_c Eq. (3.24) is evaluated by numerical integration [37]. This discretization results in a system of 278 active degrees–of–freedom when Eq. (3.32) is used, after suppressing one degree–of–freedom in the displacement potential, i.e. setting $\Psi=0$ in any arbitrary chosen node in the fluid domain.

We apply different loads to the system in Fig. 5.9. In the transient case we study the response to triangular pulse load, see Fig. 5.10. In the harmonic case we estimate the harmonic response function for a structural load in a certain frequency interval.
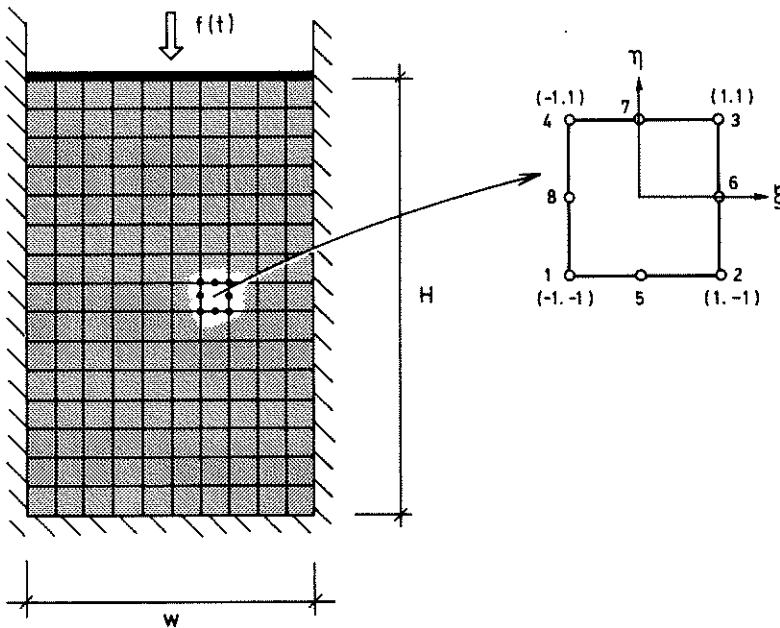
Fig. 5.9   Fluid–filled box with one flexible wall. Cavity: $H = 1.5$ m, $W = 1.0$ m, $c = 1500$ m/s, $\rho_0 = 1000$ kg/m^3. Steel plate: $E = 2.1 \cdot 10^{11}$ N/m^2, $\rho = 7800$ kg/m^3, thickness $t = 0.01$ m.
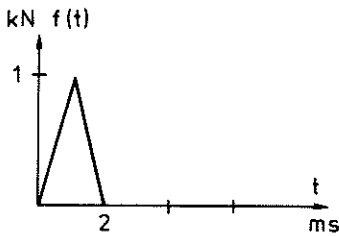
Fig. 5.10   Triangular pulse load applied to the midpoint of the plate.

The time integration scheme in the transient case is the Newmark method with $\beta = 0.25$ and $\gamma = 0.5$ (undamped) and the time step is 0.1 ms. The transient response curves are calculated in 200 time steps from 0–20 ms. In the harmonic case a resolution of 1.0 Hz is used to calculate the response function.

5.3.1   Impulsive structural load

The triangular pulse load with a peak force 1.0 kN and a duration of 2 ms, see Fig. 5.10, is applied to the plate.

Fig. 5.11 shows the plate midpoint displacement and the fluid pressure at the bottom surface of the box (midpoint), obtained by direct integration of the condensed system Eq. (3.39) and by solution of the same system reduced to the tridiagonal form Eq. (4.55) by different numbers of Lanczos vectors. No frequency shift was used in this case ($\sigma=0$). The pressure was recovered in both methods by a backsubstitution in each step according to Eq. (3.38). The structural response is captured with only 4 Lanczos vectors. The pressure response required 6 iterations to converge.
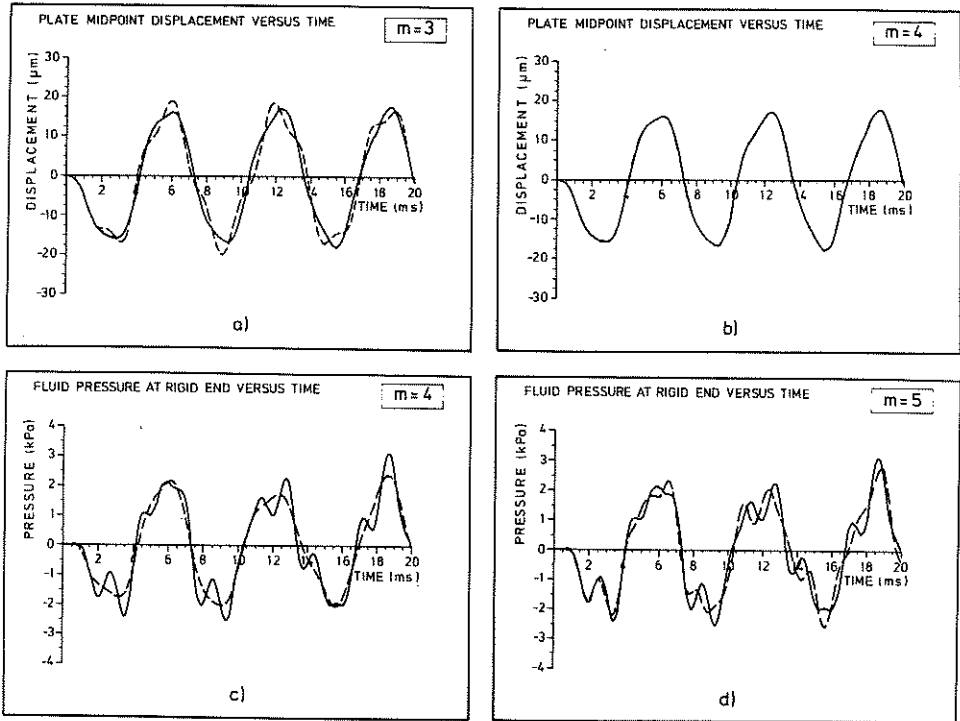
Fig. 5.11   Comparison of computed response due to structural load obtained by direct
time integration of Eq. (3.39) [a – b) Plate displacement (————), c) – d)
Pressure at the bottom surface (————)] and the same quantities obtained by
integration of the system Eq. (4.55) for different numbers of Lanczos vectors
(– – – –).

5.3.2   Harmonic structural load

We now make use of the tridiagonal form Eq. (4.56) to calculate the plate displacement versus frequency for an applied unit structural force. Let us assume that we are interested in the response in the frequency interval between 400 Hz and 800 Hz. We pick a shiftpoint inside the interval (actually the midpoint) $\sigma = 600$ Hz. Fig. 4.4 compares the direct harmonic solution of Eq. (3.39) (with no shift) and the result obtained by Eq. (4.58) with $\sigma = 600$ Hz using only 3 Lanczos vectors ($m = 3$).

From Fig. 5.12 we can again identify the characteristics of the method. The eigenvalues closest to the shiftpoint converge first. Two of the eigenvalues of the tridiagonal system Eq. (4.56) have converged to the true eigenvalues of the (unreduced) system of equations (3.39). When m is increased the number of converged eigenvalues will also be increased and the dashed line converge to the solid one.

PLATE MIDPOINT DISPLACEMENT VERSUS TIME $m = 3$
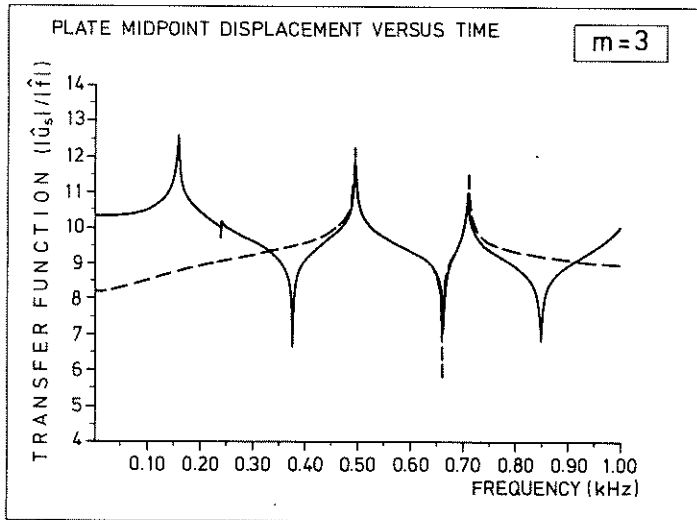
Fig. 5.12   Comparison of computed plate displacement versus frequency for an applied unit structural force plate midpoint obtained by the harmonic solution of Eq. (3.39) ($\sigma = 0$) (———) and the solution of the reduced form Eq. (4.56) for three Lanczos vectors ($\sigma = 600$ Hz) (— — — —).

5.3.3   A comparison between Lanczos and Arnoldi reduction

In Chapter 3 we derived formally equivalent symmetric and unsymmetric systems of equations for the undamped structure—acoustic problem. In this section we will compare the solution obtained by direct integration of these systems of equations with the solution obtained from the reduced systems, after the Lanczos process and Arnoldi process has been applied. For this comparison we will use the same model as described in Fig. 5.9.

Studying different choices of symmetric forms, it turns out that the coefficient matrix in the three—field form Eq. (3.32) has a very high condition number, defined as the ratio between the largest and smallest eigenvalue [34]. This was already indicated in Section 3.4, and for the model in Fig. 5.9, we get a condition number of order 10^{20} when using Eq. (3.32). Thus, we may expect large roundoff errors in each iteration of the Lanczos process if we try to reduce that problem by the algorithm in Table 4.1. However, the condensed two—field form Eq. (3.39) has a condition number of order 10^9 for the model in Fig. 3.9, and is preferable within this respect. This form was also used in the previous example.

Turning to the unsymmetric problem we may choose either Eq. (3.46) or Eq. (3.47). Interestingly we may note that, although these forms are quite similar in structure, their condition number is of different order. The pressure formulation used in Eq. (3.46) gives a condition number of order 10^{17} whereas we get a number of order 10^{13}, when using the displacement—potential formulation Eq. (3.47). Therefore we choose Eq. (3.47) to be reduced by the Arnoldi method.

We may now compare the results achieved when Eq. (3.47) is transformed to upper Hessenberg form according to Table 4.3 with the results obtained by the Lanczos process applied to Eq. (3.39). The transformed equations are solved for the loading function according to Fig. 5.10. The result is shown in Fig. 5.13 for different numbers of Lanczos and Arnoldi vectors respectively. The Lanczos results have converged to the solution obtained by direct integration with $m = 4$ (structural displacement) and $m = 6$ (fluid pressure), where m is the number of vectors in the reduced base. The convergence rate towards the direct solution is a bit slower in the unsymmetric case. An accurate solution is obtained with $m = 7$ (structural displacement) and $m = 10$ (fluid pressure).

5.16
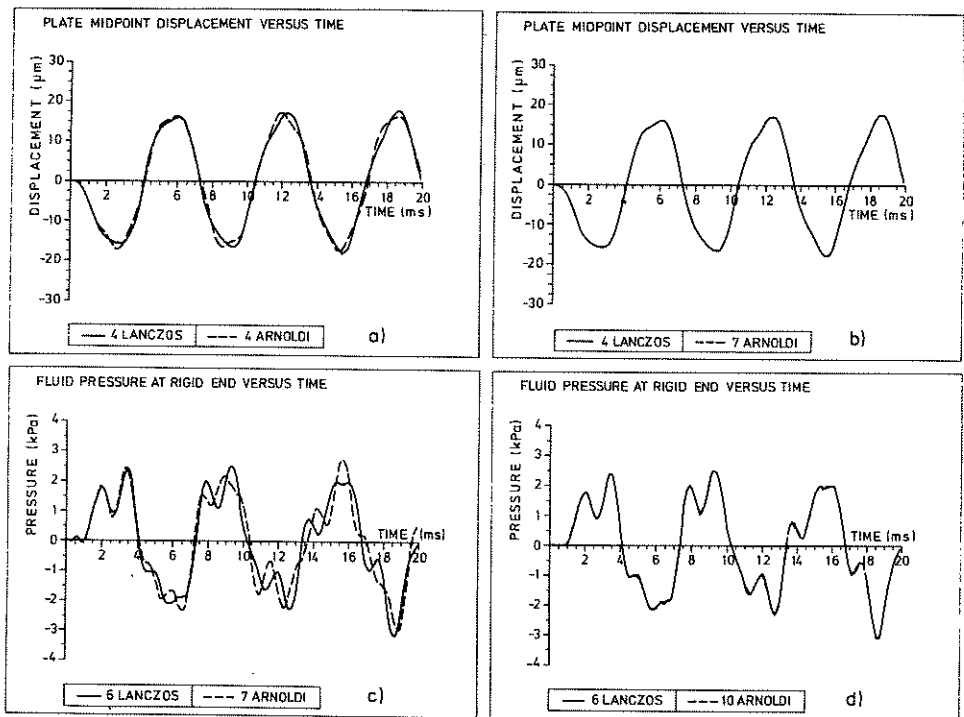
Fig. 5.13   Comparison of computed responsse due to the structural load in Fig. 5.10.
Eq. (3.39) is reduced to the tridiagonal form Eq. (4.55) by Lanczos vectors
(————) and Eq. (3.47) is reduced to Eq. (4.141) by Arnoldi vectors
(— — — —). [a–b) Plate displacement, c–d) Fluid pressure at bottom surface
(midpoint)].

Thus, we need more vectors in the reduced base when using the Arnoldi method compared
to the number of vectors required by the Lanczos process. However, although more iterations
are required in the Arnoldi algorithm than in the Lanczos algorithm, the computational effort
is far less using the Arnoldi method, in this example. Actually, the number of operations
required to obtain 10 Arnoldi vectors is a factor 16 lower than the number of operations
required to obtain 6 Lanczos vectors. A frequency shift ($\sigma = 100$ Hz) was used in Eq. (3.47)
to avoid the constant potential mode (CPM).

5.3.4 Non—proportionally damped system.

In our final example we will apply the indefinite Lanczos algorithm in Table 4.2, to a non—proportionally damped structure—acoustic system. In order to introduce a porous material we change the material data in our two—dimensional model, see Fig. 5.14. The cavity is thus filled with air and closed by a gypsum board. At the bottom of the cavity we have placed an porous absorber.
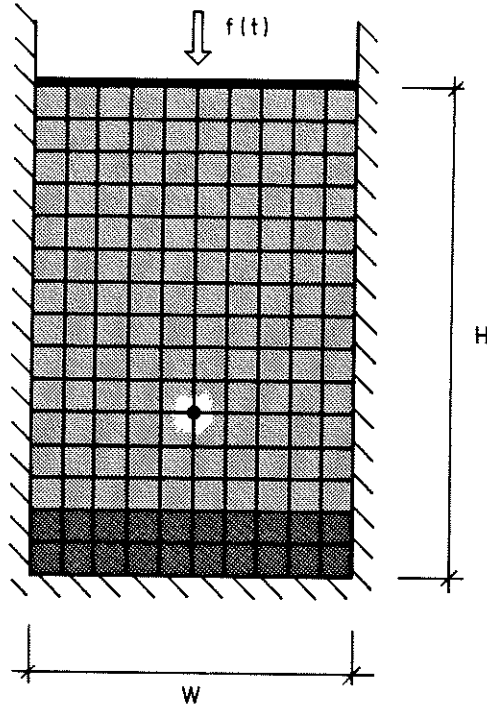
Fig. 5.14   Fluid—filled box with one flexible wall and an acoustic absorbent. Cavity: $H = 1.5$ m, $W = 1.0$ m, $c = 340$ m/s, $\rho_0 = 1.2$ kg/m^3.   Gypsum board: $E = 2.2 \cdot 10^9$ N/m^2, $\rho = 840$ kg/m^3, thickness $t = 0.023$ m. Absorbing material: $\Omega_v = 1$, $r_s = 8000$ Ns/m^4, $k_s = 4$, $c = 340$ m/s.

The two—field form Eq. (3.77), extended to include porous materials is used in this case. This system of equations is transformed to the equivalent first—order form Eq. (4.81). The number of unknowns is thus increased from 278 active degrees—of—freedom in the second—order system to 556 in the first—order system. By considering a loading configuration according to Fig. 5.14 the first—order system is tridiagonalized by the algorithm in Table 4.2 $(\sigma = 0)$.

A central difference scheme with $\alpha = 0.5$ and a time step 0.5 ms is used to solve the tridiagonal equations. The transient response shown in Fig. 5.16 and Fig. 5.17, is calculated in 280 time steps from 0–140 ms. An accurate response is achieved with 8 Lanczos vectors in this case and thus the time–integration performed in a considerably smaller system of equations, than the first–order system.
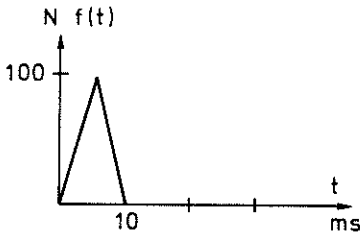
Fig. 5.15   Triangular pulse load applied to the midpoint of the gypsum board.
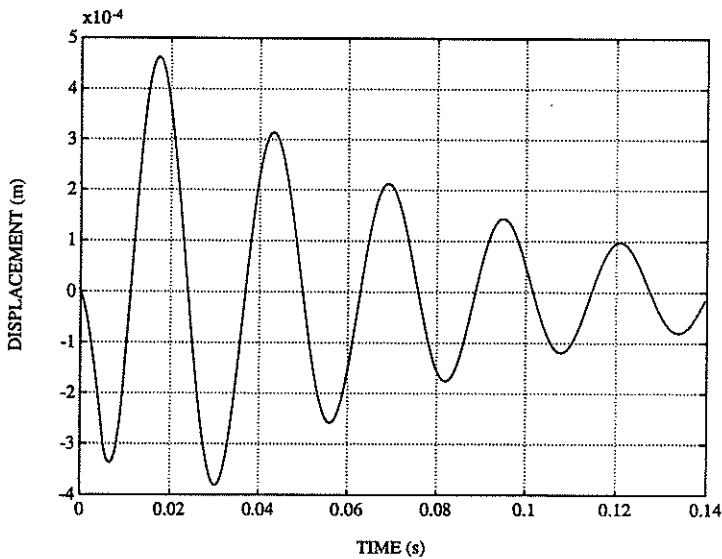
Fig. 5.16   Computed response versus time for the triangular pulse load according to Fig. 5.15. Plate midpoint displacement. $m = 8$.
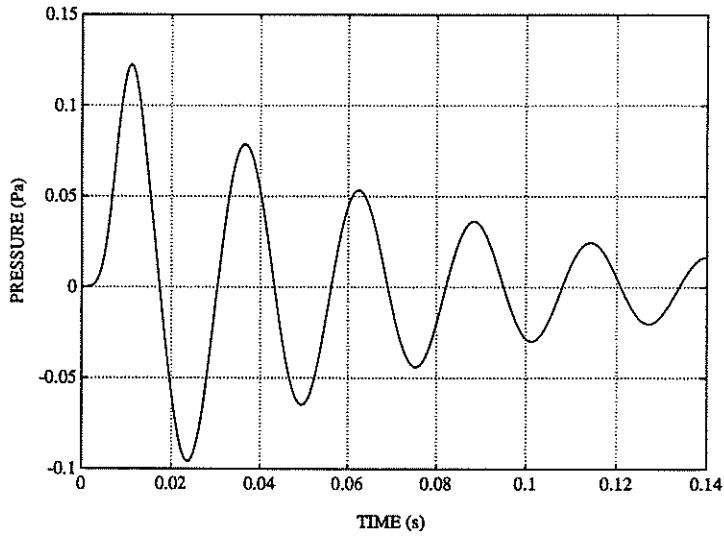
Fig. 5.17   Computed response versus time for the triangular pulse load according to Fig.
5.15. Fluid–pressure in the marked point in Fig. 5.14. $m = 8$.

6. CONCLUDING REMARKS

6.1 Conclusions

In Chapter 2, the governing equations for an acoustic fluid are shown to be of the same order of accuracy as the corresponding equations for a linear elastic solid. Navier's equation of motion for an isotropic linear elastic solid is derived on the assumption of a linear constitutive equation, small displacement velocities and small displacement gradients. For the fluid domain, the Navier–Stokes' equation is derived on the assumption of a linear constitutive equation. After neglecting fluid viscosity, the equation of motion and the continuity equation are further simplified on the assumption of small particle velocities. Finally, the time–varying density is neglected in comparison with the density in the reference state. This last approximation is found to be consistent with an assumption of small displacement gradients used in the solid equations.

In Chapter 3, the discretized weak forms of the equation of motion and of the time–integrated continuity equation, for an acoustic fluid, are combined with the discretized weak form of the equation of motion for a linear–elastic structure. Coupling is ensured by force equilibrium and a kinematic continuity condition, in the normal direction to the fluid–structure interface. The resulting symmetric system of equations, Eq. (3.32), has been previously derived in [29] for the free vibration problem and in [66] for the transient problem. Based on the system Eq. (3.32), eleven formally equivalent fluid–structure interaction formulations are derived. The resulting coupled systems of equations have been previously reported in different versions and derived in different ways, most of them by a variational principle. However, Eq. (3.32) is found to be the most general since this form includes both fluid source loads and fluid body forces, and since all other forms are derivable from this particular system of equations.

The practical use of the different forms is briefly discussed in terms of suitability and computational efficiency. Contrary to what is stated in [31], the use of Eq. (3.32) for the case of a totally enclosed fluid is straight forward, which is clear from this study. This form was also successfully used in [67] and recently in [68].

A mathematical description and a corresponding finite element model for transient acoustic analysis, including a porous medium, has been developed. The frictional retardation of the fluid flow through the pores is introduced through a velocity-dependent body force. The model for a porous medium is easily introduced in the symmetric three–field formulation Eq. (3.32), and the static condensation process resulting in the symmetric two–field form may still be applied.

In Chapter 4, non—modal reduction techniques based on load—dependent Krylov vectors, are discussed. A Lanczos process is suggested for symmetric and proportionally damped structure—acoustic systems. For symmetric and non—proportionally damped systems a variant of the Lanczos algorithm applicable for a pair of indefinite matrices is proposed. A new algorithm is developed for the reduction of unsymmetric, undamped systems of equations. Although this procedure is applied to the unsymmetric system of equations, it is found to be considerably more efficient than the Lanczos procedure, when applied to the structure—acoustic models studied in this work. Both symmetric and unsymmetric systems of equations are thus reduced without solving the associated eigenvalue problem. In the case of non—proportional damping, the second-order system of equations is transformed to a first-order system. This system is then reduced to tridiagonal form.

Further, the proposed reduction techniques utilize a load—dependent starting vector in order to make optimal use of the information about the problem to be solved. The special choice of a starting vector, in the direction of the loading gives accurate but simple expressions for the reduced system of equations in both transient and harmonic analysis.

Numerical examples are given in Chapter 5, in order to illustrate the characteristics of the proposed methods. An interesting application, shown in the examples is the study of transient acoustic problems including a porous medium.

6.2   Future developments

Because of the advantage of diagonal structural and fluid mass matrices associated with certain coupled forms, numerical studies of different lumping techniques used for evaluating these matrices are of great interest.

Further, it is of interest to study the influence of using non–matching finite element meshes in the structural and fluid domains, i.e. not using a one–to–one element coupling at the interacting surface. Considerable savings in computational time can be made if the finite element discretization is made optimal in each domain.

Structure–acoustic systems are generally ill–conditioned. An unsymmetric profile solver suitable for structure–acoustic analysis is under development. One possibility to retain the profile structure of the coefficient matrix is to use a method of iterative refinement.

Finally, the loading function considered in this work may be seen as a special case of the more general expression, viz.

$$f(t) = \sum_{i=1}^{\ell} \hat{f}_i \gamma_i(t) \tag{6.1}$$

where the loading is written as a linear combination of a set of time–independent vectors $\hat{f}_i$. The block Lanczos method has been proposed for this type of loading [51] and a block version of the Arnoldi method is of great interest.

APPENDIX A: Notations

a_0, a_1	Rayleigh constants
a	acceleration field
A	"capacity" matrix in first–order system of equations
b	body force
B	fluid pressure to fluid displacement–potential coupling matrix
B	"conductivity" matrix in first–order system of equations
c	speed of sound
C	system damping matrix
D	rate–of–deformation tensor
$e(t)$	error function
e	a vector of all ones
e_i	unit base vector
E	Young's modulus
E	infinitesimal strain tensor
f	frequency
$\hat{f}$	load amplitude
$\hat{f}$	spatial distribution of load constant in time
f_b	fluid load vector due to the body force
f_f	structure load vector due to fluid interaction
f_s^e	structure load vector due to external time–dependent load
$\overset{**}{f_s^e}$	f_s^e integrated twice with respect to time
f_q	fluid load vector due to added fluid mass
F	deformation gradient tensor
f_f	structure load due to fluid interaction
f_s	external time dependent structural load
G	shear modulus
G	Green strain tensor
H_p	pressure transfer function
H_u	displacement transfer function
H_m	$m \times m$ upper Hessenberg matrix
I	unit tensor
I_m	$m \times m$ identity matrix
k_s	structure factor for porous material

K	bulk modulus
$\mathbf{K}$	system stiffness matrix
$\mathbf{K_f}$	fluid stiffness matrix
$\mathbf{K_s}$	structure stiffness matrix
$\mathbf{K}_\sigma$	shifted system stiffness matrix
$\mathcal{K}^m$	Krylov subspace
$\mathcal{K}^m$	Krylov matrix
L	partial differential operator with respect to time and space
m	mean molecular weight
$\mathbf{M}$	system mass matrix
$\mathbf{M_c}$	structural displacement to fluid pressure coupling matrix
$\mathbf{M_f}$	fluid mass matrix
$\mathbf{M_s}$	structure mass matrix
$\mathbf{n}$	unit vector
$\mathbf{n}$	outward unit normal to the fluid domain
N_ψ	fluid displacement–potential shape function
N_P	fluid pressure shape function
N_s	structural displacement shape function
p	current fluid pressure
$\hat{p}$	pressure amplitude
p_0	pressure in reference state
p_d	pressure field in disturbed state
$\mathbf{p}$	fluid pressure vector
q	source function, added fluid mass per unit volume and time
Q	added fluid mass per unit volume
$\mathbf{Q_m}$	set of Lanczos vectors
$\mathbf{r_0}$	starting vector
r	viscous flow resistance
r_s	static flow resistance
R	universal gas constant
$\mathbf{s}_{i,m}$	eigenvector of the tridiagonal matrix $\mathbf{T_m}$
S_{fs}	fluid–structure interface
S_P	surface with prescribed pressure
S_{rs}	point reacting surface
t	time
$t^{(n)}$	traction force
$\mathbf{T_m}$	tridiagonal $m \times m$ matrix

$\mathbf{u}$	state vector
u_f	fluid displacement field
$\mathbf{u}_m$	approximate solution
$\mathbf{u}_r$	structural displacement vector corresponding to a rigid–body motion
$\hat{\mathbf{u}}_s$	structural displacement amplitude
u_s	structural displacement field
$\mathbf{u}_s$	structural displacement vector
$\overset{**}{\mathbf{u}}_s$	$\mathbf{u}_s$ integrated twice with respect to time
$\bar{\mathbf{u}}_s$	prescribed structural displacement vector
$\tilde{\ddot{\mathbf{u}}}_s$	prescribed structural acceleration vector
v	velocity field
$\mathbf{V}_m$	set of Arnoldi vectors
w	weighting function
$\mathbf{x}$	vector (x_1, x_2, x_3)
$\mathbf{x}(t)$	generalized coordinate
$\hat{\mathbf{x}}_m$	frequency dependent response function
$\mathbf{X}$	vector (X_1, X_2, X_3)
$\mathbf{Y}_m$	set with m linearly independent vectors
$\mathbf{z}$	eigenvector of system of equations
$\mathbf{z}_{i,m}$	approximate eigenvector, Ritz vector, to the system of equations
β	body force potential $b = \nabla\beta$
γ	ratio of specific heat at constant pressure to the specific heat at constant volume
$\gamma(t)$	time function
δ_{ij}	the Kronecker delta
ϵ	unit roundoff error
η	attenuation coefficient
θ	temperature
θ_o	temperature in reference state
θ_i^2	eigenvalue of $\mathbf{K}_\sigma^{-1}\mathbf{M}$
$\theta_{i,m}^2$	eigenvalue of the $\mathbf{T}_m$ matrix and approximate eigenvalue of the $\mathbf{K}_\sigma^{-1}\mathbf{M}$ matrix
λ	elastic constant
λ	eigenvalue of system of equations
μ	elastic constant
μ	dynamic viscosity
μ_i^2	shifted eigenvalue of system of equations

ν	Poisson's ratio
ρ	current density
ρ_o	density in reference state
ρ_d	density field in disturbed state
ρ_e	effective density field
σ	frequency shift
σ	the Cauchy stress tensor
φ	fluid velocity–potential
Φ	fluid velocity–potential vector
ω	angular frequency
$\bar{\omega}$	angular loading frequency
Ω_v	volume porosity for a porous material
ψ	fluid displacement–potential
Ψ	fluid displacement–potential vector
$\int_S$	surface integral
$\int_V$	volume integral
$\dfrac{d\cdot}{dt}$	material time derivative, $\left[\dfrac{\partial\cdot}{\partial t} + (\boldsymbol{v} \cdot \nabla) \cdot \right]$
∇	the del operator, $\left[\dfrac{\partial}{\partial x_1} , \dfrac{\partial}{\partial x_2} , \dfrac{\partial}{\partial x_3} \right]$
$\tilde{\nabla}$	the curl operator, $\begin{bmatrix} 0 & -\dfrac{\partial}{\partial x_3} & \dfrac{\partial}{\partial x_2} \\ \dfrac{\partial}{\partial x_3} & 0 & -\dfrac{\partial}{\partial x_1} \\ -\dfrac{\partial}{\partial x_2} & \dfrac{\partial}{\partial x_1} & 0 \end{bmatrix}$
$(\cdot)$	scalar product
$\dfrac{\partial\cdot}{\partial t}$	partial time derivative

$span\{a_1, a_2, ..., a_n\}$ subspace spanned by the vectors $a_1, a_2, ..., a_n$

APPENDIX B: References

[1]   ABAQUS, User's Manual, Version 4.9, 1990.

[2]   ANSYS, User's Manual, Swanson Analysis Systems Inc., 1987.

[3]   Antoniadis I., Kanarachos A.: Decoupling Procedures to Fluid–Structure Problems, Comp. Meth. Appl. Mech. Eng., Vol. 70, pp. 4–25, 1988.

[4]   Arnoldi W.E.: The Principle of Minimized Iteration in the Solution of the Matrix Eigenvalue problem, Quarterly of Appl. Math., Vol. 9, pp. 17–29, 1951.

[5]   Bathe K.J.: Finite Element Procedures in Engineering Analysis, Prentice–Hall, 1982.

[6]   Bayo E.P., Wilson E.L.: Use of Ritz vectors in wave propagation and foundation response, Earthquake Eng. Struct. Dyn., Vol. 12, pp. 499–505, 1984.

[7]   Beranek L.L.: Acoustic impedance of commercial material and the performance of rectangular rooms with one treated surface, Journal of Acoustical Society of America, Vol. 12, pp. 14–23, 1940.

[8]   Carlsson H., Sandberg G.: Fluid–structure interaction, Finite element analysis in a hydroacoustic application, Part 1, Report TVSM–7045, Lund Institute of Technology, Division of Structural Mechanics, Lund, Sweden, 1988.

[9]   Carlsson H.: Structure–Acoustic Interaction: Finite Element Formulations and Modal Problems, Part A in Finite Element Analysis of Interacting Structure–Acoustic Systems, Licentiate thesis, Report TVSM–3013, Lund Institute of Technology, Division of Structural Mechanics, Lund, Sweden, 1990.

[10]   Carlsson H.: Structure–Acoustic Interaction: Finite element analysis of an idealized automobile compartment, Paper B in Finite element analysis of interacting structure–acoustic systems, Licentiate thesis, Report TVSM–3013, Lund Institute of Technology, Division of Structural Mechanics, Lund, Sweden, 1990.

[11]   Carlsson H.: Structure–Acoustic Interaction: Harmonic and Transient Response using Lanczos Coordinates, Part C in Finite element analysis of interacting structure–acoustic systems, Licentiate thesis, Report TVSM–3013, Lund Institute of Technology, Division of Structural Mechanics, Lund, Sweden, 1990.

[12]   Carlsson H.: Lanczos and Arnoldi Reductions of Symmetric and Unsymmetric
       Fluid—Structure Interaction Problems, Proceedings Inter—Noise '91, pp. 1217—1220,
       Sydney, Australia, 1991.

[13]   Chen H.C., Taylor R.L.: Solution of eigenproblems for damped structural systems by
       the Lanczos method, Report UCB/SEMM—88/01, Department of Civil Engineering,
       University of California, Berkeley, USA, 1988.

[14]   Chen H.C., Taylor R.L.: A discussion of Lanczos vectors and Ritz vectors for
       computing dynamic responses, Report UCB/SEMM—88/15, Department of Civil
       Engineering, University of California, Berkeley, USA, 1988.

[15]   Chen H.C., Taylor R.L.: Vibration analysis of fluid—solid systems using a finite element
       displacement formulation. Report UCB/SEMM—88/17. Department of Civil
       Engineering, University of California, Berkeley, USA, 1988.

[16]   Christiansen P.S., Krenk S.: A recursive finite element technique for acoustic fields in
       pipes with absorption, J. Sound Vib., Vol. 122, pp. 107—118, 1988.

[17]   Clough R.W., Penzien J.: Dynamics of Structures, McGraw—Hill, 1975.

[18]   Coyette J.P.: Numerical treatment of damped acoutic finite element models using
       modal and non—modal approaches, Inter—Noise '90, pp. 877—882, Gothenburg, 1990.

[19]   Craggs A.: A finite element model for rigid porous absorbing materials, J. Sound Vib.,
       Vol. 61, pp. 101—111, 1978.

[20]   Craggs A.: Coupling of finite element acoustic absorption models, J. Sound Vib.,
       Vol. 66, pp. 605—613, 1979.

[21]   Craggs A.: A finite element model for acoustically lined small rooms, J. Sound Vib.,
       Vol. 108, pp. 327—337, 1986.

[22]   Cremer L., Müller H.A.: Principles and Applications of Room Acoustics, Vol. 1,
       Applied Science Publishers, 1978.

[23]   Dahlblom O., Peterson A.: CAMFEM — Computer Aided Modelling Based on the
       Finite Element Method, Report TVSM—3001, Lund Institute of Technology, Division
       of Structural Mechanics, Lund, Sweden, 1982.

[24]   Ericsson T., Ruhe A.: The Spectral Transformation Lanczos Method for the numerical solution of large sparse generalized symmetric eigenvalue problems, Mathematics of Computation, Vol. 35, No. 152, pp. 1251—1268, 1980.

[25]   Everstine G.C.: A symmetric potential formulation for fluid—structure interaction, J. Sound. Vib., Vol. 79, pp. 157—160, 1981.

[26]   Fahy F.: Sound and Structural Vibration: Radiation, Transmission and Response, Academic Press, 1985.

[27]   Farhat C., Wilson E.: Modal Superposition Dynamic Analysis on Concurrent Multiprocessors, Eng. Comput., Vol. 3. pp. 305—311, 1986.

[28]   Felippa C.A.: Solution of Linear Equations with Skyline—Stored Symmetric Matrix, Computers & Structures, Vol. 5, pp. 13—29, 1975.

[29]   Felippa C.A.: Symmetrization of the contained compressible—fluid vibration eigenproblem, Comm. App. Numer. Meth., Vol. 1, pp. 241—247, 1985.

[30]   Felippa C.A.: Symmetrization of Coupled Eigenproblems by Eigenvector Augmentation, Comm. Appl. Numer. Methods, Vol. 4, pp. 561—563, 1988.

[31]   Felippa C.A., Ohayon R.: Mixed variational formulation of finite element analysis of acoustoelastic/slosh fluid—structure interaction, J. Fluids and Struct., Vol. 4, pp. 35—37, 1990.

[32]   Geradin M., Roberts G., Huck A.: Eigenvalue analysis and transient response of fluid—structure interaction problems, Eng. Computations, Vol. 1, pp. 151—160, 1984.

[33]   Gladwell G.M.L., Zimmermann G.: On energy and complementary energy formulations of acoustic and structural vibration problems, J. Sound Vib., Vol. 3, pp. 233—241, 1966.

[34]   Golub G.H., Van Loan C.F.: Matrix Computations, Second Edition, The John Hopkins University Press, 1989

[35]   Göransson P.: ASKA—Acoustics. Theory and applications. FFA TN 1988—13, FFA, The Aeronautical Research Institute of Sweden, Bromma, Sweden, 1988.

[36]   Hinton E., Rock T., Zienkiewicz O.C.: A Note on Mass Lumping and Related Processes in the Finite Element Method, Earthquake Eng. Struct. Dyn., Vol. 4, pp. 245—249, 1976.

[37]   Hughes T.J.R.: The Finite Element Method: Linear Static and Dynamic Finite Element Analysis, Prentice—Hall, 1987.

[38]   Hunter S.C.: Mechanics of continuous media, Second edition, Ellis Horwood, 1983.

[39]   Ibrahimbegovic A., Wilson E.L.: Simple numerical algorithms for the mode superposition analysis of linear structural systems with non—proportional damping, Comp. Struct., Vol. 33, pp. 523—531, 1989.

[40]   Ibrahimbegovic A., Chen H.C., Wilson E.L., Taylor R.: Ritz method for dynamic analysis of large discrete linear systems with nonproportional damping, Earthquake Eng. Struct. Dyn., Vol. 19, pp. 877—889, 1990.

[41]   Ibrahimbegovic A., Wilson E.L.: Automated truncation of Ritz vector basis in modal transformation, Journal of Eng. Mech., Vol 116, pp. 2506—2520, 1990.

[42]   Izadpanah K., Harden R.L., Kansakar R., Reymond M.: Coupled Fluid—Structure Interaction Analysis, Finite Element in Analysis and Design, Vol. 17, pp. 331—342, 1991.

[43]   Lanczos C.: An iteration method for the solution of the eigenvalue problem of linear differential and integral operators, J. Res. Nat. Bur. Standard, Vol. 45, pp. 255—282, 1950.

[44]   Léger P., Wilson E.L.: Generation of Load—dependent Ritz Transformation Vectors in Structural Dynamics, Eng. Comput., Vol. 4, pp. 309—318, 1987.

[45]   Meirovitch L.: Computational methods in structural dynamics, Sijthoff & Noordhoff, 1980.

[46]   Morand H., Ohayon R.: Substructure variational analysis for the vibrations of coupled fluid—structure systems: finite element results, Int. J. Num. Meth. Eng., 14, pp. 741—755, 1979.

[47]   Morse P.M., Ingard K.U.: Theoretical Acoustics, McGraw—Hill, 1968.

[48]   Mårtensson A., Carlsson H.: The development of the finite element method. Report TVSM—7040, Lund Institute of Technology, Division of Structural Mechanics, Lund, Sweden 1987.

[49]   Nour—Omid B., Parlett B.N., Taylor R.L.: Lanczos versus Subspace iteration for solution of eigenvalue problems, Int. J. Num. Meth. Eng., Vol. 19, pp. 859—871, 1983.

[50]   Nour—Omid B., Clough R.W.: Dynamic analysis of structures using Lanczos co—ordinates, Earthquake Eng. Struct. Dyn., Vol. 12, pp. 565—577, 1984.

[51]   Nour—Omid B., Clough R.W.: Block Lanczos method for dynamic analysis of structures, Earthquake Eng. Struct. Dyn., Vol. 13, pp. 271—275, 1985.

[52]   Nour—Omid B., Parlett B.N., Ericsson T., Jensen P.S.: How to implement the Spectral Transformation, Math. Comp., Vol. 48, No. 178, pp. 663—673, 1987.

[53]   Nour—Omid B.: The Lanczos algorithm for solution of large generalized eigenproblems, pp. 582—629 in The Finite Element Method: Linear Static and Dynamic Finite Element Analysis by T.J.R. Hughes, Prentice—Hall, Englewood Cliffs, 1987.

[54]   Nour—Omid B.: Lanczos method for heat conduction analysis, Int. J. Num. Meth. Eng., Vol. 24, pp. 251—262, 1987.

[55]   Nour—Omid B.: Applications of the Lanczos method, Comput. Phys. Comm., Vol. 53, pp. 157—168, 1989.

[56]   Nour—Omid B., Regelbrugge M.E.: Lanczos method for dynamic analysis of damped structural systems, Earthquake Eng. Struct. Dyn., Vol. 18, pp. 1091—1104, 1989.

[57]   Nour—Omid B., Dunbar W.S., Woodbury A.D.: Lanczos and Arnoldi Methods for the Solution of Convection—Diffusion Equations, Comp. Mech. Appl. Mech. Eng., Vol. 88, pp. 75—79, 1991.

[58]   Nour—Omid B., Carlsson H.: Lanczos Reduction of Interacting Structure—Acoustic Systems, Proceedings Iterative Equation Solvers for Structural Mechanics Problems, pp. 37—46, ASME Winter Annual Meeting, Dec 1—6, Atlanta, USA, 1991.

[59]   Olsson L.G., Bathe K–J.: Analysis of fluid–structure interactions. A direct symmetric coupled formulation based on the fluid velocity potential, Comput. Struct., Vol. 21, pp. 21–32, 1985.

[60]   Parlett B.N.: The Symmetric Eigenvalue Problem, Prentice Hall, Englewood Cliffs, 1980.

[61]   Petersson H., Popov E.P.: Substructuring and Equation System Solutions in Finite Element Analysis, Computers & Structures, Vol. 7, pp. 197–206, 1977.

[62]   Petyt M.: The use of acoustic finite elements in a university environment, ANSYS 1989 Conference Proceedings, pp. 11.2–15, 1989.

[63]   Rajakumar C., Rogers C.R.: The Lanczos Algorithm Applied to Unsymmetric Generalized Eigenvalue Problem, Int. J. Num. Meth. Eng., Vol. 32, pp. 1009–1026, 1991.

[64]   Saad Y.: Krylov Subspace Methods for Solving Large Unsymmetric Linear Systems, Mathematics of Computation, Vol. 37, No. 155, pp. 105–126, 1981.

[65]   Saad Y.: Practical use of Some Krylov Subspace Methods for Solving Indefinite and Nonsymmetric Linear Systems, SIAM, J. Scientific and Stat. Comput., Vol. 5, pp. 203–228, 1984.

[66]   Sandberg G.: Finite element modelling of fluid–structure interaction, PhD thesis, TVSM–1002, Lund Institute of Technology, Division of Structural Mechanics, Lund, Sweden 1986.

[67]   Sandberg G., Göransson P.: A symmetric finite element formulation for acoustic fluid–structure interaction analysis, J. Sound Vib., Vol. 123, pp. 507–516, 1988.

[68]   Sandberg G.: Fluid–structure interaction, Finite element analysis of piping systems, Report TVSM–7051, Lund Institute of Technology, Division of Structural Mechanics, Lund, Sweden, 1989.

[69]   Simon H.D.: The Lanczos algorithm with partial reorthogonolization, Mathematics of Computation, 42, no. 165, pp. 115–142, 1984.

[70] Singh R.K., Kant T., Kakodbar A.: Coupled Shell–Fluid Interaction Problems with Degenerate Shell and Three–dimensional Fluid Elements, Comput. Struct, Vol. 38, pp. 515–528, 1991.

[71] Singh R.K.; Kant T., Kakodbar A.: Efficient Partitioning Schemes for Fluid–Structure Interaction Problems, Eng. Comput., Vol. 7, 1990.

[72] Spencer A.J.M.: Continuum mechanics, Longman, 1980.

[73] Strang G.: Introduction to Applied Mathematics, Wellersley–Cambridge Press, 1986.

[74] Svensson I.: A study of a dynamic system involving fluid–structure interaction, Department of Mathematics, 1987:4, Lund University, Sweden, 1987.

[75] SYSNOISE, Users Manual, Dynamic Engineering, 1989.

[76] Taylor R.L.: Solution of Linear Equations by a Profile Solver, Eng. Comput., Vol. 2, pp. 344–350, 1985.

[77] Wiberg N.–E.: System Analysis in Structural Mechanics by use of mixed force and displacement variables, Ph.D. thesis, Chalmers University of Technology, Göteborg, Sweden, 1970.

[78] Wilson E.L., Yuan M., Dickens J.: Dynamic analysis by direct superposition of Ritz vectors, Earthquake Eng. Struct. Dyn., Vol. 10, pp. 813–829, 1982.

[79] Zienkiewicz O.C., Taylor R.L.: The Finite Element Method. Fourth Edition, McGraw–Hill, 1991.

[80] Zwikker C., Kosten C.W.: Sound Absorbing Materials, Elsevier, 1949.

[81] Sandberg G.: Spectral Properties of Finite Element Formulations in Analysis of Structure–Acoustic Interaction, Svenska Mekanik–dagar, Stockholm, 1992.